Analysis of high PV Penetration Impacts and Reactive Power Management in Unbalanced Distribution Grids Including the Secondaries

Gökmen, Nuri

Publication date:
2019

Document Version
Publisher's PDF, also known as Version of record

ANALYSIS OF HIGH PV PENETRATION IMPACTS AND REACTIVE POWER MANAGEMENT IN UNBALANCED DISTRIBUTION GRIDS INCLUDING THE SECONDARIES

BY
NURI GÖKMEN

DISSERTATION SUBMITTED 2019

AALBORG UNIVERSITY
DENMARK

ANALYSIS OF HIGH PV PENETRATION IMPACTS AND REACTIVE POWER MANAGEMENT IN UNBALANCED DISTRIBUTION GRIDS INCLUDING THE SECONDARIES

PH.D. DISSERTATION

by

Nuri Gökmen

AALBORG UNIVERSITY
DENMARK

Dissertation submitted

Dissertation submitted:	September 10, 2019
PhD supervisor:	Prof. Zhe Chen, Aalborg University
Assistant PhD supervisor:	Associate Prof. Weihao Hu, Aalborg University
PhD committee:	Associate professor Jayakrishnan Radhakrishna Pillai (chair) Aalborg University
	Professor Ljupco Kocarev University in Skopje
	Professor Peng Wang Nanyang Technlogical University
PhD Series:	Faculty of Engineering and Science, Aalborg University
Department:	Department of Energy Technology

ISSN (online): 2446-1636
ISBN (online): 978-87-7210-500-0

Published by:
Aalborg University Press
Langagervej 2
DK – 9220 Aalborg Ø
Phone: +45 99407140
aauf@forlag.aau.dk
forlag.aau.dk

Printed in Denmark by Rosendahls, 2019

CV

Nuri Gökmen received the B.Eng. and M.Sc. degrees from Ege University, Izmir, Turkey, in 2011 and 2013, respectively, both in electrical and electronics engineering. He is currently pursuing the Ph.D. degree with the Deparment of Energy Technology, Aalborg University, Denmark. His research interests include photovoltaics, renewable energy integration in distribution grids, smart grids, optimization, intelligent control methods, and modern power system simulation tools.

ENGLISH SUMMARY

Environmental concerns have made governments and decision makers focus on clean energy policies to reduce greenhouse gas emissions and pollution. In this context, many countries have set ambitious targets to increase the share of renewable energy sources and accordingly lower the dependence on fossil fuels. As one of the most promising options, solar photovoltaic (PV) systems have become the fastest growing renewable energy sources over the last two decades. The remarkable rise of PV systems is expected to continue through the next decade and beyond with ongoing cost reductions and global decarbonization targets.

Even though the process is pleasing, with the increase in PV penetration levels some unfamiliar impacts are also introduced in distribution grids. Previously, when PV penetration levels were low, it was reasonable to assume that generation would offset the consumption and consequently eliminate the voltage drops, equipment loadings, and power losses. However, with the increase in PV penetration levels, these assumptions will no longer be valid; on the contrary, these problems will be exaggerated if necessary precautions are not taken in advance.

On the other hand, PV inverters are expected to play a key role in the near future. With the advances in power-electronics and communication technologies, state-of-the-art PV inverters now have the ability to provide ancillary services to the grid. Their operating points can be adjusted dynamically via intelligent control algorithms to reduce adverse PV penetration impacts. Some countries have already updated their PV interconnection standards promoting ancillary services such as active power curtailment and reactive power support from PV inverters.

It's worth to mention that, although most PVs are interconnected to secondary distribution grids, individual voltage problems at the customer sides and service transformer overloadings are usually ignored in the analysis. Traditionally, residential customers in low-voltage distribution grids had only be seen as bulk aggregated load sources for higher level voltage network studies. However, due to the smoothing effect of the aggregation, the severity of the impacts may not be observed accurately in the secondary distribution grids. Therefore, it is crucial to include both primary and secondary sections of the grid and their components in the analysis to make more accurate inferences about the PV penetration impacts.

In this thesis, first, the technical impacts of high PV penetration on distribution systems are scrutinized considering voltage variations, voltage unbalance, line and transformer loadings, surplus power, power loss, and stress on voltage regulators. For this purpose, the distribution system is modeled as detailed as possible including both primary and secondary sides. In addition, time-varying high-resolution probabilistic load and PV generation profiles are generated individually considering a variety of

device specifications, environmental effects, and human choices. Combining all of these components in a designed co-simulation environment, three-phase unbalanced power flow analysis is performed through winter and summer cases. According to the detailed analysis, problems are identified on a wide scale starting from the customer connection points to the substation in the case of high PV penetration.

Then, some mechanisms are investigated to maintain the voltage variations and voltage unbalance within the allowable limits. Accordingly, reactive power management strategies based on PV inverters are developed to mitigate the voltage variations and voltage unbalance by including the behavior of secondary distribution systems under high PV penetration levels.

Regarding the voltage variation problem, two different techniques are proposed to mitigate the voltage variations both in primary and secondary distribution systems. Both techniques utilize reactive power support capabilities of PV inverters. While in the first technique, only global solar irradiance measurements are used for all the inverters to reduce the system complexity, in the second technique, individual load and PV generation measurements are used to increase the system accuracy. With both techniques, it's shown that reactive power support could be a very promising solution in mitigation of the voltage variations problem.

Regarding the voltage unbalance problem, PV inverters are coordinated in two different techniques to mitigate the voltage unbalance in distribution systems. Both proposed techniques are based on reactive power support capabilities of PV inverters and three-phase voltage-sensitivity analysis. While in the first technique (self-node balancing strategy), coordination of PV inverters is limited among the individual node phases to reduce the system complexity, in the second technique (cooperative-node balancing strategy) coordination of PV inverters is extended among all unbalanced node phases to include the mutual effect between the nodes. Following this logic, optimal reactive power deviations for each participating PV inverter is obtained via an optimization process. As in the voltage variations problem, it's shown that reactive power support of PV inverters can also be used to effectively mitigate the voltage unbalance problem in distribution systems.

DANSK RESUME

Miljømæssige bekymringer har gjort regeringer og beslutningstagere opmærksom på rene energipolitikker for at reducere drivhusgasemissioner og forurening. I den forbindelse har mange lande sat ambitiøse mål for at øge andelen af vedvarende energikilder og dermed mindske afhængigheden af fossile brændstoffer. Som en af de mest lovende muligheder er solfotovoltaisk (PV) systemer blevet de hurtigst voksende vedvarende energikilder i de sidste to årtier. Den bemærkelsesværdige stigning i PV-systemer forventes at fortsætte gennem det næste årti og derover med løbende omkostningsreduktioner og globale decarboniseringsmål.

Selvom processen er tilfredsstillende, med stigningen i PV-penetrationsniveauer, introduceres også nogle ukendte virkninger i distributionsnet. Tidligere, da PV-penetrationsniveauerne var lave, var det rimeligt at antage, at generationen ville kompensere for forbruget og dermed eliminere spændingsfaldene, udstyrsbelastningerne og strømforløbene. Men med stigningen i PV-penetrationsniveauer vil disse antagelser ikke længere være gyldige; Tværtimod vil disse problemer være overdrevne, hvis det ikke er nødvendigt at træffe forholdsregler forinden.

På den anden side forventes PV-omformere at spille en central rolle i den nærmeste fremtid. Med fremskridt inden for strømelektronik og kommunikationsteknologier har de nyeste PV-omformere nu mulighed for at yde supplerende tjenester til nettet. Deres driftspunkter kan justeres dynamisk via intelligente kontrolalgoritmer for at reducere negative PV-penetrationspåvirkninger. Nogle lande har allerede opdateret deres PV-sammenkoblingsstandarder, der fremmer hjælpeydelser som aktiv strømindskrænkning og reaktiv strømstøtte fra PV-omformere.

Det er værd at nævne det, selvom de fleste PV'er er sammenkoblet med sekundære distributionsnet, individuelle spændingsproblemer på kundens sider, og servicetransformatoroverbelastninger ignoreres normalt i analysen. Traditionelt var boligkunder i lavspændingsdistributionsnet kun betragtet som bulkaggregerede belastningskilder til højere spændingsundersøgelser. På grund af aggregerings udjævningseffekt er det dog ikke sikkert, at sværhedsgraden af virkningerne bliver nøjagtigt i sekundærfordelingsnettet. Derfor er det afgørende at inkludere både primære og sekundære dele af nettet og deres komponenter i analysen for at gøre mere præcise konklusioner om PV-penetrationspåvirkningerne.

I denne afhandling undersøges først de tekniske virkninger af høj PV-penetration på distributionssystemer i betragtning af spændingsvariationer, spændingsbalance, linie- og transformatorbelastninger, overskydende effekt, effekttab og stress på spændingsregulatorer. Til dette formål er distributionssystemet modelleret så detaljeret som muligt inklusive både primære og sekundære sider. Derudover

genereres tidsvarierende højopløselige probabilistiske belastnings- og PV-generationsprofiler individuelt under hensyntagen til forskellige enhedsspecifikationer, miljøeffekter og menneskelige valg. Ved at kombinere alle disse komponenter i et designet co-simuleringsmiljø udføres tre-fase ubalanceret strømgennemstrømningsanalyse gennem vinter- og sommerfaser. Ifølge den detaljerede analyse er problemer identificeret i stor målestok, startende fra kundens forbindelsespunkter til transformatorstationen i tilfælde af høj PV-penetration.

I denne afhandling udvikles reaktive strømstyringsstrategier baseret på PV-omformere for at afbøde spændingsvariationerne og spændingsbalancen ved at inddrage adfærden af sekundære distributionssystemer under høje PV-penetrationsniveauer.

Hvad angår spændings variationer problemet foreslås to forskellige teknikker til at afbøde spændingsvariationerne både i primære og sekundære distributionssystemer. Begge teknikker udnytter PV-omformere med reaktiv strømforsyning. I den første teknik anvendes kun globale solstrålingsmålinger til alle invertere for at reducere systemkompleksiteten. I den anden teknik bruges individuelle belastnings- og PV-generationsmålinger til at øge systemets nøjagtighed. Med begge teknikker er det vist, at reaktiv strømforsyning kunne være en meget lovende løsning til begrænsning af spændingsvariationer.

Hvad angår spændings ubalance problemet, er PV-omformerne koordineret i to forskellige teknikker for at afbøde spændingsbalancen i distributionssystemerne. Begge de foreslåede teknikker er baseret på reaktive strømstyrkefunktioner af PV-omformere og trefasespændingsfølsomhedsanalyse. I den første teknik (selvreguleringsbalancestrategi) er koordinering af PV-omformere begrænset mellem de individuelle nodefaser for at reducere systemkompleksiteten, i den anden teknik (kooperativ-knudebalanceringsstrategi) koordineres PV-omformerne blandt alle ubalancerede node faser for at indbefatte den gensidige effekt mellem knuderne. Efter denne logik opnås optimale reaktive effektafvigelser for hver deltagende PV-inverter via en optimeringsproces. Som i spændingsvariationerproblemet er det vist, at reaktiv strømstøtte af PV-omformere også kan bruges til effektivt at begrænse spændingsbalanceproblemet i distributionssystemerne.

ACKNOWLEDGMENTS

This study is supported in part by the Danish Council for Strategic Research (Grant DSF 09-067255) under the project "Development of a Secure, Economic and Environmentally-friendly Modern Power System (SEEMPS)" and in part by the EUDP/ForskEL (Grant 64017-0047/12561) under the project of "Voltage Control and Protection for a Grid towards 100% Power Electronics and Cable Network (COPE)". Hereby, I would like to express my sincere thanks to these institutions, and also to Otto Mønsteds Fond, Department of Energy Technology, and Aalborg University for giving me this precious research opportunity.

I would like to express my deep gratitude to my supervisor Prof. Zhe Chen for his patient guidance, enthusiastic encouragement, kindness, and constructive discussions. His valuable support, understanding, and expertise have been very important in completing this study. Assistance provided by co-supervisor Associate Prof. Weihao Hu was also greatly appreciated.

I would like to express my very great appreciation to Associate Prof. Engin Karatepe who has encouraged me throughout this journey to achieve many great things from the very beginning.

I wish to acknowledge the help provided by all academic and support staff of the Department of Energy Technology and on behalf of them special thanks to Tina Larsen, Corina Busk Gregersen, and Eva Janik for their invaluable help during my study in Aalborg University.

I would sincerely thank my colleagues in our research group, Baohua Zhang, Peng Hou, Rui Hu, Dong Liu, Yanbo Wang, Weihua Zhou, and Kaiqi Ma. Besides, a special thanks to Mostafa Astaneh, Iker Diaz de Cerio Mendaza, and Miguel Canas Carreton for helping me a lot from my very first days at Aalborg University. I am also so grateful to all my other friends and guest researchers in the Department of Energy Technology for spending pleasant times with them. Furthermore, I would like to thank research assistants Özge Canlı and Gizem Kalender, and also Prof. Dr. Yeşim Zoral for their warm hospitality during my study abroad period at Dokuz Eylul University.

Very special thanks to my close friend Berk Çelik. We have started this journey together and supported each other all the time. And, Faruk Ugranlı, Sabin Bana, Robert Popescu, Saher Shakhshir, Jose Simon thank you all for being great friends.

And Ezgi Bayar, iyi ki…

Lastly, I would like to give my deepest gratitude to my family for their endless love, care, and support. I wouldn't have done it without you. Thank you so much.

Nuri Gökmen

August 2019
Aalborg, Denmark

TABLE OF CONTENTS

TABLE OF FIGURES

CHAPTER 1. INTRODUCTION

1.1. BACKGROUND AND MOTIVATION

It is of vital importance to reduce the greenhouse gas emissions for the continuation of life on earth. In this direction, many countries have set ambitious targets to increase the share of renewable energy sources and accordingly lower the dependence on fossil fuels [1]. In virtue of these global decarbonization targets, solar PV systems have received a great deal of attention over the last few decades. With an average annual growth rate of 48% since 2007, worldwide PV system installation capacity has reached 403 GW by the end of 2017 as shown in Figure 1.1 [2].

Moreover, PV systems have become the least costly power generation option in many countries. With the ongoing cost reductions, utility-scale PV systems are now cheaper than nuclear, coal, and combined cycle gas turbine power plants [3]. As an indicator of this, there have been more PV installations than fossil fuel and nuclear power plants in 2017, and PV systems have almost doubled its renewable energy competitor, wind power, in the new installation capacities. With the increase in competitiveness and determined green energy policies, the upward trend of PV systems is expected to continue also in the forthcoming years [4].

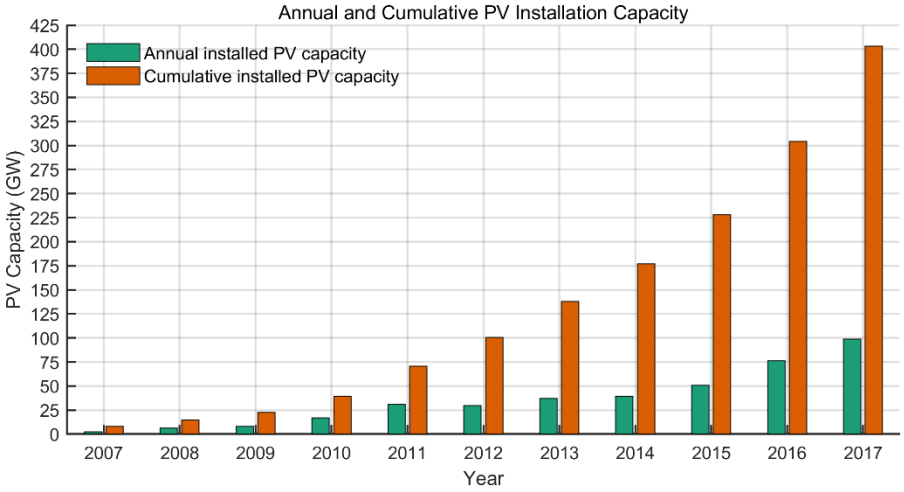

Figure 1.1 Remarkable upward trend of PV systems in the last decade

The vast majority of PV systems are integrated into existing low-voltage distribution grids which were originally not designed to host any kind of generation [5]. The proliferation of PV systems and other distributed generation sources have changed our

perspectives on distribution grids. With the integration of distributed generation sources, passive distribution networks have been progressively transformed into active distribution networks [6]. Today, end-users have also the opportunity to generate their own electricity and inject surplus power to the grid [7]. Even a new definition, prosumer, has been emerged for these kinds of end-users due to being both consumer and producer at the same time [8]. The process that began with the deregulation of the power markets [9], integration of the distributed renewable energy sources [10], and the development of smart grid concept [11] have made the previously neglected customers and low-voltage distribution grids the very center of the attention today [12].

However, with the increase in PV penetration levels, some unfamiliar impacts have also begun to appear in distribution systems. Voltage variations [13], voltage unbalance [14], line and transformer overloadings [15], the excessive operation of voltage regulation devices [16], increase in power losses [17] and the substantial amount of surplus power [18] can be exemplified as the experienced problems so far. As it is well-known, the whole purpose of power system operations is to balance the load and generation instantaneously. Unfortunately, both of them are intermittent and highly variable in distribution systems [19]. For these reasons, further increasing PV penetration levels can also increase the degree of load and generation imbalance, and consequently lead to the technical problems above [20]. Therefore, there is an urgent need for understanding the associated impacts and taking necessary precautions to continue the proliferation of PV systems [21].

In addition, it's important to emphasize that although most PVs are interconnected to secondary distribution grids, individual voltage problems at the customer sides and service transformer overloadings are usually ignored in the analysis [22]. Traditionally, residential customers in low-voltage distribution grids had only be seen as bulk aggregated load sources for medium or high voltage level grid studies [23]. However, due to the smoothing effect of the aggregation, the severity of the impacts may not be observed accurately in the secondary distribution grids. Therefore, it is crucial to include both primary and secondary sections of the grid and their components in the analysis to make more accurate inferences about the PV penetration impacts.

As being expressed in literature, due to the inadequacy of conventional methods, more up-to-date solutions are required to mitigate these unfamiliar impacts [24]. Modern solutions to deal with the high PV penetration problems include the options of active power curtailment [25], reactive power support [26], demand-side management [27] and energy storage systems [28]. Although conventional devices such as load tap changers, voltage regulators, and switched capacitors are still being used today, they do not have the capability to tolerate the fast variations of load and generation [29]. Having this ability, PV inverters are expected to play a key role in the mitigation of high PV penetration impacts in the near future [30]. With the advances in power

electronics and communication technologies, now state-of-the-art PV inverters are able to provide ancillary services to the grid. Their operating points can be adjusted dynamically with intelligent control algorithms to reduce the adverse PV penetration impacts.

Considering the mentioned problems, there's presently a growing need to model the secondaries in detail taking into account both individual loads and renewable generation. Besides, advanced inverter capabilities should be integrated into distribution management systems to seamlessly increase PV penetration levels. In this context, this thesis comprises of the following three stages. In the first stage, modeling of loads, PV generation, and distribution networks are performed combining both primary and secondaries. In the second stage, the technical impacts of high PV penetration are analyzed in detail considering the time-varying nature of load and generation. In the third stage, reactive power support capabilities of PV inverters are utilized as ancillary service to mitigate the voltage variations and voltage unbalance.

1.2. RESEARCH QUESTIONS AND OBJECTIVES

The main objective of this thesis is to analyze the technical impacts of high PV penetration in depth by including the secondary distribution systems and to provide modernized solutions based on new reactive power management strategies to mitigate the voltage variations and voltage unbalance problems. To accomplish this objective, the following research questions will be answered step by step throughout this thesis.

How to include individual characteristics of end-user loads in distribution grids?

Traditionally, end-users in low-voltage distribution grids have been represented by aggregated load models for the analysis of medium and high voltage sections of the electricity grid. After the deregulation of power markets and the birth of the smart grid concept, previously neglected individual end-user behaviors now have become the center of interest.

In this thesis, individual loads of end-users will be represented by physical load models to include their time-varying nature in the analysis. Moreover, loads will be diversified at three different levels by assigning random device parameters (device level), different thermal and structural characteristics (house level), and diverse human behaviors (human level). Adapting this diversification approach, high-resolution time-varying probabilistic load profiles will be generated to be used in the analysis.

How to include PV generation considering environmental effects and how to utilize PV inverter capabilities?

There has been an enormous growth of solar energy in the last two decades and this is anticipated to continue also in the forthcoming years. On the other hand, the output power of the PV system highly varies throughout the day depending on the solar irradiance and temperature changes. Thus, it's crucial to represent the variations of PV output as accurate as possible in distribution system studies. In addition, PV inverters are expected to play a key role in the near future by providing ancillary services to the grid. In connection with this, the capacity of PV inverter has become a key parameter which may directly affect the contribution of reactive power support.

In this thesis, apart from the irradiance and temperature effects on PV generation, wind speed effect will also be investigated to more accurately estimate the variations of PV system output. In addition, a mechanism will be explored how to effectively use the capabilities of PV inverters as an ancillary service to maintain the voltage variations within the allowable range.

How to construct a co-simulation environment with multitudinous individual end-users having both loads and generation?

Many studies disregard the variability of individual end-user loads and PV systems in secondary distribution grids due to the difficulties to perform their simulations in a single platform.

In this thesis, to efficiently use the computer resources, two different simulation platforms, GridLAB-D and Matlab, will be incorporated together through a Python programming language interface. In this way, the advanced modeling technique in GridLAB-D and friendly user interface of Matlab will be combined to perform the three-phase unbalanced power flow analysis. In this framework, high PV penetration impacts will be investigated on both primary and secondary distribution systems including HVAC, EWH, lighting loads, and PV generation systems.

How to use reactive power support by PV inverters to mitigate the voltage variations?

Loads in distribution systems are intermittent and highly variable due to diverse device characteristics and human behaviors. While this to a certain extent already causes some voltage variation problems, on top of it, adding highly variable PV generation may lead to more severe voltage variations. This phenomenon may cause frequent operation of load tap changers, voltage regulators, and switched capacitors; and consequently, reduce their lifetimes. Moreover, voltage sensitive devices may also be damaged.

In this thesis, new reactive power management strategies will be explored to mitigate the voltage variations via PV inverters. It's aimed to determine the set points of PV inverters in a simple analytical way by metering different types of parameters such as solar irradiance, load, and PV measurements.

How to coordinate PV inverters in an intelligent way to mitigate the voltage unbalance problem?

Voltage unbalance problem may arise due to the differences in phase voltage magnitudes. If the voltage unbalance level exceeds the safe limits, it can damage three-phase motor windings and shorten the insulation life of three-phase transformers by excessive heating. On the other hand, distribution grids are to some extent inherently unbalanced due to untransposed lines, multiphase structure, and unevenly distributed single-phase loads. The increasing trend of PV system installations on single-phase laterals may introduce additional uncertainty in phase voltages and forthrightly affect the degree of voltage unbalance level.

In this thesis, benefitting from voltage sensitivity analysis and reactive power support capabilities of PV inverters, new techniques will be explored to mitigate the voltage unbalance problem in multi-phase distribution systems. It's aimed to reveal some mechanisms to coordinate the PV inverters in different ways and consequently contribute to the solution of the voltage unbalance problem.

1.3. METHODOLOGY

To analyze the technical impacts of high PV penetration, a co-simulation environment has been designed with both primary and secondary sections of the grid as shown in Figure 1.2. The test system is made flexible so that any IEEE distribution test feeder can be used as the primary section of the grid and accordingly secondaries can be populated automatically with a Matlab script.

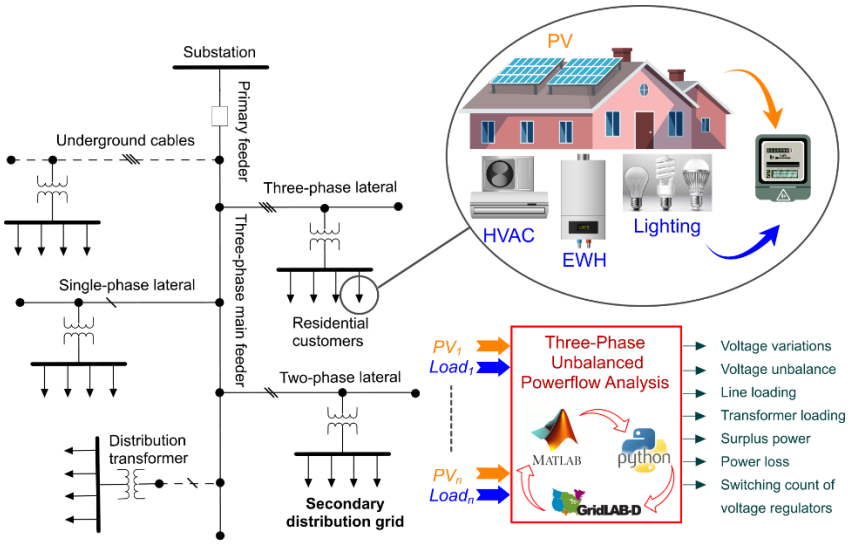

Figure 1.2 Design of a co-simulation environment to analyze the technical impacts of high PV penetration

Each house in secondaries is equipped with HVAC, EWH, and lighting loads, and also a PV generation system. Matlab scripts are written to generate probabilistic random values for hundreds of different input parameters considering diverse household demographics, thermal and structural characteristics of buildings, device specifications, weather characteristics, and also human behaviors. Then, these generated values are used as inputs to GridLAB-D simulation tool to obtain the high-resolution time-varying probabilistic load and PV generation profiles.

These two simulation platforms are communicated through an interface which is designed with Python programming language to perform the three-phase power flow analysis. With the powerflow analysis, the technical impacts of interest are reported including voltage variations, voltage unbalance, line and transformer loading, surplus power, power loss, and switching count of voltage regulation devices.

After the analysis of technical impacts, reactive power support capabilities of PV inverters have been used to mitigate the voltage variations as illustrated in Figure 1.3.

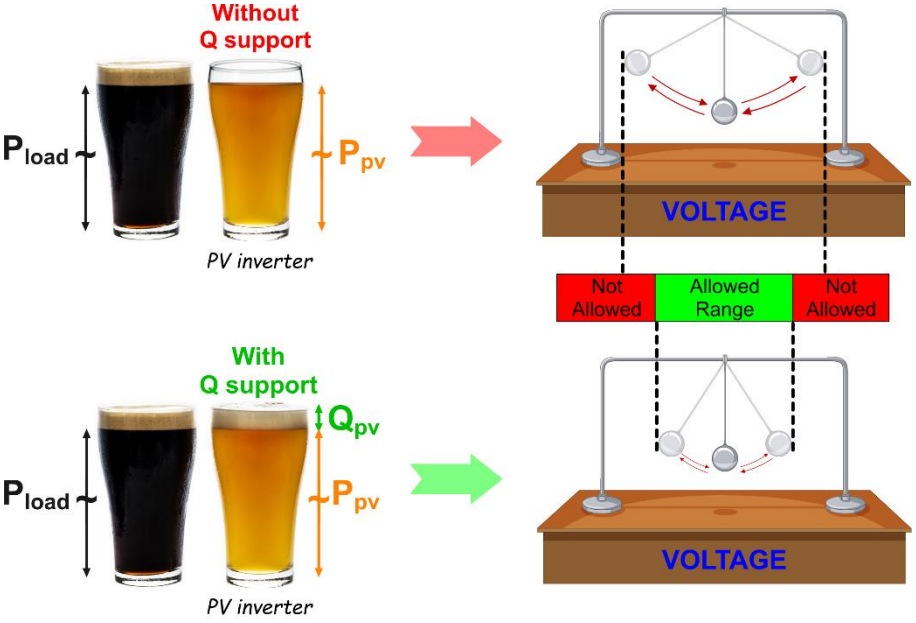

Figure 1.3 Reactive power support to mitigate the voltage variations

The primary objective of a PV inverter is to generate active power (P_{pv}) and most of its capacity can be used for this purpose. On the other hand, the leftover or extra capacity can be used to provide some reactive power (Q_{pv}) as an ancillary service. By using this small capacity for reactive power support, voltage variations can be mitigated as shown in Figure 1.3.

In this thesis, two different techniques are proposed to mitigate the voltage variations by using reactive power support of PV inverters. The first technique only requires two solar irradiance components (global and diffuse horizontal irradiance) which can easily be obtained from weather stations. It's aimed to reduce the system costs by eliminating the need for additional sensors. The power factor of each inverter is regulated in proportion to solar irradiance by a simple analytical conversion. On the other hand, the second technique requires active power measurements of load and PV generation. Moreover, the weekly changing patterns of load and generation are also taken into account to more accurately determine and scale the maximum quantity of reactive power for each PV inverter. Depending on the instantaneous imbalance of load and generation, inductive or capacitive power factors are applied to tolerate the voltage variations locally. Similar to the first technique, required reactive power deviations for each PV inverter is also obtained with a simple analytical approach.

Afterward, the voltage unbalance problem is tackled in distribution grids. First of all, node/phase relationships (d*V*/d*Q* sensitivity) are revealed with an enhanced three-phase voltage sensitivity analysis. Then, this information is used to optimally set the required reactive power amount for each single-phase PV inverter. Accordingly, phase voltages are pulled back to the allowable voltage unbalance zone as shown in Figure 1.4.

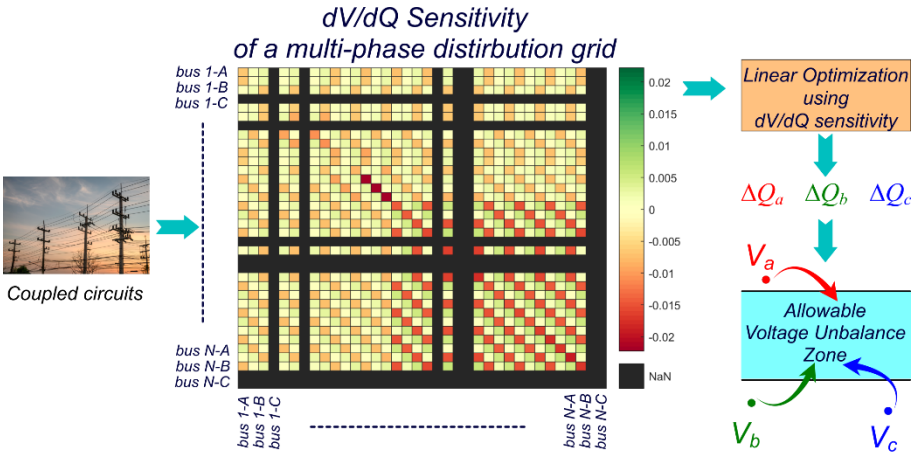

Figure 1.4 The outline of voltage unbalance mitigation strategies

Using the explained logic, two different methods are proposed to mitigate the voltage unbalance problem. While in the first method (self-node balancing), only the unbalanced node's own phases (self-effect) is considered, in the second method (cooperative balancing), not only unbalanced node's own phases (self-effect), but the impact of other node phases (mutual-effect) on the unbalanced node is also considered to optimally adjust the reactive power deviations for each phase.

1.4. THESIS OUTLINE

This thesis is written as a monograph and chapters are organized in a systematic way as depicted in Figure 1.5. The research consists of three main stages as modeling, analysis, and reactive power management strategies that are distributed over five core chapters.

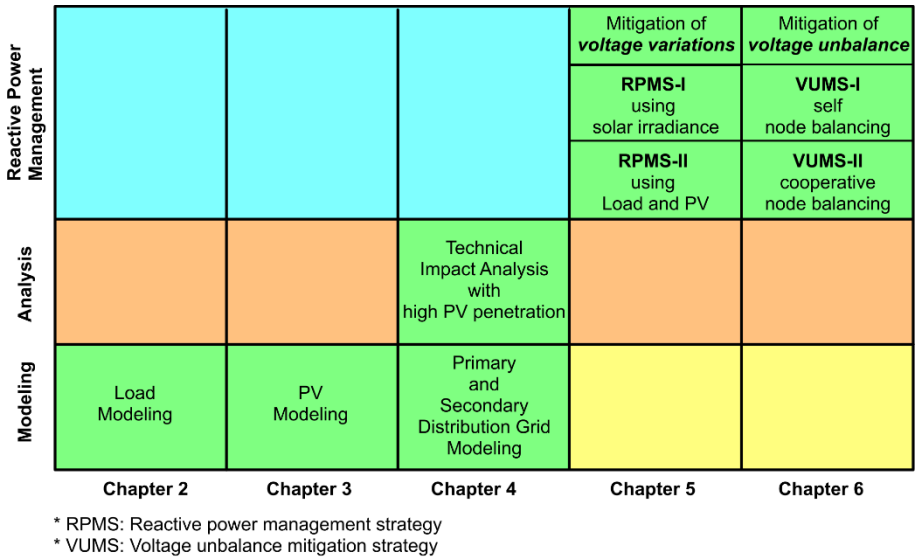

Figure 1.5 Thesis structure

The rest of the thesis is organized as follows:

Chapter 2 presents a probabilistic approach to model the end-user loads in secondary distribution grids. Heating, ventilation, and air conditioning system (HVAC), electric water heater (EWH), and lighting loads have been considered. A gray-box bottom-up approach is presented using both physical load models and statistical data. High-resolution time-varying load profiles are generated for each individual load.

Chapter 3 focuses on overall PV system modeling. Apart from the solar irradiance and temperature effects, wind effect is also investigated to more accurately estimate the PV generation variations. Then, individual time-varying high-resolution PV generation profiles are generated considering the diverse PV module and inverter characteristics. In addition, it's discussed how to utilize PV inverter capabilities for a more effective reactive power support.

Chapter 4 analyzes the technical impacts of high PV penetration on a large scale from customer connection points to the substation. For this purpose, first, the distribution

system is modeled as a whole including both primary and secondary sections. Second, the three-phase unbalanced power flow technique is presented. Third, using the previously generated high-resolution time-varying individual load and PV generation profiles, a comprehensive technical impact analysis is conducted.

Chapter 5 proposes two different techniques to mitigate the voltage variations in the case of high PV penetration. While the first technique requires solar irradiance measurement, the second technique requires active power measurements of load and PV generation. Accordingly, power factors of PV inverters are regulated with a simple analytical approach. The effectiveness of the proposed techniques is tested under different seasons and compared with the conventional approaches.

Chapter 6 proposes two different techniques to mitigate the voltage unbalance in distribution grids. Both techniques are based on three-phase voltage sensitivity analysis and reactive power support capabilities of PV inverters. The first one is called self-node balancing due to only individual phases of unbalanced node participate in the mitigation strategy. On the other hand, the second one is called cooperative balancing which also includes the other node phases to contribute to the solution. According to the chosen strategy, optimal reactive power deviations for all participating PV inverters are determined with an optimization process and consequently, voltage unbalance problem is mitigated.

Chapter 7 draws a conclusion and summarizes the main contributions of this thesis. In addition, some research proposals are made and introduced as future works.

1.5. LIST OF PUBLICATIONS

[C.1] **N. Gökmen**, W. Hu, and Z. Chen, "A simple PV inverter power factor control method based on solar irradiance variation," in *2017 IEEE Manchester PowerTech*, 2017, pp. 1–6.

[C.2] **N. Gökmen**, W. Hu, X. Xu, and Z. Chen, "A novel reactive power control strategy for distribution grids with large scale rooftop PV systems," in *2018 IEEE PES Asia-Pacific Power and Energy Engineering Conference (APPEEC)*, 2018, pp. 382–387.

[C.3] **N. Gökmen**, W. Hu, and Z. Chen, "Technical Impacts of Overhead-Line to Underground-Cable Transition in Distribution Grids," in *2018 11th IET International Conference on Advances in Power System Control, Operation and Management (APSCOM),* 2018.

[J.1] **N. Gökmen**, W. Hu, P. Hou, Z. Chen, D. Sera, and S. Spataru, "Investigation of wind speed cooling effect on PV panels in windy locations," *Renewable Energy*, vol. 90, pp. 283–290, May 2016.

[J.2] **N. Gökmen**, W. Hu, and Z. Chen, "Mitigation of voltage unbalance in multiphase distribution grids," *IEEE Trans. Smart Grid*, 2019 (submitted).

CHAPTER 2. LOAD MODELING

Loads could be regarded as the most essential components of power systems. It is of vital importance, first to understand the nature of loads and then move one step forward to understanding how power systems actually work.

With the evolution of power grids, previously neglected residential customers have become the very center of the attention. Increase in renewable energy integration levels has made it necessary to properly understand and model the behaviors of end-users to achieve sustainable energy development. Therefore, having an accurate customer demand model is critical for efficient planning, operation, and control of power systems.

In this chapter, first, a comprehensive literature review is given about load modeling. Then all data sources are introduced and steps to create a probabilistic household database for any location and grid is explained. For the largest three loads in the houses, physical load models are presented, and in the final stage, individual probabilistic load profiles are generated by the proposed load diversification methods. These generated high-resolution time-varying load profiles will be used in the following chapters to analyze the distribution grids.

2.1. LITERATURE REVIEW

Traditionally, low voltage distribution networks where residential customers are connected to the electricity grid would have been represented by bulk aggregate load models for the analysis of the medium and high voltage sections of the grid [23]. After the deregulation of power markets and the birth of smart grid concept, previously neglected end-users now have become the very center of the attention [31]. A good understanding and estimation of end-user behaviors are of vital importance for sustainable energy development [32].

In the light of these developments, there is renewed interest in load modeling at the end-user side. By studying behavioral patterns of end-users, system flexibility can be increased with the demand side management techniques and demand response programs [33]. By taking time-variant load profiles into account, renewable energy integration levels can be boosted [34]. Furthermore, resources in distribution grids can be allocated more efficiently with improved planning, operation, and control algorithms [35].

However, load modeling in low-voltage distribution grids poses some significant challenges as:

- Knowledge on load models is usually not sufficient [36].
- Having a great diversity, parameters of load models are difficult to obtain [37].
- Lacking individual measurements, it is not easy to characterize a specific end-user device [38].
- Loads are in time-varying nature [39].
- Demand is discrete both in magnitude and duration, and also highly volatile [40].

Energy consumption of a house depends on many parameters such as environmental conditions, socio-economic situation, type and size of the house, number of occupants, number and feature of the devices, time of the year, and also human behaviors [41]. Due to many parameters, it is not so easy to consider all of these and accordingly model the residential loads.

In literature, it is observed that authors use different terms for classification of load modeling techniques. The categorization types can be listed as:

- Component-based and measurement-based [42],
- Bottom-up and top-down (aggregated) [35],
- Black-box, gray-box, and white-box [41] modeling techniques.

First and second category fundamentally refer to the same techniques, but with different names. Component-based (or bottom-up) modeling approach considers individual load characteristics to build up the load model. On the other hand, measurement-based (or top-down (aggregated)) modeling use direct measurements of aggregated load profiles at substations or bulk connection points of the grid. In the last category, white-box model refers that the load is modeled based on its physical characteristics. On contrary, the black-box model does not use any physical modeling, but benefits from statistical or empirical data. Lastly, in gray-box models, both physical characteristics and statistical methods can be used.

Besides these, there is a more general categorization of load models as static and dynamic load models [43]. Static load models neglect time-dependence and are often used for steady-state power system studies (sometimes for dynamic studies, if the load is time-independent). Exponential and polynomial (ZIP) models are the most used variants of static load models. On the other hand, dynamic load models are time-dependent and they are generally used for dynamic power system studies (such as analysis of frequency stability, short-term voltage stability) [44].

There have been many studies for both individual and aggregated load modeling purposes in literature. Bottom-up modeling approaches are presented to model individual electrical loads by using Markov chains or other Markov processes [45], [46]. Residential loads are aggregated in reference to similar consumption profiles of

customers with clustering techniques [47], [48], [49]. Load disaggregation methods are proposed by using bulk smart meter measurements to distinguish individual load profiles [50], [51]. Parameter values of static load models are provided considering both individual electrical devices and aggregated loads for power system analysis [33], [43]. A measurement-based dynamic load modeling approach is presented for time-domain simulations [36]. For large-scale non-linear load simulations, frequency-domain models are proposed as claimed to be faster than the time-domain simulations [52]. Lastly, long term load models without losing individual load characteristics are presented for the purpose of power system planning studies [53].

Another important point that should be emphasized is the increasing trend of using high-resolution data in end-user load modeling. In time, more and more residential users will join real-time energy balancing strategies by the favor of smart grid developments. The time-varying dynamics of end-users should be identified in order to better adapt fast balancing needs [47]. It's reported that resolution over 15-minute is not practical for low-voltage grid studies [43]. Furthermore, in the case of load aggregation, sampling time should also be reduced in proportion to the aggregation level to not lose the behavioral characteristics of the individual customers [54]. Therefore, in accordance with the technological developments and needs, the temporal resolution of the data is expected to get higher as already pointed out in literature with 15-minute [55], 10-minute [56], 5-minute [47], and 1-minute [57] resolutions.

After a comprehensive literature review, in the following sections, a gray-box bottom-up modeling approach is presented. Three different load types as HVAC (heating ventilation and air conditioning system), EWH (electric water heater), and lighting loads that share the top consumption levels in U.S. households are considered in this study. Both physical models and statistical data are used to generate individual probabilistic load profiles in one-minute resolution. If required, generated device level load profiles can also be aggregated to represent a house or group of houses without losing individual load characteristics.

2.2. DATA SOURCES

In this section, three different data sources are introduced which are going to be used for load modeling purpose and also afterward for other parts of the thesis. The first one is weather data for the three distinctive locations to consider the effect of different climate zones, and the second one is a residential survey data to populate the houses with diversified structural characteristics, and the last one is an international energy conversion code that is used to generate thermal characteristics of the houses according to the requirements.

2.2.1. WEATHER DATA FOR DIFFERENT CLIMATE ZONES

In order to take into account different weather conditions, three locations are chosen as being in a cold, mixed-humid, and hot-dry climate zones which are defined by the U.S. Department of Energy Building America Program [58]. The specifications of the study locations are given in Table 2.1.

Table 2.1 The specifications of study locations

State	**Colorado**	**Tennessee**	**California**
County	Jefferson	Roane	Los Angeles
City	Golden	Oak Ridge	Los Angeles
Latitude	39.74211	35.92996	33.966674
Longitude	-105.17514	-84.30952	-118.42282
Elevation	1793	245	27
Timezone	MST	EST	PST
Timezone Offset	-7	-5	-8
Climate Type	Cold	Mixed-Humid	Hot-Dry

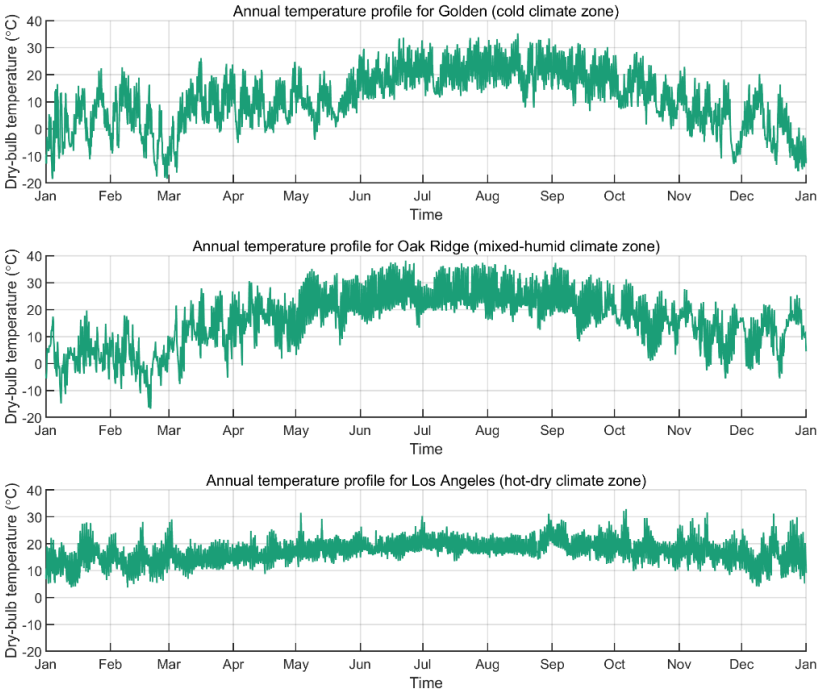

Figure 2.1 Temperature profiles for a whole year of the selected locations

One-minute resolution weather raw data for the preselected locations are obtained from the Measurement and Instrumentation Data Center (MIDC) [59] of National Renewable Energy Laboratory (NREL). For Golden and Oak Ridge, 2015; and for Los Angeles, 2013 data sets have been used which are complete for the whole year. Among many variables, irradiance (global horizontal, direct normal, and diffuse horizontal), dry-bulb temperature, relative humidity, wind speed, wind direction, and station pressure recordings are separated and used for the studies hereupon.

Annual temperature profiles for the study locations are shown in Figure 2.1. To easily compare locational differences, statistical measures are also provided in Table 2.2.

For the chosen cold, mixed-humid, and hot-dry locations minimum temperatures are recorded as -18.50 °C, -16.81 °C, and 3.67 °C; and average temperatures are recorded as 10.86 °C, 15.75 °C, and 16.92 °C, respectively.

Table 2.2 Annual air temperature statistics for the locations

City	Climate Type	Min (°C)	Avg (°C)	Max (°C)	Standard deviation
Golden	Cold	-18.50	10.86	35.28	10.41
Oak Ridge	Mixed-Humid	-16.81	15.75	38.17	10.01
Los Angeles	Hot-Dry	3.67	16.92	32.91	4.13

2.2.2. SURVEY DATA FOR HOUSEHOLD STRUCTURAL CHARACTERISTICS

To create a database of houses with different structural characteristics, it is benefitted from a residential energy consumption survey (RECS) [60] which is provided by U.S. Energy Information Administration (EIA). From this survey, the tabulated data of year of construction, housing unit type, average square footage, and the number of bedrooms are used to diversify the households. For the preselected study locations data is degraded as given in Table 2.3, Table 2.4, Table 2.5, and, Table 2.6.

Table 2.3 Average square footage

	Golden (Mountain North) (ft^2)	Oak Ridge (East South Central) (ft^2)	Los Angeles (Pacific) (ft^2)
Square footage	2107	1895	1605

Table 2.4 Distribution of houses based on year of construction

Year of Construction	Golden (Mountain North) (number of houses, million)	Oak Ridge (East South Central) (number of houses, million)	Los Angeles (Pacific) (number of houses, million)
Before 1950	0.5	0.7	2.7
1950 to 1959	0.3	0.6	2.2
1960 to 1969	0.3	0.8	2.2
1970 to 1979	0.8	1.2	3.2
1980 to 1989	0.6	1.0	2.6
1990 to 1999	0.7	1.3	2.3
2000 to 2009	0.8	1.2	2.2
2010 to 2015	0.0	0.3	0.5

Table 2.5 Distribution of houses based on housing unit type

Housing Unit Type	Golden (number of houses, million)	Oak Ridge (number of houses, million)	Los Angeles (number of houses, million)
Single Family Detached	2.7	5.0	10.6
Single Family Attached	0.2	0.2	1.1
Apartments in 2 to 4 Buildings	0.0	0.4	1.4
Apartments in 5 or More Buildings	0.6	0.8	4.0
Mobile Homes	0.4	0.8	0.8

Table 2.6 Distribution of houses based on number of bedrooms

Number of bedrooms	Golden (number of houses, million)	Oak Ridge (number of houses, million)	Los Angeles (number of houses, million)
None (Studio/Eff.)	0.0	0.0	0.6
1	0.3	0.5	2.2
2	1.0	1.7	4.8
3	1.5	3.6	6.3
4	0.9	1.1	3.1
5 or More	0.4	0.2	0.8

2.2.3. LOCATION SPECIFIC THERMAL ENVELOPE DATA FOR HOUSEHOLD THERMAL CHARACTERISTICS

To populate the houses with different thermal envelope characteristics, the requirements based on their climate zones are obtained from 2009 International Energy Conversion Code [61]. According to this code, thermal envelope of a building shall meet the minimum insulation and fenestration criteria. R (thermal resistance) and U (thermal transmittance) values for residential buildings are adapted from this code based on preselected locations and their climate zones as given in Table 2.7.

Table 2.7 Building thermal envelope requirements

R (ft^2·°F·h/BTU) U (BTU/h·°F·ft^2)	**Golden (Colorado)**	**Oak Ridge (Tennessee)**	**Los Angeles (California)**
R-roof	38	38	30
R-wall	[13-17]	[5-10]	[5-8]
R-floor	30	19	19
U-door	0.35	0.35	0.5
U-windows	0.35	0.35	0.5

2.3. GENERATION OF PROBABILISTIC HOUSEHOLD DATABASE

To diversify load profiles among the houses, the next step is to create a database which consists of many households with unique thermal and structural characteristics. Benefitting from data sources that are introduced in section 2.2, a matlab code is written to create a probabilistic household database based on a specified study location. The values are assigned to each house for each variable with the inverse transform sampling method [62].

Table 2.8 An example of a created household database

House no	**House ID**	**House unit type**	**House constr. year**	**House square footage**	**House bedrooms**	**House occupants**
1	H_632A_1	Apt	1971	1580	1	2
2	H_632A_2	Sf	1983	1638	1	1
3	H_632A_3	Apt	1950	1578	3	3
4	H_632A_4	Sf	1999	1762	2	2
⋮	⋮	⋮	⋮	⋮	⋮	⋮
464	H_680C_16	Apt	1971	1454	2	2

The code is made flexible meaning that it may be adapted to any distribution grid with any number of the houses in a specified location. An example of a created household database based on Los Angeles location and specifically designed for IEEE13 distribution grid can be seen in Table 2.8.

To identify the houses in a smart way, a unique ID is given for each one of them considering the distribution grid node-phase where they are connected to and the corresponding sequence number of the house in that specific node-phase. For example, H_632B_12 represents the house that is connected to B phase of the node 632, and it is also the twelfth house in that specific node-phase couple. In the housing unit type section of the table, the abbreviations of Apt. and Sf. are used to symbolize the apartment and single-family houses, respectively.

To take into account the effect of end-user behaviors on consumption patterns, an additional variable is also attached to the database which is called “house occupants”. The number of occupants is assigned to each house as a function of the housing unit type and number of bedrooms, and calculated by [63]

$$N_{occupants} = \begin{cases} round(0.59xN_{bedrooms} + 0.87), & single\text{-}family \\ round(0.92xN_{bedrooms} + 0.63), & Apartment \end{cases} \quad (2.1)$$

2.4. RESIDENTIAL LOADS

As sharing the top three consumption levels in U.S. households, “Heating, ventilation, and air conditioning system (HVAC)”, “electric water heater (EWH)”, and “lighting” loads have been considered in this study. For these loads, GridLAB-D simulation tool has been used due to having very detailed physical load models. Besides that, Matlab scripts are written to generate probabilistic values for hundreds of input parameters and time-varying consumption patterns for different human behaviors. Details of the modeling technique is presented in the following subsections.

2.4.1. HEATING VENTILATION AND AIR CONDITIONING SYSTEM (HVAC)

The largest load in a house is generally the HVAC system. Throughout the year, it draws energy to maintain the indoor temperature of a house at a specific interval through the set points. Performance of the system is also dependent on nonelectrical parameters such as insulation level of the building, outdoor temperature, and time of the year. In this section, modeling approach is introduced and then the procedure to diversify HVAC loads is explained.

2.4.1.1 HVAC load model

To represent the behavior of a residential HVAC system, GridLAB-D tool uses the equivalent thermal parameter (ETP) model [64]. In this model, various thermal parameters are taken into account such as mass which shows how much thermal energy is stored in the building and envelope that defines how fast energy is being transferred to the outside. These parameters are dependent on the actual physical parameters of the building (structural and thermal characteristics). The diagram of the ETP model can be seen in Figure 2.2.

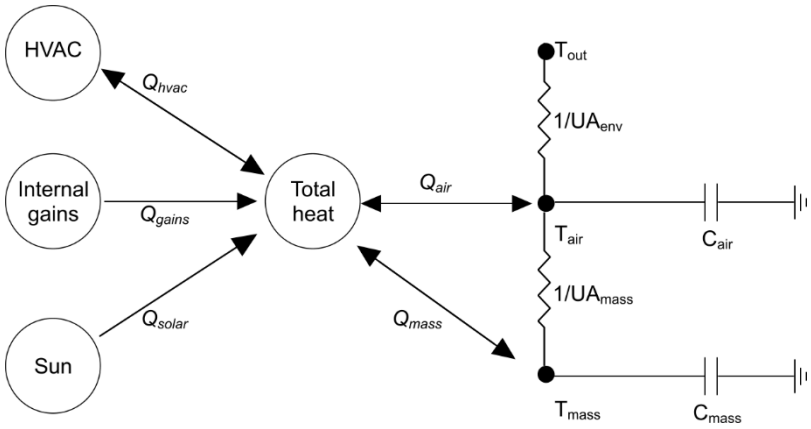

Figure 2.2 Equivalent thermal parameter (ETP) model of an HVAC system

where

C_{air} : air heat capacity (joules/°C)
C_{mass} : mass heat capacity (joules/°C)
UA_{env} : the gain/heat loss coef. between air and outside (W/°C)
UA_{mass} : the gain/heat loss coef. between air and mass (W/°C)
T_{out} : air temperature outside the house (°C)
T_{air} : air temperature inside the house (°C)
T_{mass} : mass temperature inside the house (°C)
Q_{hvac} : heat rate from HVAC (watts)
Q_{gains} : heat rate from other appliances (watts)
Q_{solar} : heat gain from sun (watts)
Q_{mass} : heat rate to house mass (watts)
Q_{air} : heat rate to house air (watts)

HVAC, sun, and internal gains (the extra heat source from other loads, lights, and people) are the main sources of the heat that flows into the house then transferred to the air and mass of the building. While some of the heat is stored in air and mass, some of it goes outside (losses).

In the ETP model, two ordinary differential equations are used to describe the heat flow as

$$\frac{dT_{air}}{dt} = \frac{1}{C_{air}}\left[T_{mass}UA_{mass} - T_{air}\left(UA_{env} + UA_{mass}\right) + Q_{air} + T_{out}UA_{env}\right] \tag{2.2}$$

$$\frac{dT_{mass}}{dt} = \frac{1}{C_{mass}}\left[UA_{mass}\left(T_{air} + T_{mass}\right) + Q_{mass}\right] \tag{2.3}$$

Equations 2.2 and 2.3 can be transformed to a single second-order differential equation as

$$a\frac{d^2T_{air}}{dt^2} + b\frac{dT_{air}}{dt} + cT_{air} = d \tag{2.4}$$

where:

$$a = \frac{C_{mass}C_{air}}{UA_{mass}}$$

$$b = \frac{C_{mass}\left(UA_{env} + UA_{mass}\right)}{UA_{mass}} + C_{air}$$

$$c = UA_{env}$$

$$d = Q_{mass} + Q_{air} + UA_{env}T_{out}$$

By solving Equation 2.4 simultaneously for T_{air} and T_{mass}, cooling/heating load of an individual house can be obtained as a function of time. This is the simple logic of the ETP modeling approach.

In order to calculate the energy consumption of the HVAC system, additional parameters are required by the simulation tool such as floor area, R-values of several parts of the house, and also the technical specifications of the HVAC device. Due to these are out of the scope for this study, complex mathematical relations of these additional parameters are not given here, but more information can be found in the technical manual [64].

2.4.1.2 Diversification of HVAC loads

Three types of diversification methods have been applied for HVAC loads. First one is at device level where random characteristics are assigned to heat pumps such as different heating and cooling COPs (coefficient of performance). The second one is at building level where thermal and structural characteristics of houses are diversified, and in the last one human behaviors are taken into account.

How values of some parameters are generated at device and household levels is shown in Table 2.9.

Table 2.9 Randomized input parameters for HVAC systems

	Value	Data source
Floor area *(household level)*	σ*rand+μ	Table 2.3
R-roof, R-floor *(household level)*	σ*rand+μ	Table 2.7
R-wall *(household level)*	U(min,max)	Table 2.7
U-door, U-windows *(household level)*	σ*rand+μ	Table 2.7
Heating COP *(device level)*	N(2.5, 0.05)	Internet research
Cooling COP *(device level)*	N(3.5, 0.05)	Internet research

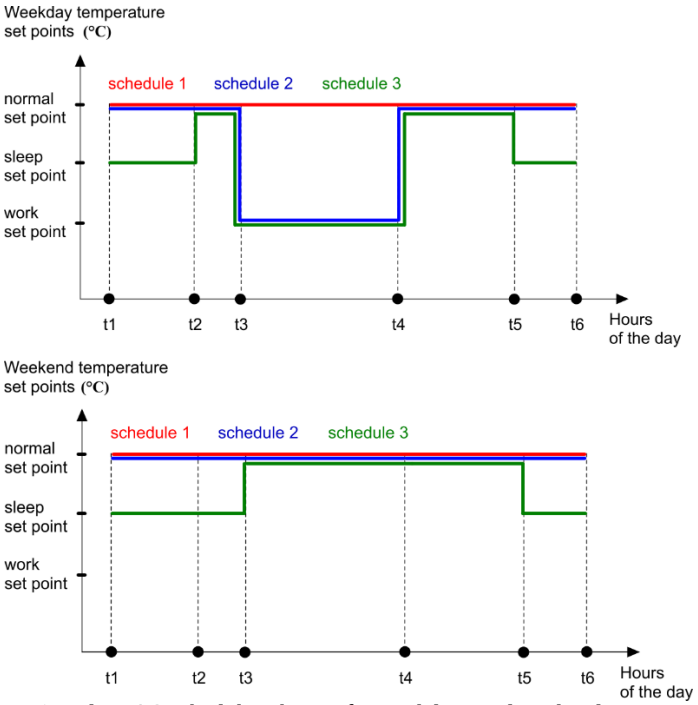

Figure 2.3 Designed HVAC schedule schemes for weekdays and weekends

Additionally, considering diverse human choices three different schedules are designed as shown in Figure 2.3. In these schedules, weekdays and weekends are treated separately. Thermostat setpoints of schedules are given in Table 2.10 and Table 2.11, for winter and summer periods, respectively.

Table 2.10 Thermostat setpoints of designed schedules in winter

	Sch. 1 (week d.)	**Sch. 2 (week d.)**	**Sch. 3 (week d.)**	**Sch. 1 (week e.)**	**Sch. 2 (week e.)**	**Sch. 3 (week e.)**
Normal set point (°C)	21.67	21.67	21.67	21.67	21.67	21.67
Sleep set point (°C)	21.67	21.67	17.50	21.67	21.67	17.50
Work set point (°C)	21.67	19.44	17.50	-	-	-
Deadband (°C)	2.78	2.78	2.78	2.78	2.78	2.78
t1 (hour of day)	0	0	0	0	0	0
t2 (hour of day)	-	-	5	-	-	-
t3 (hour of day)	-	7	7	-	-	7
t4 (hour of day)	-	16	16	-	-	-
t5 (hour of day)	-	-	22	-	-	22
t6 (hour of day)	23	23	23	23	23	23

Table 2.11 Thermostat setpoints of designed schedules in summer

	Sch. 1 (week d.)	**Sch. 2 (week d.)**	**Sch. 3 (week d.)**	**Sch. 1 (week e.)**	**Sch. 2 (week e.)**	**Sch. 3 (week e.)**
Normal set point (°C)	25.56	25.56	25.56	25.56	25.56	25.56
Sleep set point (°C)	25.56	25.56	29.44	25.56	25.56	29.44
Work set point (°C)	25.56	27.78	29.44	-	-	-
Deadband (°C)	2.78	2.78	2.78	2.78	2.78	2.78
t1 (hour of day)	0	0	0	0	0	0
t2 (hour of day)	-	-	5	-	-	-
t3 (hour of day)	-	7	7	-	-	7
t4 (hour of day)	-	16	16	-	-	-
t5 (hour of day)	-	-	22	-	-	22
t6 (hour of day)	23	23	23	23	23	23

Deadband control strategy is applied to control the HVAC system meaning that indoor temperature is allowed to fluctuate around the set-point by the value of ±deadband/2. Assuming '*s*' is the thermostat set-point and, '*d*' is the dead-band value, HVAC operating states can be summarized as in Table 2.12.

Table 2.12 HVAC operation states

	HVAC ON	**HVAC OFF**
Heating mode	T_{in} < (s-d/2)	T_{in} > (s+d/2)
Cooling mode	T_{in} > (s+d/2)	T_{in} < (s-d/2)

To see how the HVAC model behaves, a random house is chosen and simulated for a representative winter and summer day as shown in Figure 2.4

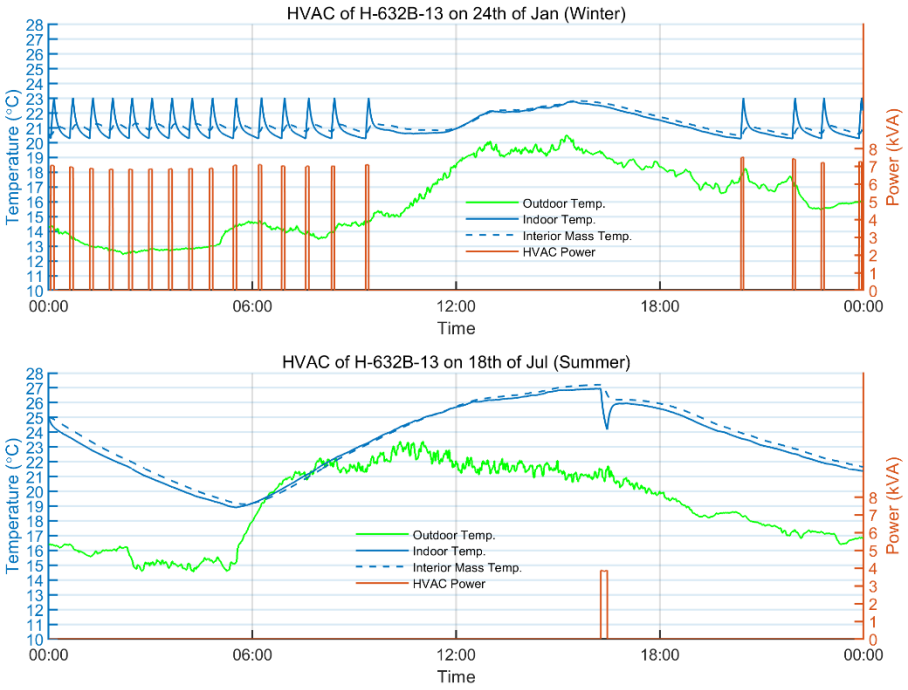

Figure 2.4 HVAC model response for a winter and summer day

According to the HVAC device settings of this specific house, "*schedule 1*" strategy is chosen which means that in winter HVAC starts to heat the house when the indoor temperature is below 20.28 °C, and stops heating if the indoor temperature is above 23.06 °C. In summer, heating mode is closed and HVAC is only adjusted to cool down

the house if the indoor temperature is above 26.94 °C and stop cooling when the indoor temperature is below 24.17 °C. It can be seen that due to higher cooling efficiency of the heat pump (higher COP), in summer period, required operational power is much less than the winter. On a side note, as can be observed from the figure, outside temperature is also a significant parameter that may affect the operational states of the HVAC remarkably.

2.4.2. ELECTRIC WATER HEATER (EWH)

Hot water is needed for daily human activities such as washing clothes and dishes, having shower, sink, et cetera. To heat the water, electrical water heaters (EWH) are being used as the second largest loads in U.S. houses. In this section, modeling technique is introduced and then, the procedure to generate realistic hot water usage demand profile for each house is presented.

2.4.2.1 EWH load model

In the typical EWH design, water is generally heated by the two elements as shown in Figure 2.5. Lower element is located close to the bottom where cold water enters the tank, and the upper element is usually located at a higher point which is closer to the hot water output. Both elements have independent thermostats but only one of them is permitted to heat the water at a time. Generally lower element heats the water, but during the excess hot water usage if cold water layer reaches to the level of the higher element, then lower element stops and higher element starts to heat the water to meet the immediate demand.

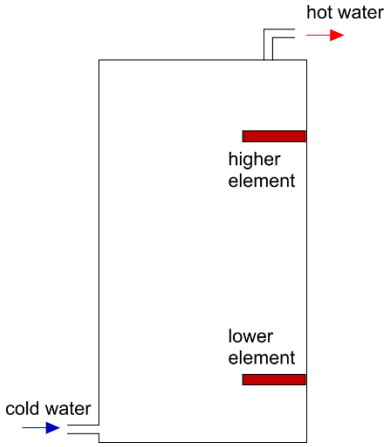

Figure 2.5 Typical two-element water heater design

Because of its simplicity, one-node model has been used to simulate the EWHs [64]. In this model, an average water temperature is assumed in the entire tank and the system is simplified with a lumped-parameter model as shown in Figure 2.6.

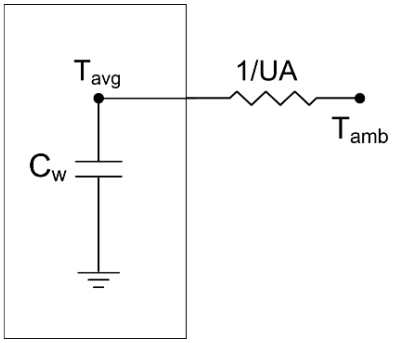

Figure 2.6 Equivalent water heater model

where

C_w : thermal capacitance of the water (joules/°C)
T_{avg} : average water temperature inside the tank (°C)
UA: thermal conductance of the tank shell (W/°C)
T_{amb} : ambient temperature (°C)

In one-node model, the heat balance can be written as

$$Q_{elec} - \dot{m}C_p\left(T_w - T_{inlet}\right) + UA\left(T_{amb} - T_w\right) = C_w \frac{dT_w}{dt} \tag{2.5}$$

Here, Equation 2.5 can be rearranged to find the required time (Δt), to change the initial temperature of the tank to a new temperature

$$\Delta t = \frac{1}{b}\log\left(a + bT_w\right)\Big|_{Tw,initial}^{Tw,final} \tag{2.6}$$

where

$$a = \frac{Q_{elec} + \dot{m}C_p T_{inlet} + UA \times T_{amb}}{C_w}$$

$$b = \frac{-\left(UA + \dot{m}C_p\right)}{C_w}$$

Equation 2.5 can also be rearranged to calculate the final temperature of the water when a predefined time passes from an initial state as

$$T_{final} = \frac{Q_{elec} + \dot{m}C_p T_{inlet} + UA \times T_{amb}}{UA + \dot{m}C_p} - \left(\frac{Q_{elec} + \dot{m}C_p T_{inlet} + UA \times T_{amb}}{UA + \dot{m}C_p} - T_{init} \right) e^{b\Delta t} \quad (2.7)$$

2.4.2.2 Diversification of EWH loads

EWH loads are also diversified by randomizing device specifications, thermostat settings, and also human usage patterns as summarized in Table 2.13.

Table 2.13 Randomized input parameters for EWH systems

Parameter	Value	Data source
Tank volume	$f(N_{bedrooms})$	logic
Thermostat setpoint (*s*)	U(50, 60) °C	internet research
Thermostat deadband (*d*)	U(2, 6) °C	internet research
Initial outlet water temperature	U(*s-d/2*, *s+d/2*)	logic
Water demand	stochastic	[65]

In Table 2.13, tank volume (liter) is determined by simple logic that the more people live in a house, the bigger the tank size should be. According to that, tank volume is determined as a function of the number of bedrooms

$$f\left(N_{bedrooms}\right) = \begin{cases} tank\_volume = 113, & \text{if } N_{bedrooms} = 1 \\ tank\_volume = 151, & \text{if } N_{bedrooms} = 2 \,||\, 3 \\ tank\_volume = 189, & \text{if } N_{bedrooms} \geq 4 \end{cases} \quad (2.8)$$

In addition to that, to take into account human behaviors, an advanced tool has been used which can generate realistic hot water events such as having showers in the morning/evening, washing clothes, etc., according to the real probability distributions of many real-life parameters [65]. Climate location, number of bedrooms, and time step parameters are required to generate annual domestic hot water demand events in this tool.

Generated hot water demand profiles for five random houses with different number of bedrooms is shown in Figure 2.7, for a representative winter and summer day, respectively.

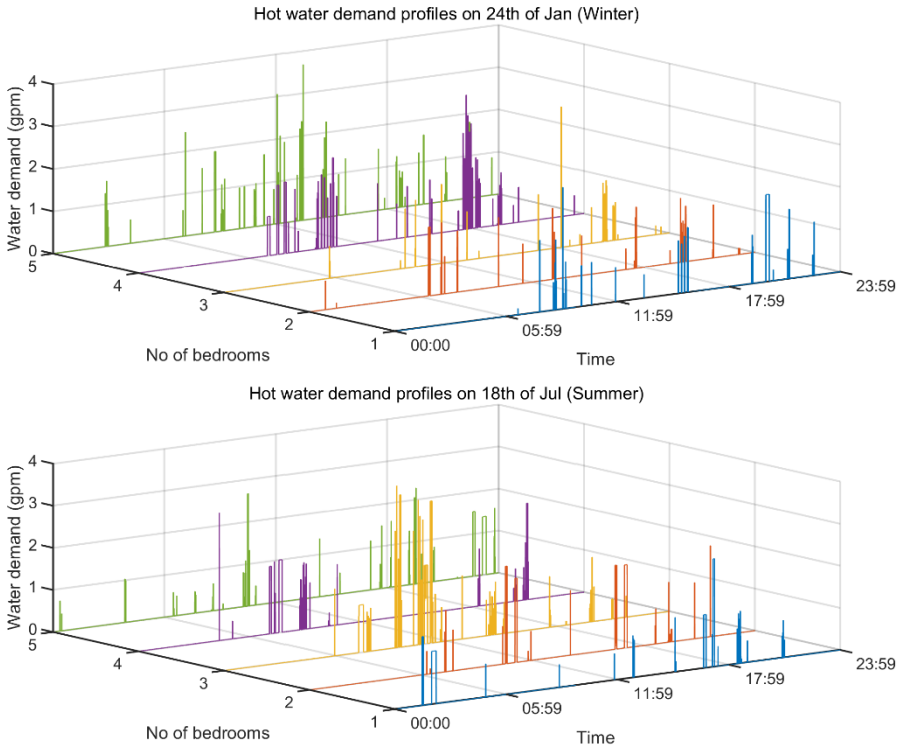

Figure 2.7 Hot water demands for 5 different houses in a winter and summer day

As in HVAC control, deadband control strategy is also applied to EWH system where water temperature is allowed to fluctuate around the thermostat set-point by the value of ±deadband/2. Assuming '*s*' is the thermostat set-point and, '*d*' is the dead-band value, EWH operating states can be summarized as in Table 2.14.

Table 2.14 EWH operation states

EWH ON	**EWH OFF**
$T_{water} < (s-d/2)$	$T_{water} > (s+d/2)$

Finally, to see how the EWH model behaves, a random house is chosen and simulated for a representative winter and summer day as shown in Figure 2.8. As can be seen from the figure, even though at some instants hot water is not drawn, EWH switches on and tries to keep the water temperature around the setpoint to compensate the losses. Therefore, energy consumption also depends on other parameters such as insulation level of the tank and outside temperature.

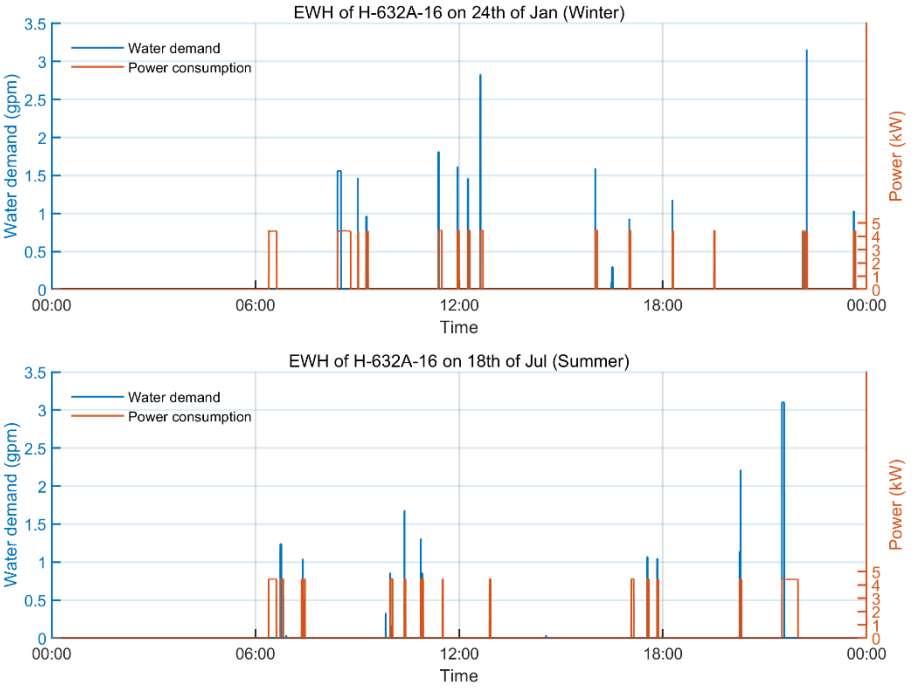

Figure 2.8 EWH model response for a winter and summer day

2.4.3. LIGHTING

Lighting is the third largest residential load after HVAC and EWH systems in U.S. households. In the following subsections, modeling approach is presented and then the steps to create unique lighting consumption profiles for all the houses are explained in detail.

2.4.3.1 Lighting load model

ZIP modeling approach has been chosen to model the lighting loads in residential houses [66]. In this technique, load is modeled as a combination of constant impedance (Z), constant current (I), and constant power (P) loads. As one of the benefits of this model, voltage dependency can also be taken into account when calculating the power consumption.

In ZIP modeling technique, depending on the terminal voltage, real and reactive power can be calculated by

$$P_i\left(V_a\right) = \left|S_n\right|\left(\left|\frac{V_a^2}{V_n^2}\right| Z_{\%} Z_{pf} + \left|\frac{V_a}{V_n}\right| I_{\%} I_{pf} + P_{\%} P_{pf}\right) \tag{2.9}$$

$$Q_i(V_a) = |S_n| \left(\left| \frac{V_a^2}{V_n^2} \right| Z_{\%} \sin\left(\text{acos}\left(Z_{pf}\right)\right) + \left| \frac{V_a}{V_n} \right| I_{\%} \sin\left(\text{acos}\left(I_{pf}\right)\right) + P_{\%} \sin\left(\text{acos}\left(P_{pf}\right)\right) \right) \tag{2.10}$$

Equation 2.9 and 2.10 must also satisfy the following criteria

$$Z_{\%} + I_{\%} + P_{\%} = 1 \tag{2.11}$$

where

P: real power consumption of the load (W)
Q: reactive power consumption of the load (VAr)
V_a: actual terminal voltage (V)
V_n: nominal terminal voltage (V)
S_n: nominal power consumption (VA)
$Z_{\%}$: ratio of the load that is constant impedance
$I_{\%}$: ratio of the load that is constant current
$P_{\%}$: ratio of the load that is constant power
Z_{pf}: power factor of constant impedance component
I_{pf}: power factor of constant current component
P_{pf}: power factor of constant power component

In this study, three different lamp types have been considered as incandescent, compact fluorescent, and LED lamps. The proper ZIP coefficients for these lamp types are given in Table 2.15 [66].

Table 2.15 ZIP coefficients for the lamp types

Lamp Type	**$Z_{\%}$**	**$I_{\%}$**	**$P_{\%}$**	**Z_{pf}**	**I_{pf}**	**P_{pf}**
Incandescent	0.5711	0.4257	0.0032	1	-1	0.9996
Compact fluorescent	0.4085	0.0067	0.5849	-0.8785	0.4208	-0.7792
LED	-0.455*	0.4573	0.9977	-0.8191	-0.9843	-0.8613

*- sign is just fictious, comes from the equality constraint in (2.11)

2.4.3.2 Diversification of lighting loads

To diversify the lighting loads, lamp types are distributed randomly for each house with respect to the distribution in Table 2.16 [63].

Table 2.16 Lamp distribution ratios

Lamp Type	Distribution
Incandescent	66%
Compact fluorescent	21%
LED	13%

Moreover, unique consumption profiles are generated with another tool which takes into account the number of occupants in the house and solar irradiance level [67]. Generated load profiles for five random houses with different number of occupants can be seen in Figure 2.9, for a winter and summer day, respectively.

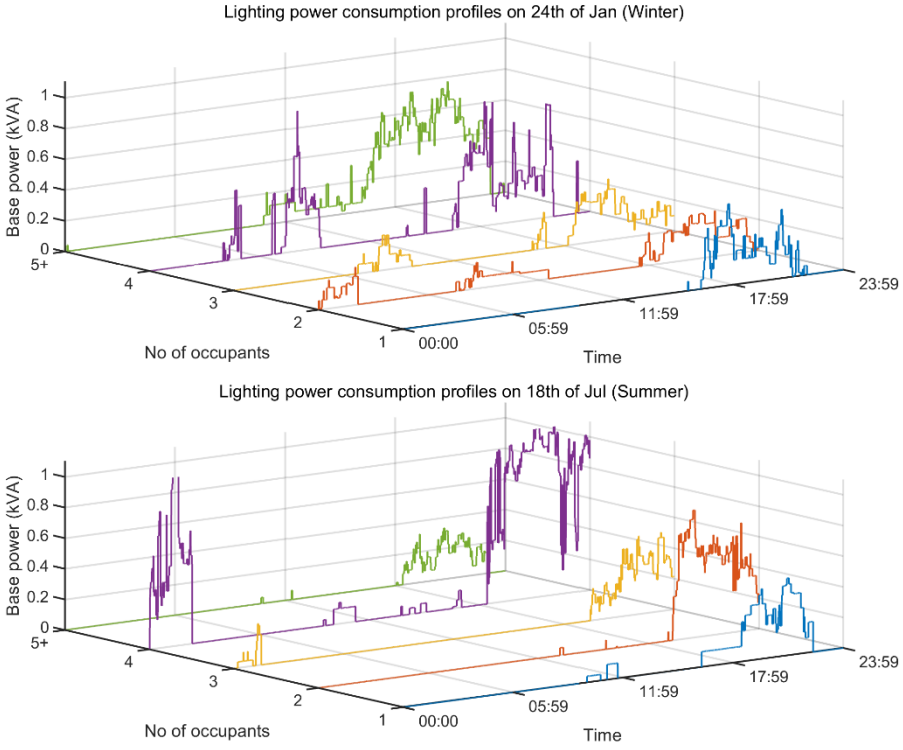

Figure 2.9 Lighting load of 5 different houses in a winter and summer day

As can be observed from the figure, the likelihood of using the lights increases as the solar irradiance level outside decreases. Furthermore, the number of people living in

a house also increases the possibility of switching on the lights at different time intervals during the day.

2.5. SUMMARY AND DISCUSSION

Previously, residential customers in low-voltage distribution grids had only be seen as bulk aggregated load sources for medium and high voltage studies. Development of smart grid, increase in renewable energy sources and controllable smart devices have changed our perspective to these customers. Now, it is of critical importance to understand and accordingly model the chaotic behaviors of end users to achieve sustainable energy development. However, modeling of end-user loads poses some tremendous challenges due to diversity in load parameters, lack of individual measurements, and diverse human behaviors. In this chapter, unique individual load profiles are generated considering as many parameters as possible such as household demographics, different thermal and structural characteristics of the buildings, random device parameters, realistic human behaviors, and also varying time and weather characteristics. Furthermore, if required, generated load profiles may be also aggregated accurately without losing individual customer information for medium and high voltage level studies.

CHAPTER 3. PHOTOVOLTAIC SYSTEM MODELING

Solar photovoltaic (PV) systems are the most preferred renewable energy generation sources in low-voltage distribution grids. Unlike the past, today, end-users have also the opportunity to generate their own electricity. Even a new term, prosumer, has been derived from the combination of consumer and producer for this kind of end-users.

With many great advantages, PV systems can be used almost anywhere wherever sunlight is available. The applications can be scaled from micro-level consumer electronics to macro-level utility power plants. Nowadays, PV systems have even become the most competitive power generation option with the ongoing cost reductions in recent years.

As it's well-known the output power a PV system is highly variable depending on the solar irradiance and temperature variations. Several power quality issues can be experienced in the grid with the increase in PV penetration levels. Therefore, it is very important to accurately model PV system components to be able to understand the dynamics of PV power generation and accordingly, develop more effective strategies to mitigate the related problems.

In this chapter, first, a brief overview of PV systems has been presented including the latest figures, developments, and trends. Then, step by step how the PV system components are modeled is explained in detail. It is started with the estimation of total solar irradiance on a tilted surface by using the available horizontal irradiance components and then continued with the estimation of PV module temperature by including the wind speed parameter to be more accurate. In the next steps, models to calculate DC output power of a PV array and AC output power of a PV inverter are given, respectively. To be more realistic in the simulations, a probabilistic PV system database is created consisting of different types of PV modules and PV inverters. Lastly, the importance of PV inverter sizing is discussed and some suggestions are made for a more effective reactive power provision.

3.1. OVERVIEW OF PV SYSTEM TECHNOLOGIES

PV systems have grown rapidly during the last two decades and become the most favorable power generation systems among renewable energy resources [68]. Just in ten years from 2007 to 2017, total installed PV capacity all over the world has increased more than 4300% and reached 404.5 GW. In 2017 compared to the previous year, an additional 99.1 GW has been added to the total PV capacity with an annual increase rate of 30%. With an exceptional growth in 2017, China has overtaken the

global leadership in total installed PV capacity by reaching out a market share of 32% which is followed by Europe 28%, the United States 13%, Japan 12%, and India 5% [3].

In many countries, PV systems have become the most affordable power option with dramatic cost reductions in recent years. It has been reported that now utility-scale PV systems are cheaper than nuclear, coal, and combined cycle gas turbine power plants [3]. In the light of these, there have been more PV installations than fossil fuel and nuclear power plants in 2017, and PV systems almost doubled the new installation capacities compared to its renewable peer, wind power [3].

Not just economic benefits but also environmental concerns have made governments and decision makers focus on clean energy policies to reduce the pollution and greenhouse gas emissions [69]. Concordantly, as one of the most promising options PV systems are expected to play a key role in future sustainable energy development. The prominent advantages of PV systems can be described as follows [70]

- can be installed almost anywhere
- do not make any noise
- require little or no maintenance
- free energy source
- clean and environmentally friendly

A typical PV system consists of PV modules, battery, charge controller, and inverter. Solar cells are the basic units of PV modules which generate electricity from sunlight through the photovoltaic effect. These cells are connected in series and parallel to form a PV module at the desired voltage and current level. Battery is used to store surplus energy and provide the stored energy back whenever needed. The charging/discharging operation of the battery is controlled by charge controller in an optimal way to preserve the useful lifetime of the battery. Lastly, DC output of the PV array can be converted to AC power with a PV inverter for either grid connection or self-consumption [71].

Solar cell technologies depending on the raw material used and commercial maturity level can be grouped into three categories as crystalline silicon (c-Si), thin film, and organic cell technologies [72]. Currently, 90% of the PV market is dominated by c-Si solar cells due to successful commercial integration and high-efficiency characteristics. With ongoing development and achievement, monocrystalline (mono-Si) and its cheaper variant polycrystalline (poly-Si) cells have reached 26.7% and 22.3% efficiencies, respectively [73]. On the other hand, thin film technologies are very promising alternatives to c-Si technologies with up to 99% less material usage. Due to being thin, flexible and lightweight they can be applied to any surface. Amorphous silicon (a-Si), cadmium telluride (CdTe), and copper indium gallium selenide (CIGS) are the three mostly commercialized thin film types [74]. Even

though they are still not as efficient as c-Si cells, especially CdTe and CIGS cell efficiencies have been significantly improved in recent years by reaching 21.0% and 22.9% levels, respectively [73]. However, there are still some challenges which should be dealt with such as toxicity and scarcity of the raw materials and high degradation rates. Besides these, organic cells are also being developed by using organic semiconductors such as polymers. They are also thin, flexible, semitransparent, ecological, and less costly than silicon-based production. Nevertheless, there should be more research on organic cells to increase their lifetime and efficiency in order to compete with the mature c-Si cell technology [71].

PV systems depending on the connection type can be either grid-connected or standalone (off-grid). In the grid-connected systems, PV owner can sell surplus energy to the grid at high generation and low consumption periods and draw energy from the grid at low generation and high consumption times. On the other hand, standalone systems are designed to be self-sufficient without a need for external grid connection. Standalone PV systems can be used in many applications such as street lighting, satellites, spacecraft, telecommunications, water pumping, consumer products, and also for the purpose of remote area electrification [71].

Power generation level of a PV system during the daylight varies depending on the absorbed solar irradiance and solar cell operating temperature. These two parameters are affected by the PV technology itself, installation location, tilt angle and orientation, mounting type, and meteorological variables. PV system may also produce less energy due to shading, soiling/dust, and degradation problems [75].

As it is well-known output power of a PV system throughout the day is highly variable which may lead to some power quality issues in the grid. Voltage violation and fluctuations, harmonics, large reverse power flow, overloading of line and transformers are some of the faced technical problems with the increasing integration of PV systems [76]. Therefore, several organizations and technical committees get involved in providing PV interconnection standards to ensure reliable and compatible operation of PV systems. These standards contain recommended practices and guidelines that are being updated regularly to keep up with the current grid requirements. Some of the recognized national and international PV interconnection standards are listed as follows [77]

- IEC 61727, IEC 62109, IEC 62116 (International)
- IEEE 1547, IEEE 929, UL 1741 (USA)
- EN 50438 (Europe)
- VDE 0126-1-1 (Germany)
- RD 1663/661 (Spain)
- DK 5940 (Italy)
- G83/1-1 (UK)
- PV 501 (South Korea)

- GB/T 19964, GB/T 29319, Q/GDW 617 (China)
- AS 4777 (Australia)

On the other hand, PV inverters are also expected to play an important role in the near future. With the advances in power-electronics and communication technologies, state-of-the-art PV inverters now have the ability to provide ancillary services to the grid. By controlling active and reactive power output of the PV systems, power quality issues can be mitigated [78]. Especially, reactive power support is critical to enhance the local voltage profile at the connection point. Even though the first version of IEEE 1547 standard forbids reactive power provision, recently revised version promotes reactive power support to increase the voltage quality [79].

Despite these developments, according to 2017 figures, only 12.1% of the global power demand is met by the renewables [3]. This clearly indicates that we are still in the beginning stage of the clean energy revolution. In this context, with its huge potential, solar energy could be the perfect match to reach the global decarbonization targets.

3.2. PV SYSTEM MODELING

In this section, the modeling approach of a whole PV system is explained in detail. First, it is started with the estimation of total solar irradiance on a tilted surface. Then, it is shown how to estimate the operating temperature of PV modules more accurately by considering the wind speed cooling effect. After presenting the power efficiency model to calculate the DC output power of a PV array, in the last stage, a dynamic efficiency inverter model is introduced for the DC to AC power conversion process.

3.2.1. ESTIMATION OF TOTAL SOLAR IRRADIANCE ON TILTED PV MODULE SURFACE

Meteorological stations generally record solar irradiance components on horizontal surfaces. However, PV modules are inclined with a tilt angle in reference to the horizontal plane to maximize the absorbed solar radiation. For this reason, total irradiance either should be measured directly on the tilted surface or should be estimated from the horizontal measurements.

To estimate the total irradiance on a tilted surface, three individual components are required as beam (direct), diffuse, and reflected irradiance. Beam irradiance directly comes from the sun without being scattered throughout the atmosphere. Contrarily, diffuse irradiance is highly scattered due to dust, clouds, and different molecules. Both beam and diffuse irradiance can also be reflected by the ground and then reach to the module surface, this component, reflected irradiance, should also be included in the calculation for a more accurate estimation.

Beam irradiance calculation is quite straightforward due to being purely geometric. It can be obtained by

$$G_{\beta,b} = G_b \cdot \frac{a}{b} \tag{3.1}$$

where

$\frac{a}{b} = \frac{\max(0, \cos\theta)}{\max(0.087, \cos\theta_z)}$, and G_b is horizontal beam irradiance, θ is incidence angle, and, θ_z is zenith angle.

In literature, to calculate the diffuse irradiance component, various models have been proposed. These approaches can be grouped into two categories as isotropic and anisotropic models. Due to assuming of uniform diffuse irradiance density all over the sky dome, it is reported that accuracy of isotropic models is not good enough to estimate the diffuse irradiance component [80]. On the other hand, anisotropic models are reported as being more accurate due to taking into account circumsolar diffuse and horizon-brightening components. Therefore, a well-known anisotropic model (Perez model) has been used in this study to calculate the tilted diffuse irradiance component by [81]

$$G_{\beta,d} = G_d \left[(1 - F_1)\left(\frac{1+\cos\beta}{2}\right) + F_1 \frac{a}{b} + F_2 \sin\beta \right] \tag{3.2}$$

where β is tilt angle, G_d is horizontal diffuse irradiance, and coefficients of F_1 and F_2 express the degree of circumsolar and horizon anisotropy, respectively. These coefficients are the functions of sky clearness and sky brightness indexes and can be calculated easily from the related table in [81].

The last component, ground-reflected irradiance can be obtained by

$$G_{\beta,r} = (G_b + G_d) \cdot \rho \cdot \left(\frac{1-\cos\beta}{2}\right) \tag{3.3}$$

where ρ is albedo which is actually the reflectance of the ground and a constant value of 0.2 is generally taken in most studies.

Finally, total irradiance on a tilted surface can be calculated by summation of the three individual irradiance components as

$$G_\beta = G_{\beta,\mathrm{b}} + G_{\beta,\mathrm{d}} + G_{\beta,r} \tag{3.4}$$

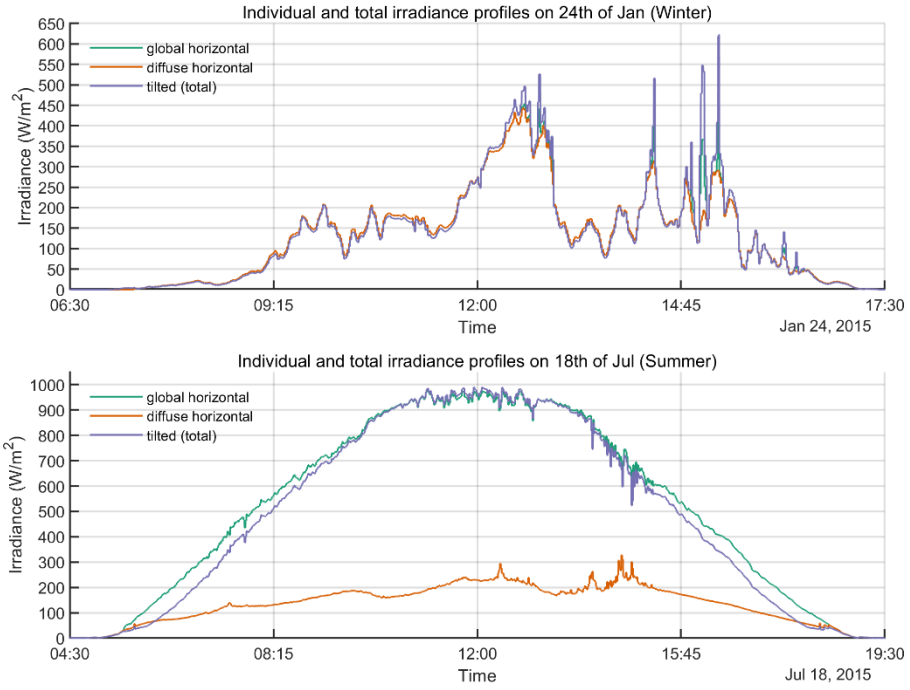

Figure 3.1 Individual and total irradiance profiles for a winter and summer day

To give an example, total irradiance profile of a PV module has been estimated from available global and diffuse horizontal irradiance components for a representative winter and summer day as shown in Figure 3.1. It is assumed that PV module is installed with an optimal tilt angle of 31° with respect to ground and located in Los Angeles city.

3.2.2. ESTIMATION OF PV MODULE TEMPERATURE

Temperature is the second important parameter that affects the output power of PV systems significantly. Depending on many parameters such as ambient air temperature (T_a), plane of array irradiance (G_β), mounting type of PV arrays (ω), and wind speed (V_f), solar cell operating temperature (T_c) can vary.

In literature, it is observed that in many studies, wind speed parameter is still ignored and not taken into account. Following explicit equation or its derivatives are commonly being used to estimate the operating temperature of PV modules [82]

$$T_c = T_a + \left(\frac{T_{noct} - 20}{800} \right) \cdot G_\beta \tag{3.5}$$

Even though Equation 3.5 or its derivatives may give satisfactory results for low wind locations, it may not give accurate results for moderate or high wind locations. Therefore, this phenomenon has been investigated over a northern European city, Aalborg in Denmark [83].

Using experimental data from a 1.9 kWp rooftop PV system located at the Department of Energy Technology in Aalborg University, recorded temperature and power measurements are compared with the simulated ones. It is intended to see if considering wind speed parameter makes any improvement on the estimation of PV module temperature and output power. To include the wind speed effect the following equation is used

$$T_c = T_a + \omega \cdot \left(\frac{0.32}{8.91 + 2V_f} \right) \cdot G_\beta \tag{3.6}$$

where ω is mounting coefficient that varies according to the installation types as given in Table 3.1 [84] and V_f is the free stream wind speed.

Table 3.1 Mounting coefficients according to different installation types [84]

Mounting Type	**Mounting Coefficient**
Free standing	1.0
Flat roof	1.2
Sloped roof	1.8
Façade integrated	2.4

First experimental data is from 11 December 2010, a windy and cold winter day. The day length is very short (6 hours and 50 minutes) and an average of 15.2 m/s wind speed, 7.6 °C ambient temperature, and 146.5 W/m^2 irradiance value is recorded during the daylight. Simulated temperature and output power values with the measured ones are shown in Figure 3.2.

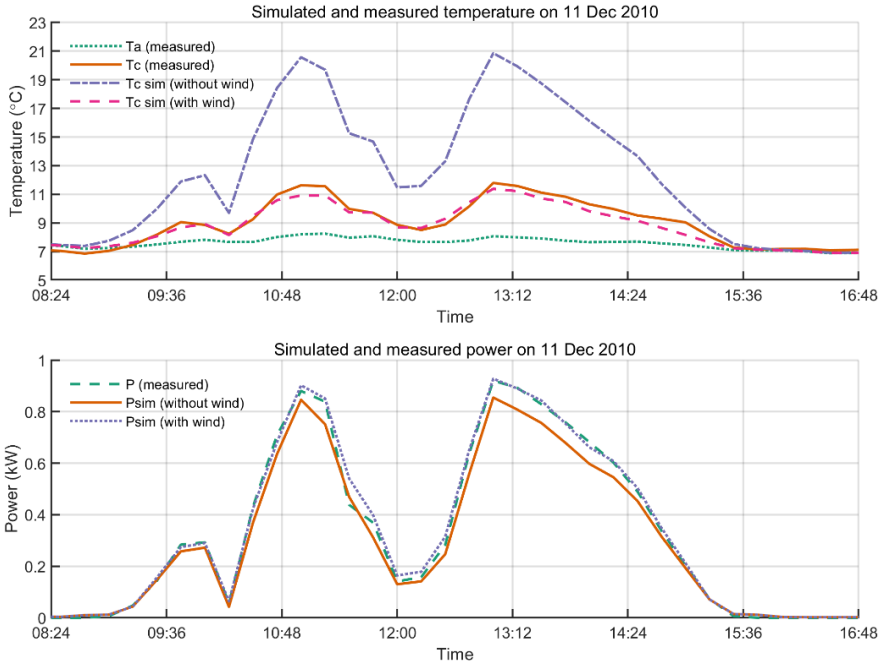

Figure 3.2 Effect of wind speed parameter on a winter day [83]

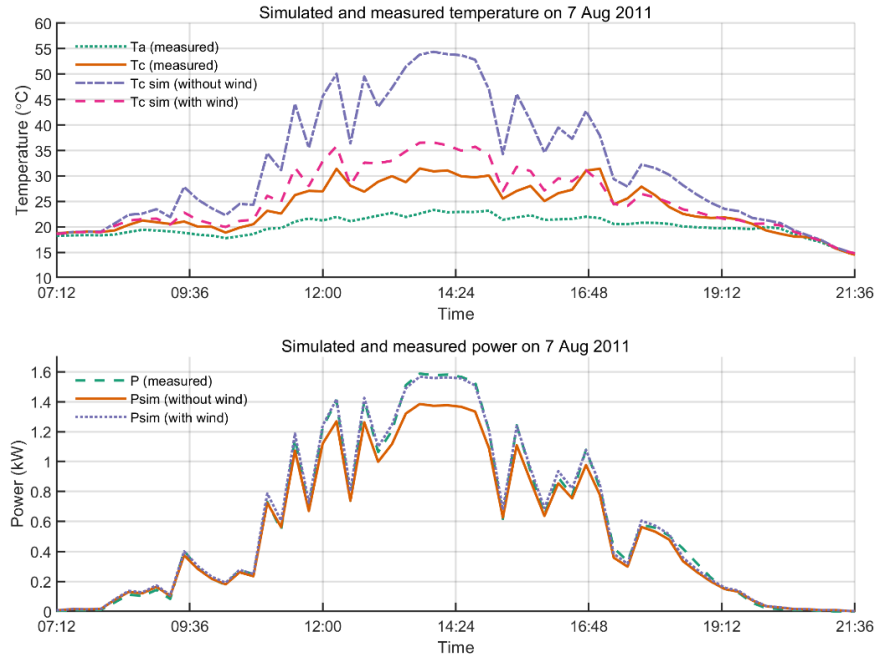

Figure 3.3 Effect of wind speed parameter on a summer day [83]

As can be seen from Figure 3.2, PV module temperature at some time intervals is being overestimated up to 10 °C when the wind speed parameter is not considered. This has led to 2% simulation error on daily energy estimation compared to real measurements. On the other hand, when the wind speed parameter is considered as in Equation 3.6, the error is reduced to 0.5% and energy is more accurately estimated.

Second experimental data is from 7 August 2011, a less windy and hot summer day. The day length is very long (15 hours and 50 minutes) and an average of 5.9 m/s wind speed, 20 °C ambient temperature, and 373.4 W/m^2 irradiance value is recorded during the daylight. Simulated temperature and output power values with the measured ones are shown in Figure 3.3.

As can be seen from Figure 3.3, temperature estimation error goes up to 25 °C when the traditional method is used, and accordingly, daily energy is estimated 4.4% less than the measured one. On the other hand, if the wind speed parameter is taken into account the temperature error goes down to 5 °C and correspondingly, daily energy estimation error is successfully reduced to 0.7%.

As a result, it is observed and validated that by considering the wind speed parameter, temperature and output power can be estimated more accurately. This valuable information can be used at the planning stage to reduce the overall system costs and also at the operational stage to allocate the resources more efficiently.

3.2.3. CALCULATION OF DC POWER OUTPUT

PV module efficiency model has been used to calculate the DC output power of a PV system [87]. As input parameters, this model requires the total area of PV modules (A_{pv}), solar irradiance on the tilted surface (G_β), and a set of conversion efficiency values (η_{pv}). Based on these parameters, DC output power of a PV array can be calculated by [87]

$$P_{pv} = \eta_{pv} \cdot A_{pv} \cdot G_\beta \tag{3.7}$$

Here, the conversion efficiency can be expressed as

$$\eta_{pv} = \eta_{loss} \cdot \eta_{ref} \cdot \left(1 + k_T \left(T_c - T_{ref}\right)\right) \tag{3.8}$$

where η_{loss} represents the losses in DC side, η_{ref} is reference PV module efficiency, k_T is maximum power temperature coefficient, T_{ref} is reference temperature (25 °C), and T_c is the operating temperature of the PV module. Parameter values of η_{ref} and k_T depend on solar cell material and generally given on datasheets of the manufacturers. To account for all the losses in DC side such as maximum power point tracking loss, subarray mismatch loss, etc., a constant value of 0.86 is used for η_{loss} parameter [83].

To represent how the model behaves, a PV system (6500 kWp) of a house has been randomly chosen and then simulated for two different days. The efficiency and maximum power temperature coefficient of the PV modules are read from the database as 0.1607 and -0.417 %/°C, respectively. Variation of DC output power according to the total irradiance and PV module temperature is illustrated for a winter and a summer day, respectively as in Figure 3.4 and Figure 3.5.

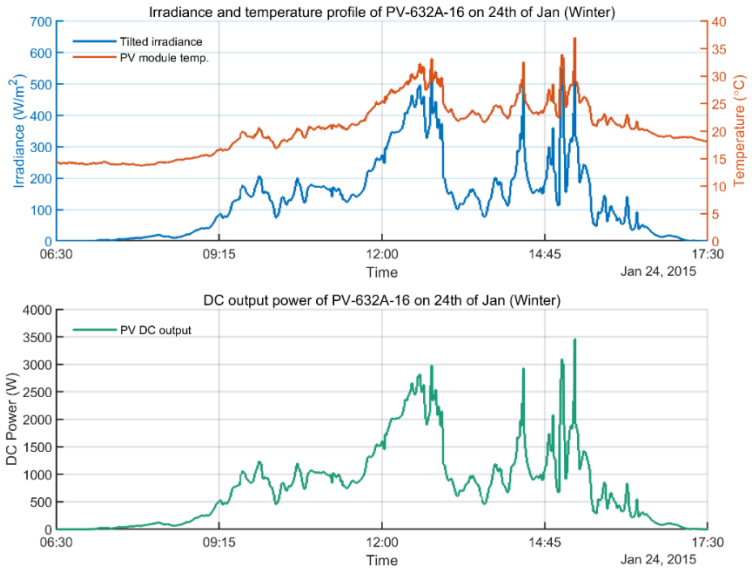

Figure 3.4 Variation of DC output power of the PV system on a winter day

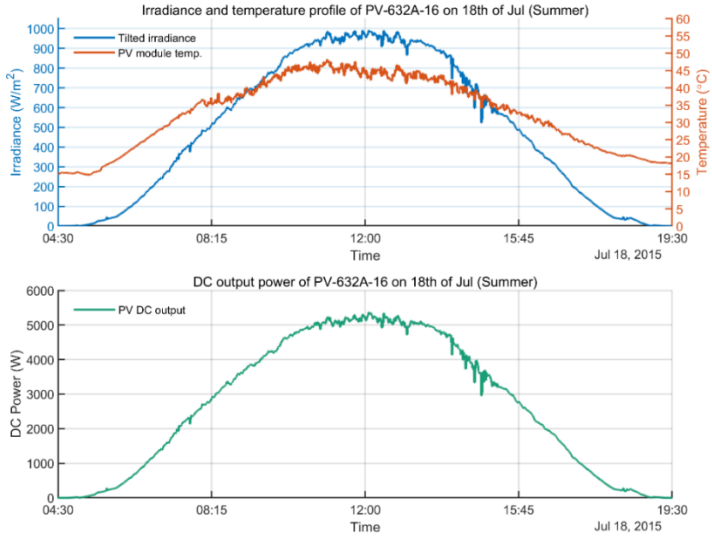

Figure 3.5 Variation of DC output power of the PV system on a summer day

As can be observed from the figures, the shapes of the DC output power profile and total irradiance profile are almost alike, but the magnitudes vary depending on both irradiance and temperature variations. Moreover, as expected, the variation of the generated power in winter is much more compared to the summer case due to the passing clouds which cause frequent fluctuations in solar irradiance.

3.2.4. CALCULATION OF AC POWER OUTPUT

Generated DC power from PV array should be converted to AC power with PV inverters either for own consumption of end-users or to supply energy to the electricity grid. To state the efficiency of this power conversion process, usually the inverter efficiency parameter is defined which is simply the ratio of AC output power to DC input power. PV inverter manufacturers typically provide a single peak efficiency value, but the efficiency of this conversion process actually varies according to the input power and voltage level.

Therefore, to reflect the dynamic efficiency characteristics of PV inverters, Sandia inverter model has been used which is based on both manufacturer specifications and empirically derived coefficients [85]. According to the model, AC output power can be calculated by

$$P_{ac} = \left[\frac{P_{ac,0}}{A-B} - C\left(A-B\right) \right]\left(P_{dc}-B\right) + C\left(P_{dc}-B\right)^2 \tag{3.9}$$

where

$$A = \; P_{dc,0}\left[1 + C_1\left(V_{dc} - V_{dc,0}\right)\right]$$
$$B = \; P_{s,0}\left[1 + C_2\left(V_{dc} - V_{dc,0}\right)\right]$$
$$C = \; C_0\left[1 + C_3\left(V_{dc} - V_{dc,0}\right)\right]$$

And parameters,

P_{dc} : PV array DC power (W)
$P_{dc,0}$: maximum DC power (W)
$P_{s,0}$: power consumption during operation (W)
$P_{ac,0}$: maximum AC power (W)
P_{ac} : PV inverter output power (W)
V_{dc} : DC string voltage (V)
$V_{dc,0}$: nominal DC voltage (V)
$V_{ac,0}$: nominal AC voltage (V)

Empirical C coefficients for a specific PV inverter can be obtained from the Sandia Inverters library [85], and the other coefficients are usually given in manufacturer datasheets. On a side note, maybe $P_{s,0}$ parameter which is the required DC power for PV inverter to start the conversion process, may not be given in the specifications but can be taken as 1% of the inverter rated power with a reasonable estimate.

Finally, the power conversion efficiency of the inverter can be expressed as

$$\eta_{inv} = \frac{P_{ac}}{P_{dc}} \tag{3.10}$$

To illustrate how the inverter model behaves, a random PV inverter is chosen from the created database and then simulated for a winter and summer day as shown in Figure 3.6. As can be seen from the figure, especially during the sunrise and sunset hours, the efficiency of the inverter is quite low. This is mostly because of self-consumption power required by the inverter to be able to start the conversion process at low power levels. As the solar irradiance level increases, accordingly the DC input power and voltage level increase, and then the inverter starts to operate more efficiently.

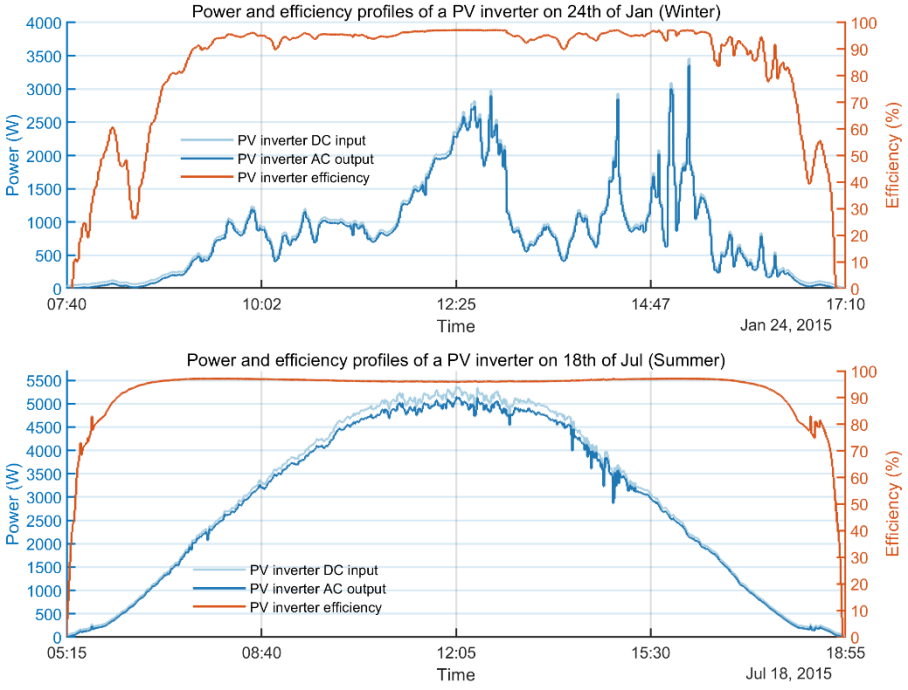

Figure 3.6 Dynamic behavior of PV inverter model for a winter and summer day

3.3. RANDOM ALLOCATION OF PV SYSTEMS IN SECONDARY DISTRIBUTION GRIDS

To increase the diversity as in residential loads, different types of PV modules and PV inverters from a variety of manufacturers are recorded to a PV equipment database as listed in Table 3.2 and Table 3.3, respectively. Then, a Matlab script is written to distribute these devices randomly to each house according to a specific PV penetration level for a preselected location and distribution grid.

Table 3.2 PV module database

	Mod. I	**Mod. II**	**Mod. III**	**Mod. IV**	**Mod. V**	**Mod. VI**
P_{mp} **(W)**	150	150	199	199	240	244
I_{mp} **(A)**	6.7	4.3	7.63	5.0	8.3	7.9
V_{mp} **(V)**	22.5	34.8	26.2	40.0	29.1	30.8
I_{sc} **(A)**	7.30	4.70	8.12	5.40	8.80	8.50
V_{oc} **(V)**	28.5	43.6	33.4	47.8	36.9	37.5
k_T **(%/°C)**	-0.556	-0.491	-0.432	-0.417	-0.526	-0.461
η_{ref} **(%)**	11.75	11.96	13.61	16.07	14.78	14.85
A_m **(m²)**	1.277	1.260	1.469	1.244	1.630	1.643
material	mc-Si	c-Si	mc-Si	c-Si	mc-Si	c-Si

Table 3.3 PV inverter database

	Inv. I	**Inv. II**	**Inv. III**	**...**	**Inv. IX**
$P_{ac,0}$ **(W)**	4000	4500	5000	...	8000
$P_{dc,0}$ **(W)**	4186	4731	5163	...	8402
$V_{dc,0}$ **(V)**	600	600	600	...	600
$P_{s,0}$ **(W)**	19.73	28.09	38.12	...	34.63
η_{ref} **(%)**	96.08	95.76	96.42	...	95.82
C_0 **(1/W)**	-6.58e-06	-7.28e-06	-2.37e-06	...	-3.34e-06
C_1 **(1/V)**	4.73e-05	1.82e-05	-2.86e-05	...	4.90e-05
C_2 **(1/V)**	0.00202	0.000998	0.00024	...	0.00162
C_3 **(1/V)**	0.000285	-0.00032	-0.00205	...	-7.52e-05

To give an example, using the script a probabilistic PV system database is created for Los Angeles city and IEEE 13 distribution grid as shown in Table 3.4. The system has

a total number of 464 houses and the PV penetration level is specified as 50%. For this location, optimum tilt and orientation angles are calculated as 31° and 180°, respectively [83].

Table 3.4 An example of a created PV system database

House No	PV System ID	PV Mod. Type	Rated Power (W)	PV Inv. Type	Tilt Angle (°)	Orientation Angle (°)
1	PV_632A_1	Mod. I	5500	Inv. IV	31	180
2	PV_632A_2	Mod. V	6500	Inv. VI	31	180
3	PV_632A_3	Mod. II	7000	Inv. VII	31	180
4	PV_632A_4	Mod. IV	4000	Inv. I	31	180
⋮	⋮	⋮	⋮	⋮	⋮	⋮
464	PV_680C_16	Mod. V	5500	Inv. IV	31	180

As done in the household database, to identify the PV systems in a smart way, a unique ID is given for each one of them considering the distribution grid node-phase where they are connected to and the corresponding sequence number of the house in that specific node-phase. For example, PV_632B_12 represents the PV system of the house (H_632B_12) that is connected to the B phase of the node 632, and it is also the twelfth PV system in that specific node-phase.

3.4. IMPORTANCE OF PV INVERTER SIZING ON REACTIVE POWER SUPPORT

In the near future, it is anticipated that PV inverters will also provide reactive power support for helping to keep the voltage level at the connection point within the limits. By adjusting the magnitude and direction of the reactive power, terminal voltage can be increased or decreased according to the specific needs at that moment. This flexible operating scheme of the inverter is shown in Figure 3.7.

Assuming that the main purpose of the inverter is to generate active power, normally only leftover inverter capacity can be used to provide reactive power as

$$-\sqrt{S_{max}^2 - P^2} \leq Q \leq \sqrt{S_{max}^2 - P^2} \tag{3.11}$$

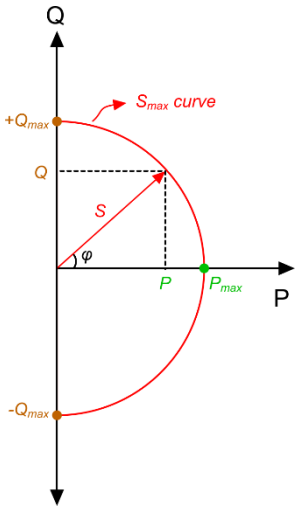

Figure 3.7 P-Q diagram of a PV inverter

This could be a major obstacle in reactive power provision if the inverter size is not chosen a bit larger in the planning stage. Because there will be times where all the inverter capacity is only used for generation of active power and consequently there will not be any leftover space for the reactive power support [88].

Unfortunately, in practice, PV inverters are generally being sized for the purpose of active power feed-in only. Size is usually determined by a techno-economic optimization procedure considering annual solar irradiance and ambient air temperature profiles, tilt angle, orientation, mounting type, revenues, and cost of PV inverters, but not reactive power support.

Even though rated power capacity of a PV array is generally given for the standard test conditions (1000 W/m^2 irradiance and 25 °C solar cell temperature), it is not possible to reach that maximum generation levels most of the time. Therefore, PV inverter sizes are determined in average 0.9 times of the nominal DC power by the optimization. This is also reported in a study where hundreds of different PV system installations are investigated and then maxima of the frequency distribution of sizing ratios found to be between 0.85 and 0.95 [86].

As illustrated in Figure 3.8, choosing the inverter capacity less than (~ $S_{0.9}$) or even equal to ($S_{1.0}$) rated nominal DC power could be an improper choice if it is desired to have an adequate reactive power support whenever it is required without the need of active power curtailment.

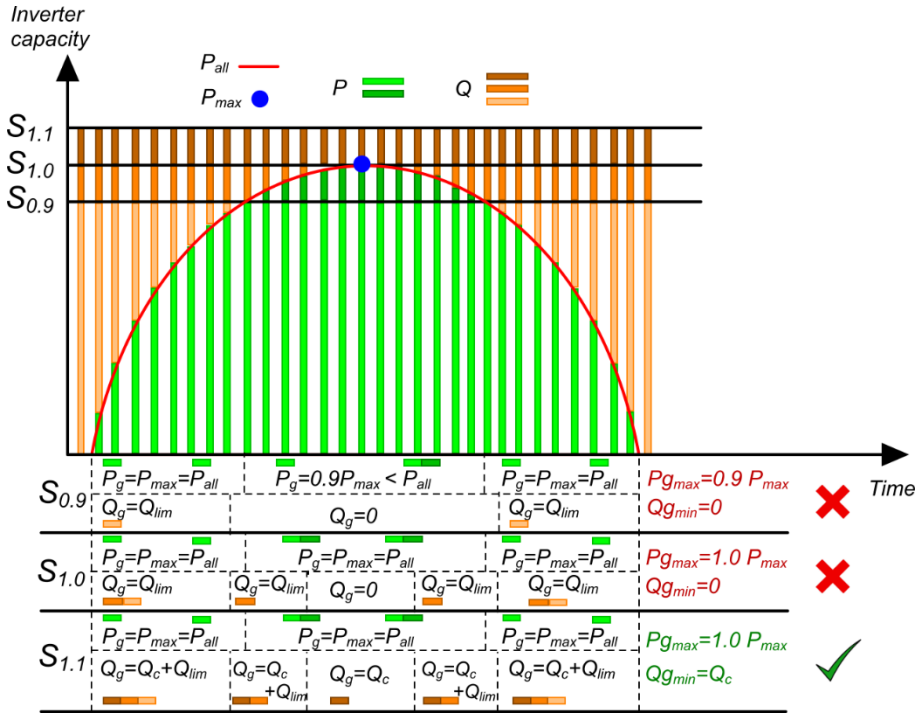

Figure 3.8 The effect of inverter sizes on active and reactive power generation

If the PV inverter size is chosen with the traditional optimization methods ($S_{0.9}$), it is not possible to provide reactive power (Q_g=0) around the midday (even active power is curtailed at high irradiance levels, P_g=0.9P_{all}), and during the other periods of the time, reactive power support (Q_{lim}) will be limited and highly variable.

On the other hand, if the inverter capacity is chosen to fit the nominal DC power exactly ($S_{1.0}$), then active power will never have to be curtailed (P_g=1.0P_{all}), but still, during the high irradiance periods, there will not be any reactive power support (Q_g=0). In other periods, reactive power capacity will still be highly variable and limited (Q_{lim}), but compared to $S_{0.9}$, more reactive power can be provided.

The best option seems to be choosing the inverter size a bit larger as in $S_{1.1}$ case. Therefore, there will be always some room for constant reactive power support (Q_c) and also some additional reactive power (Q_{lim}) depending on the leftover capacity remaining from the active power generation. Besides, all available active power can be provided (P_g=1.0P_{all}) at any instant without any curtailment.

Finally, it is important to note that state-of-the-art PV inverters are technologically ready to provide ancillary services to the grid. They have programmable logic controllers (PLC) with the ability of fast response times (in milliseconds) [76].

Therefore, sophisticated control algorithms can be developed and embedded in their microchips to mitigate the power quality issues locally by controlling their active and reactive power outputs dynamically.

3.5. SUMMARY AND DISCUSSION

In this chapter, a comprehensive overview is given for the PV system technologies including the latest figures and developments. It has been reported that with the ongoing cost reductions, now utility-scale PV systems have become the cheapest power generation options. Therefore, the enormous growth of solar energy in the last two decades is expected to continue without slowing down in the forthcoming years. On the other hand, the output power of a PV module highly varies throughout the day depending on the solar irradiance and temperature changes. Hence, it's crucial to accurately estimate these variations to reveal the true dynamics of PV systems. For this reason, more precise models have been used for the estimation of total solar irradiance, PV module temperature, and DC-AC output powers. It is also emphasized that especially in windy locations, wind speed parameter should not be ignored due to affecting PV system performance. Lastly, PV inverters are expected to play a key role in the near future by providing ancillary services to the grid. Therefore, it is suggested that the capacity of PV inverters should be chosen a bit larger especially for a more reliable and effective reactive power support to mitigate the voltage variations.

CHAPTER 4. TECHNICAL IMPACTS OF HIGH PV PENETRATION IN DISTRIBUTION GRIDS

There has been a tremendous interest in solar PV systems since the last two decades due to green environmental policies and ongoing cost reductions. Despite this huge progress, PV systems still only cover a very small portion of the energy resources. Therefore, this phenomenal growth of PV systems is expected to continue also in the forthcoming years.

With the increase in PV penetration levels, some unfamiliar impacts are also introduced in distribution grids such as voltage rise, voltage unbalance, line and transformer overloadings, the excessive operation of voltage regulators, increase in power losses, and also a substantial amount of surplus power towards substation. Therefore, it is critical to understand the associated impacts and take necessary precautions to continue the proliferation of PV systems.

In this chapter, the technical impacts of high PV penetration are analyzed in depth considering voltage variations, voltage unbalance, line and transformer loading, surplus power, power loss, and also stress on step-voltage regulator. In the first part, an overview of the PV integration challenges is provided including a comprehensive literature review. Secondly, how a whole distribution system can be modeled is explained in detail including the primary and secondary sides together. Then, the three-phase unbalanced powerflow technique is presented to be used as the main tool in the impact analysis. After that, by using the previously generated high-resolution time-series load and generation data as inputs, sequential power flow is run for the default and high PV penetration case considering the winter and summer periods separately. Finally, technical impacts are scrutinized in detail.

4.1. OVERVIEW OF PV INTEGRATION CHALLENGES

Solar PV systems are amongst the fastest growing renewable energy sources across the globe. Each passing day, more and more PV systems are being interconnected to electrical power grids and this is anticipated to continue through the next decade and beyond. Even though the process is pleasing, with the increase in PV penetration levels some unfamiliar impacts are also introduced in distribution grids. Therefore, there is an urgent need for understanding the associated impacts and taking necessary precautions to continue the proliferation of PV systems [89].

The vast majority of PV installations are being hosted by secondary distribution grids where commonly residential customers are located. Although these grids are originally not designed to host generation, it is reported that installed PV capacities in some low-voltage grids have already overpassed the peak load by a factor of ten [90]. Previously, when PV penetration levels were low, it was reasonable to assume that generation would offset the consumption and consequently eliminate the voltage drops, equipment loadings, and power loss [91]. However, with the increase in PV penetration levels, these assumptions will no longer be valid; on the contrary, these problems will be exaggerated if necessary precautions are not taken in advance [92].

Benefitting from the related studies in literature, high PV penetration impacts can be grouped under different categories as follows

- voltage problems (voltage rise [93], [94], voltage variations [95], [96], and voltage unbalance [97], [98])
- stress on grid equipment and components (line and transformer overloading [99], [100], the excessive operation of load tap changers, voltage regulators, and switched capacitors [101], [29])
- increase in power loss [102], [103]
- surplus power towards substation [104], [22]
- misoperation of protection devices [105]
- reliability issues [106]

To summarize the main findings of the impact studies, the severity of these impacts may vary depending on the PV installation size and location, weather conditions, load and generation imbalance, and the electrical characteristics of distribution systems [107]. It's reported that low PV penetration levels usually do not cause any significant issues. Contrary, they may even help to reduce the voltage drops, line and transformer loadings, and power losses. However, it's more likely to experience these local and/or systemwide impacts with the increase in PV penetration levels [93].

First of all, voltage rise is generally defined as the most restrictive obstacle in PV integration [94]. Especially, endpoints of rural feeders are more inclined to the overvoltage problems due to high feeder impedances [95]. Secondly, as one of the power quality problems, voltage variations are also critical especially for voltage sensitive devices. Both load and generation are intermittent and highly variable by nature and their interaction with each other may increase the degree of voltage variations [96]. As a result, this phenomenon may lead to frequent operation of load tap changers, voltage regulators, and switched capacitors; and consequently, reduce their lifetimes [29].

On the other hand, distribution grids are inherently unbalanced due to untransposed lines, multiphase structure, and unequal load distribution. In addition to that, the presence of the PV systems on single-phase laterals may cause an additional increase

in voltage unbalance levels [98]. Voltage unbalance over the safe limits may damage the three-phase motor windings [97] and shorten the insulation life of three-phase transformers [108] by excessive heating.

Besides these, especially during the low consumption and high generation periods due to the significant amount of surplus power, distribution lines [99] and transformers [100] can be overloaded. This may lead to costly grid reinforcement measures to avoid congestion of lines and transformers [109]. Power loss is also another important grid parameter which is considered as a key performance indicator by the electric utilities [103]. Up to a certain PV penetration level power loss can be decreased, but after that level is exceeded, power loss tends to increase again [102].

Although it's not within the scope of this thesis, it's worth to mention that high level of PV penetration can make the protection schemes more complex and cause misoperation of the protection devices [105]. In addition, system reliability can also be affected and additional measures may be required to improve the network safety [110]. Transmission systems can also be affected due to substantial amount of surplus power from the substation [104]. For this reason, joint simulations may be needed to analyze high PV penetration impacts systemwide including low-voltage, medium-voltage and high-voltage grids [22].

To evaluate the impacts more accurately, detailed models are required for loads, PV systems, and also the grid itself. Simplified models may not fully reflect the degree of impacts and may lead to erroneous evaluations [92. Many studies also disregard the variability of individual end-user loads and PV systems in secondary distribution grids [111]. Individual voltage problems at customer connection points and service transformer overloadings are usually ignored in the analysis [22].

Considering these flaws, a comprehensive PV impact study is conducted in this chapter. Very detailed models are used for loads, PV systems, and also distribution system itself. High-resolution time-series load and generation profiles had already been created in the previous chapter. In this chapter, distribution systems are also modeled with both primary and secondary parts. After that, three-phase unbalanced powerflow algorithm is presented and technical impacts are investigated for a high PV penetration case in the designed distribution grid.

4.2. DISTRIBUTION SYSTEM MODELING

In this section, a distribution test system is designed combining both primary and secondary parts of the grid. It will be used as a testbed for power system analysis hereupon to investigate and mitigate the technical impacts of high PV penetration.

4.2.1. MODELING PRIMARY AND SECONDARY DISTRIBUTION SYSTEMS

Distribution systems typically consist of two parts as primary and secondaries. In primary part, one or more individual feeders may exist to serve industrial and commercial customers at medium-voltage level (4.16-34.5 kV), whereas in secondary part, voltage is usually reduced to low-voltage level (120/240 V in U.S. or 230/400 V in Europe) with distribution transformers to serve the end-users.

Considering both primary and secondary parts, a simulation test system is designed in this section. A modified IEEE 13 node feeder is used as a primary part of the grid and also a secondary distribution system is constructed taking U.S. infrastructure as reference as shown in Figure 4.1 and 4.2, respectively.

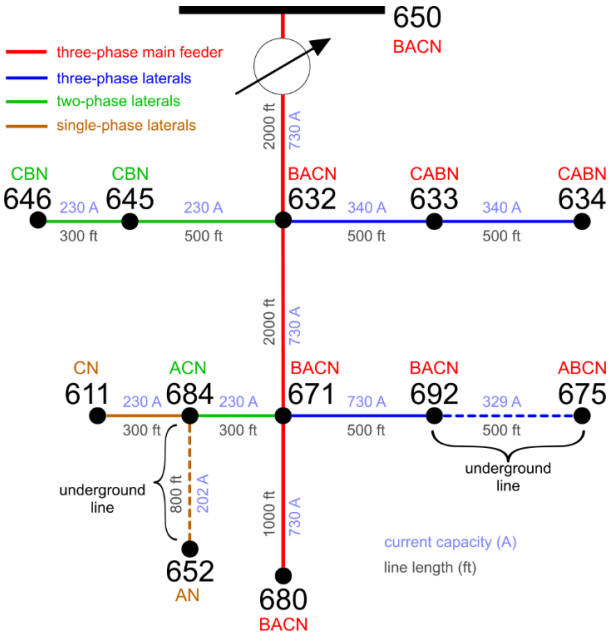

Figure 4.1 Modified IEEE 13 node test feeder as primary distribution system

In the modified version of IEEE 13 distribution grid, all constant loads, static capacitor banks, the switch between nodes 671 and 692, and the transformer between nodes 633 and 634 have been removed. Instead of the switch and transformer, three-phase overhead lines are inserted to the related places. Moreover, constant loads have been replaced with time-varying end-user load and generation profiles which are generated in previous chapters.

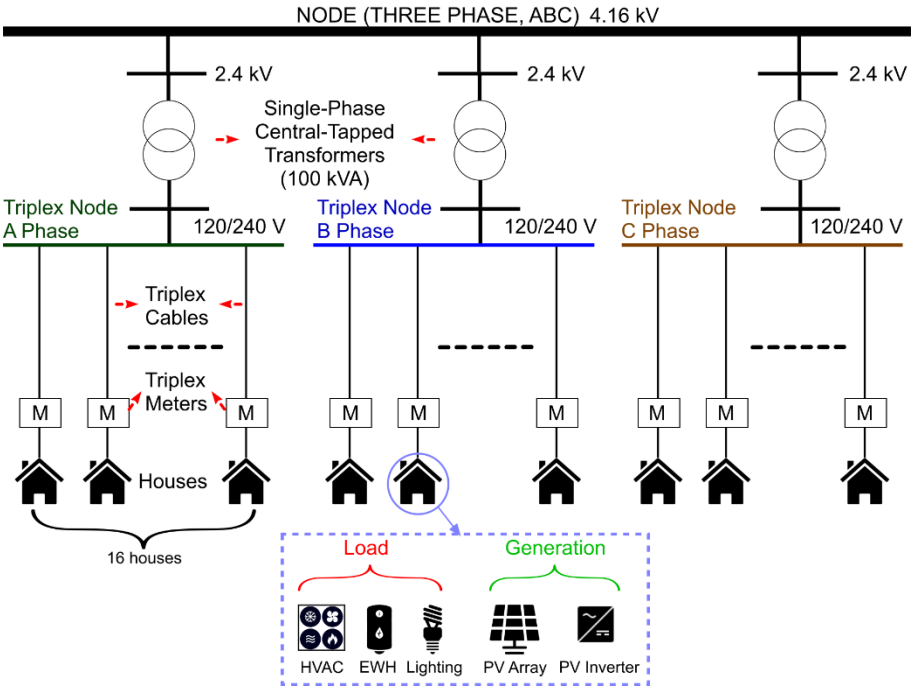

Figure 4.2 Designed secondary distribution system infrastructure

In secondaries, for each existing phase of a primary node, a single-phase central-tapped transformer (distribution transformer) has been used to form a single-phase triplex node system. Depending on the transformer capacity, number of houses that can be interconnected to a triplex node may change. A triplex cable (two phase wires and one ground wire) is provided for each house to be able to feed the loads either with 120 V (one phase) or 240 V (two phases). Each house is equipped with load (HVAC, EWH, and lighting) and generation sources (rooftop PV systems). Furthermore, a triplex meter is installed to each house for the measurement purpose.

4.2.2. MODELS OF INDIVIDUAL DISTRIBUTION SYSTEM COMPONENTS

In this section, how distribution system components are modeled is briefly described. It is started with the configuration of overhead lines and underground cables, and after that, models are introduced for the distribution lines, transformers, voltage regulators, loads, and shunt capacitors, respectively. Modeling approach for individual system components is adapted from Kersting's distribution system modeling and analysis book [112].

4.2.2.1 Conductor configuration of overhead lines and underground cables

Commonly used conductor configurations by IEEE distribution test systems for both overhead lines (OVH) and underground cables (UGC) are shown in Figure 4.3. Here, two more configurations are added (e, f) to be able to easily modify the grid in case of a complete transformation from OVH lines to UGC systems for further studies [113].

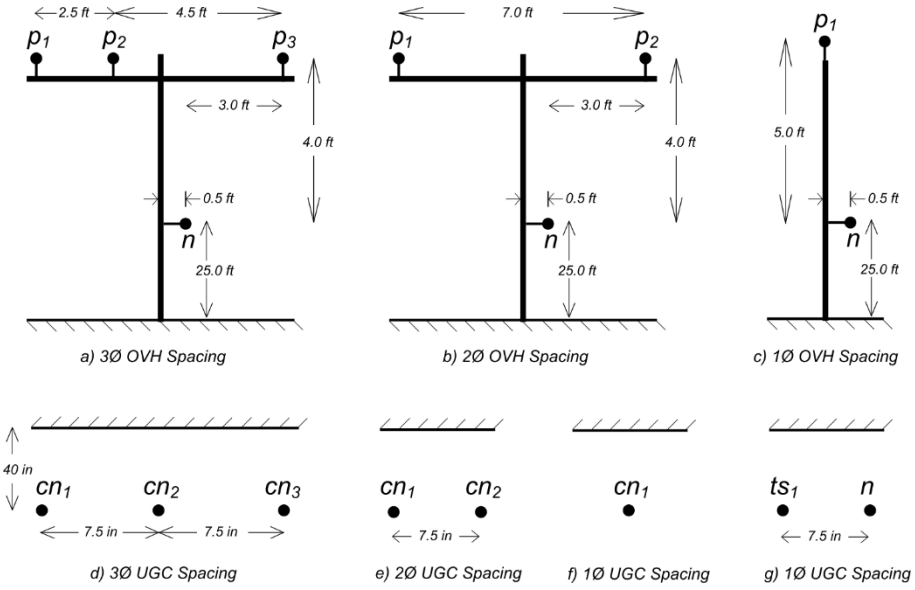

Figure 4.3 Conductor configuration of overhead lines and underground cables

4.2.2.2 Line model

The exact line segment model has been used for the distribution lines as shown in Figure 4.4 [112].

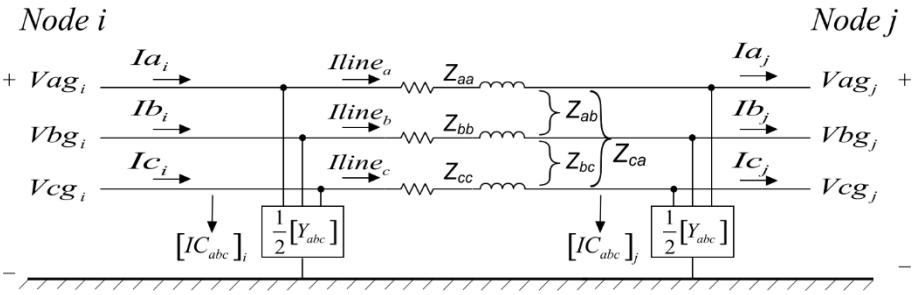

Figure 4.4 Three-phase exact line segment model of the distribution systems

To express the relationship between input voltage and currents (node *i*) with the output voltage and currents (node *j*), generalized three-phase line matrices (**a_{line}, b_{line}, c_{line}, d_{line}, A_{line}, B_{line}**) can be used as follows

$$[VLG_{abc}]_i = [a_{line}] \cdot [VLG_{abc}]_j + [b_{line}] \cdot [I_{abc}]_j \quad (4.1)$$

$$[I_{abc}]_i = [c_{line}] \cdot [VLG_{abc}]_j + [d_{line}] \cdot [I_{abc}]_j \quad (4.2)$$

$$[VLG_{abc}]_j = [a_{line}] \cdot [VLG_{abc}]_i - [b_{line}] \cdot [I_{abc}]_i \quad (4.3)$$

$$[I_{abc}]_j = -[c_{line}] \cdot [VLG_{abc}]_i + [d_{line}] \cdot [I_{abc}]_i \quad (4.4)$$

$$[VLG_{abc}]_j = [A_{line}] \cdot [VLG_{abc}]_i - [B_{line}] \cdot [I_{abc}]_j \quad (4.5)$$

Where **U** is 3x3 unit matrix, and

$$[a_{line}] = [U] + \frac{1}{2} \cdot [Z_{abc}] \cdot [Y_{abc}],\ [b_{line}] = [Z_{abc}],$$

$$[c_{line}] = [Y_{abc}] + \frac{1}{4} \cdot [Y_{abc}] \cdot [Z_{abc}] \cdot [Y_{abc}],\ [d_{line}] = [U] + \frac{1}{2} \cdot [Z_{abc}] \cdot [Y_{abc}],$$

$[A_{line}] = [a]^{-1}$, and $[B_{line}] = [a]^{-1} . [b]$

4.2.2.3 Transformers

Generalized matrices can also be used to represent the transformers in distribution systems as follows

$$[VLN_{abc}]_j = [A_t] \cdot [VLG_{abc}]_i - [B_t] \cdot [I_{abc}]_j \quad (4.6)$$

$$[VLN_{abc}]_i = [a_t] \cdot [VLG_{abc}]_j + [b_t] \cdot [I_{abc}]_j \quad (4.7)$$

$$[I_{abc}]_i = [c_t] \cdot [VLN_{abc}]_j + [d_t] \cdot [I_{abc}]_j \quad (4.8)$$

Here, **VLN (**or **VLG)** voltage matrix may represent the line-to-neutral or line-to-ground voltages for ungrounded and grounded wye connections, respectively. On the

other hand, for a delta connection, it represents the equivalent line-to-neutral voltage. Depending on the transformer connection type, generalized transformer matrices ($\mathbf{a_t}$, $\mathbf{b_t}$, $\mathbf{c_t}$, $\mathbf{d_t}$, $\mathbf{A_t}$, $\mathbf{B_t}$) should be calculated separately.

4.2.2.4 Voltage regulators

Using the same logic as lines and transformers, step-type voltage regulators are also modeled with the generalized matrices as

$$\left[VLN_{abc}\right]_j = \left[A_{reg}\right]\cdot\left[VLG_{abc}\right]_i - \left[B_{reg}\right]\cdot\left[I_{abc}\right]_j \tag{4.9}$$

$$\left[VLN_{abc}\right]_i = \left[a_{reg}\right]\cdot\left[VLG_{abc}\right]_j + \left[b_{reg}\right]\cdot\left[I_{abc}\right]_j \tag{4.10}$$

$$\left[I_{abc}\right]_i = \left[c_{reg}\right]\cdot\left[VLN_{abc}\right]_j + \left[d_{reg}\right]\cdot\left[I_{abc}\right]_j \tag{4.11}$$

To be able to regulate phase voltages individually, a separate single-phase voltage regulator is considered for each phase. Meaning that, each regulator has its own line drop compensator unit to determine the optimal tap setting for that specific phase. If a line drop compensator decides a tap change to mitigate the voltage drop or rise on that phase, then these generalized regulator matrices ($\mathbf{a_{reg}}$, $\mathbf{b_{reg}}$, $\mathbf{c_{reg}}$, $\mathbf{d_{reg}}$, $\mathbf{A_{reg}}$, $\mathbf{B_{reg}}$) should be recalculated according to the flowchart in Figure 4.5.

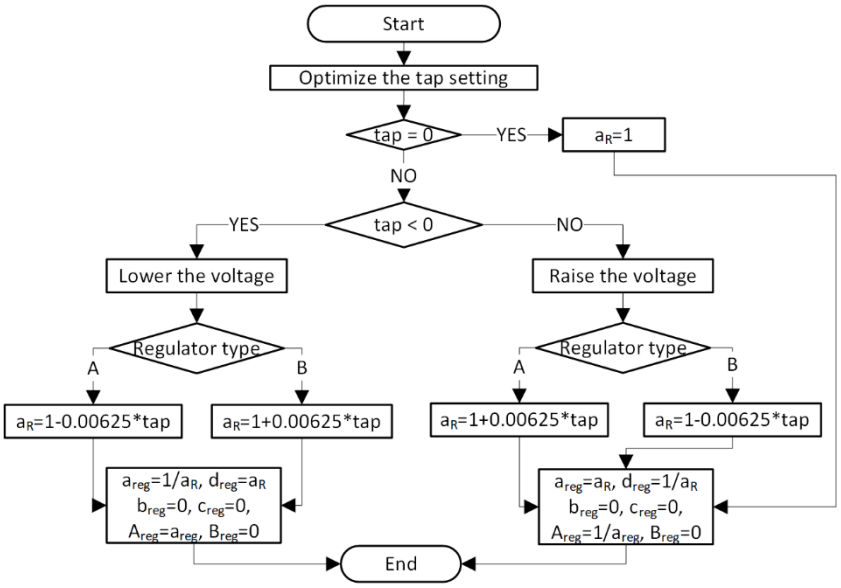

Figure 4.5 Determining generalized regulator matrices depending on the tap setting

4.2.2.5 Loads

ZIP modeling approach is adapted to integrate the loads in distribution grids. In this modeling approach, loads can be partitioned into three parts as constant impedance (Z), constant current (I), and constant power (P) portions. Total load current can be found by summing up these three individual components as

$$I_{abc} = I_Z Z_{\%} + I_I I_{\%} + I_P P_{\%} \tag{4.12}$$

Satisfying the following constraint

$$Z_{\%} + I_{\%} + P_{\%} = 1 \tag{4.13}$$

All loads can initially be defined as complex power per phase, but depending on the connection type either line-to-neutral (wye) or line-to-line (delta) parameters should be used for the calculation of the load currents.

If the load is wye-connected, then using the following matrices

$$S = \begin{bmatrix} |S_a|\angle\theta_a \\ |S_b|\angle\theta_b \\ |S_c|\angle\theta_c \end{bmatrix},\ V = \begin{bmatrix} |V_a|\angle\delta_a \\ |V_b|\angle\delta_b \\ |V_c|\angle\delta_c \end{bmatrix},\ V_{init} = \begin{bmatrix} |V_a|\angle 0^\circ \\ |V_b|\angle -120^\circ \\ |V_c|\angle +120^\circ \end{bmatrix}, \text{ and } Z_{load} = \frac{|V_{init}|^2}{S^*}$$

Three-phase line current entering the load terminals can be calculated by

$$IL_{abc} = \left[\frac{|V|}{|Z_{load}|}\angle(\delta-\theta)\right]Z\% + \left[\left|\left(\frac{S}{V_{init}}\right)^*\right|\angle(\delta-\theta)\right]I\% + \left[\frac{|S|}{|V|}\angle(\delta-\theta)\right]P\% \tag{4.14}$$

Where $\boldsymbol{\delta}$ and $\boldsymbol{\theta}$ matrices (3x3) represent the line-to-neutral voltage angles and power factor angles, respectively.

On the other hand, if the load is delta-connected, then using the following matrices

$$SD = \begin{bmatrix} |S_{ab}|\angle\theta_{ab} \\ |S_{bc}|\angle\theta_{bc} \\ |S_{ca}|\angle\theta_{ca} \end{bmatrix},\ VD = \begin{bmatrix} |V_{ab}|\angle\delta_{ab} \\ |V_{bc}|\angle\delta_{bc} \\ |V_{ca}|\angle\delta_{ca} \end{bmatrix},\ D = \begin{bmatrix} 1 & -1 & 0 \\ 0 & 1 & -1 \\ -1 & 0 & 1 \end{bmatrix},\ DI = \begin{bmatrix} 1 & 0 & -1 \\ -1 & 1 & 0 \\ 0 & -1 & 1 \end{bmatrix},$$

$$VD_{init} = D \times V_{init} \text{ and } ZD_{load} = \frac{|VD_{init}|^2}{SD^*}$$

Three-phase delta current entering the load terminals can be calculated by

$$ID_{abc} = \left[\frac{|VD|}{|ZD_{load}|}\angle(\delta-\theta)\right]Z\% + \left[\left|\left(\frac{SD}{VD_{init}}\right)^{*}\right|\angle(\delta-\theta)\right]I\% + \left[\frac{|SD|}{|VD|}\angle(\delta-\theta)\right]P\% \tag{4.15}$$

Where $\boldsymbol{\delta}$ and $\boldsymbol{\theta}$ matrices (3x3) represent the line-to-line voltage angles and power factor angles, respectively.

Finally, for the conversion of delta currents to line currents following equation can be used

$$IL_{abc} = DI \times ID_{abc} \tag{4.16}$$

4.2.2.6 Shunt capacitors

Shunt capacitor banks are also connected as either wye or delta to the distribution lines and can be represented by the constant susceptance model.

If the capacitor banks are wye-connected, then using the following matrices

$$S_c = \begin{bmatrix} jQ_a \\ jQ_b \\ jQ_c \end{bmatrix},\ V = \begin{bmatrix} |V_a|\angle\delta_a \\ |V_b|\angle\delta_b \\ |V_c|\angle\delta_c \end{bmatrix},\ V_{init} = \begin{bmatrix} |V_a|\angle 0^{\circ} \\ |V_b|\angle -120^{\circ} \\ |V_c|\angle +120^{\circ} \end{bmatrix}$$

Where phase capacitor units are specified in kVar in $\boldsymbol{S_c}$ matrix and voltages are defined in kV for the $\boldsymbol{V}$ and $\boldsymbol{V_{init}}$ matrices. Constant susceptance ($\boldsymbol{B_c}$) matrix can be computed by

$$B_c = \frac{S_c}{|V_{init}/1000|^2 \times 1000} \tag{4.17}$$

Then, three-phase line currents can be found by

$$IC_{abc} = jB_c \times V \tag{4.18}$$

If the capacitor banks are delta-connected, then using the following matrices

$$VD = \begin{bmatrix} |V_{ab}|\angle\delta_{ab} \\ |V_{bc}|\angle\delta_{bc} \\ |V_{ca}|\angle\delta_{ca} \end{bmatrix},\ D = \begin{bmatrix} 1 & -1 & 0 \\ 0 & 1 & -1 \\ -1 & 0 & 1 \end{bmatrix},\ DI = \begin{bmatrix} 1 & 0 & -1 \\ -1 & 1 & 0 \\ 0 & -1 & 1 \end{bmatrix},\ VD_{init} = D \times V_{init}$$

Constant susceptance ($\boldsymbol{B_c}$) matrix can be computed by

$$B_c = \frac{S_c}{\left|VD_{init} / 1000\right|^2 \times 1000} \tag{4.19}$$

Three-phase delta current entering the capacitor terminals can be calculated by

$$ICD_{abc} = jB_c \times VD \tag{4.20}$$

Finally, delta currents can be converted to line currents as

$$IC_{abc} = DI \times ICD_{abc} \tag{4.21}$$

4.3. THREE-PHASE UNBALANCED POWERFLOW

It is fundamental to carry out a powerflow study to analyze the power systems under steady-state operating conditions. Prior to the analysis, feeder characteristics, the three-phase voltages at the substation, complex power of loads and generators are usually known. Using these parameters as inputs for the powerflow algorithm, distribution feeder analysis can be performed. With the powerflow analysis, voltage magnitude and angles at each node, power and current flow at each line segment, loading ratios of lines and transformers, power loss, total feeder power, and operational status of switching devices can be obtained.

Conventional powerflow algorithms such as Gauss-Seidel, Newton-Raphson, and their derivatives are more suitable for transmission system analysis where the network is mesh structured and balanced. Therefore single-phase assumption can be applied to represent the three-phase transmission grid. On the other hand, distribution systems are radial and highly unbalanced due to untransposed conductors, multi-phase structure, and unequal load/generation distribution; therefore single-phase assumption can not be applied. For these reasons, conventional algorithms may not handle unbalanced distribution systems and have some convergence issues while trying to solve the powerflow problem by defining the system as ill-conditioned.

In this thesis, forward-backward sweep (FBS) algorithm has been used for the distribution system powerflow analysis due to its simplicity and better convergence characteristics for the radial and unbalanced grids. Basic feature of a radial distribution network is that there only exists one unique path from any given node to the source. FBS based methods are designed to update the voltages and currents along these unique paths in an iterative way until the convergence criterion is met. As one of the main advantages of the FBS method, Kirchoff's current and voltage laws can directly be applied with the generalized line, transformer, and voltage regulator ABCD matrices as modeled in the previous subsection.

In FBS powerflow algorithm, it is necessary to follow a specific sequence while updating the voltage and currents during the sweep operation. To do that each node and lateral should be indexed in a systematic way to guide the FBS algorithm properly. For this purpose, the breadth-first (BF) graph algorithm has been used as proposed in [114]. To give an example, it is used on the IEEE 13 grid as shown in Figure 4.6.

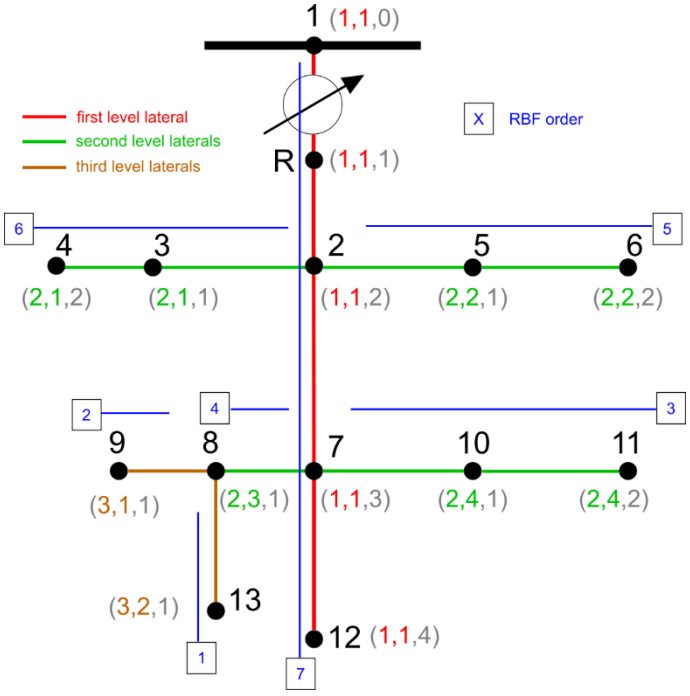

Figure 4.6 Bus and lateral indexing to determine the ordering in FBS algorithm

Using BF algorithm, each node in the grid can be represented with an ordered triple as (l, m, n). Here, l represents the level of the lateral such that main feeder is assigned as the first level, and its sublaterals are second, and their sublaterals would be third, and so on. Laterals within level l are indexed according to the order of appearance (m) during the BF search and each lateral can be represented by an ordered pair as (l, m). Finally, buses within a specific lateral can be indexed according to the appearance order (n) in that lateral.

After this indexing process, laterals are sorted in descending order with the reverse breadth-first (RBF) ordering as shown in Figure 4.6 with the boxed numbers. This RBF sequence is used in the backward sweep stage to update the currents from end point to source, whereas in the forward sweep, the reverse of RBF sequence is used to update the node voltages from source to end.

Using a simplified distribution grid section as shown in Figure 4.7, stages of the FBS algorithm is explained below.

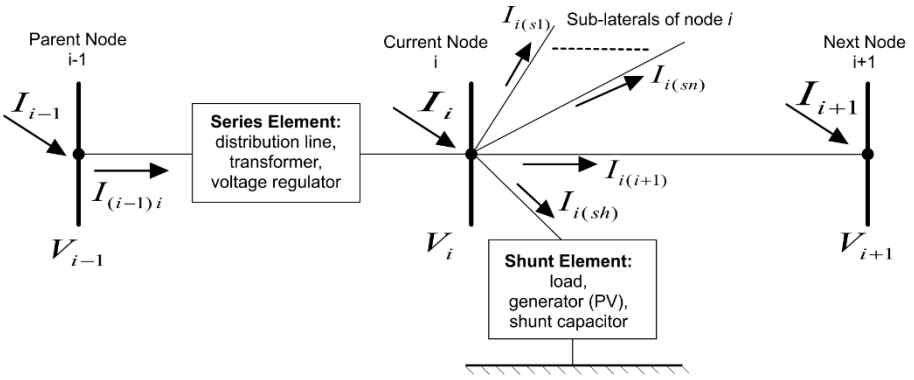

Figure 4.7 Simple radial distribution grid section used to represent the FBS stages

Stages of the FBS powerflow algorithm:

- Initialization

Initialize all the voltages with the nominal value (1.0 pu), and currents with zeros.

- Forward sweep

Starting from the last lateral, update the voltages from source to end

$$V_i = A_{(i-1)(i)} V_{i-1} - B_{(i-1)(i)} I_i \tag{4.22}$$

- Backward sweep

Starting from the first lateral, update the currents from end to source

a) Accumulate shunt element currents

$$I_{i(sh)} = I_{i,load} + I_{i,gen} + I_{i,cap} \tag{4.23}$$

b) Update the node current

$$I_i = I_{i(sh)} + I_{i(i+1)} + \sum_{k=1}^{n} I_{i(sk)} \tag{4.24}$$

c) Update the parent branch current

$$I_{(i-1)i} = c_{(i-1)i} V_i + d_{(i-1)i} I_i \tag{4.25}$$

d) Update the parent node voltage

$$V_{i-1} = a_{(i-1)i} V_i + b_{(i-1)i} I_i \tag{4.26}$$

- Convergence criterion

If the difference of voltage magnitudes with the current and previous iteration is less than the specified tolerance, then terminate the FBS, otherwise, continue with the next iteration.

4.4. INVESTIGATION OF HIGH PV PENETRATION IMPACTS

Technical impacts of large-scale PV integration in secondary distribution grids have been analyzed in this section. Voltage variations, voltage unbalance, line and distribution transformer loading, surplus power towards substation, total power loss, and excessive operation of tap-changers are investigated in detail.

IEEE 13 distribution grid has been used as the simulation testbed with the integrated secondaries as introduced in the previous sections. Each house is equipped with HVAC, EWH, and lighting loads, and a PV system of which generation capacity is randomly chosen between 4 and 8 kW. Time-series load and PV profiles are generated in one-minute resolution with the modeling approach explained in Chapter 2 and Chapter 3, respectively.

One random week is chosen for both winter and summer cases and three-phase powerflow analysis is performed for these periods. Overall analysis scheme can be seen in Figure 4.8. Results are interpreted and discussed in the following subsections.

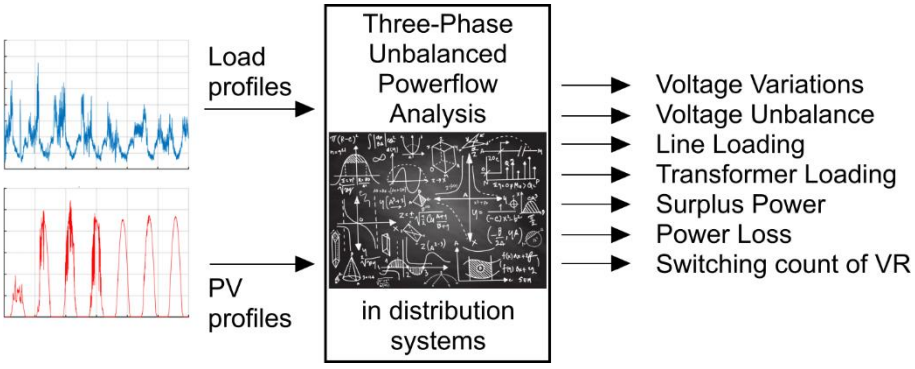

Figure 4.8 Scheme of high PV penetration impact analysis in distribution grids

4.4.1. VOLTAGE VARIATIONS

According to ANSI C84.1-2006 standard, voltage should preferably stay within 0.95 and 1.05 p.u. at the service entrance of the end-users. On the other hand, an exceedance of those reference values is recommended when PVs are interconnected to the system by limiting the variations within ±2% and ±3% for medium-voltage and low-voltage nodes, respectively [107]. In this thesis, the latter recommendation is considered to analyze the voltage impacts of PV systems.

Voltage profiles of both primary and secondary distribution grids with and without PV systems are shown in Figure 4.9 and Figure 4.10 for winter and summer cases, respectively. Voltage impact metrics are also given in Table 4.1 considering all nodes in primaries and customer connection points in secondaries.

Table 4.1 Voltage impact metrics with and without PV systems

Grid Section	Voltage Impact Metrics	Winter		Summer	
		No PV	PV	No PV	PV
Primary Distribution Grid	V_{min} (V)	0.9649	0.9652	0.9761	0.9844
	V_{max} (V)	1.0057	1.0241	1.0072	1.0263
	$V_{rise\_violation}$ (total)	0	856	0	1390
	$V_{drop\_violation}$ (total)	24	27	0	0
Secondary Distribution Grid	V_{min} (V)	0.9428	0.9431	0.9607	0.9717
	V_{max} (V)	1.0054	1.0379	1.0072	1.0426
	$V_{rise\_violation}$ (total)	0	32951	0	50929
	$V_{drop\_violation}$ (total)	10239	9717	452	0

First of all, it can be deduced that secondary grids are more vulnerable to voltage variations than primary grids. With the increase in feeder impedances, magnitudes of voltage-drops and voltage-rises are also getting bigger towards the end of the lines.

When PVs are interconnected to the system, voltage usually tends to increase with the sunrise, reach a peak around noon, and gradually decrease until the sunset. Both in primary and secondary distribution grids voltage rise violations are observed. However, compared to the primary grid, secondaries are affected more from these voltage rise violations.

On the other hand, PV systems may help to eliminate the voltage-drops in secondary distribution grids as an indirect contribution. As can be seen in Table 4.1, especially in summer periods, all voltage drops, due to excessive HVAC usage, are mitigated. On the contrary, voltage rises are also increased especially in high generation and low consumption periods.

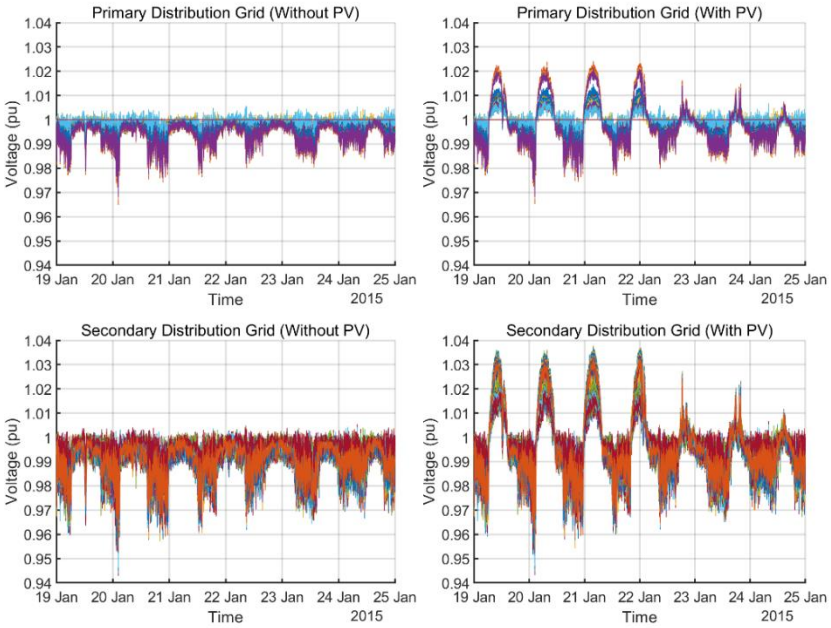

Figure 4.9 Voltage profiles of primary and secondary distribution grids with and without PV penetration (winter case)

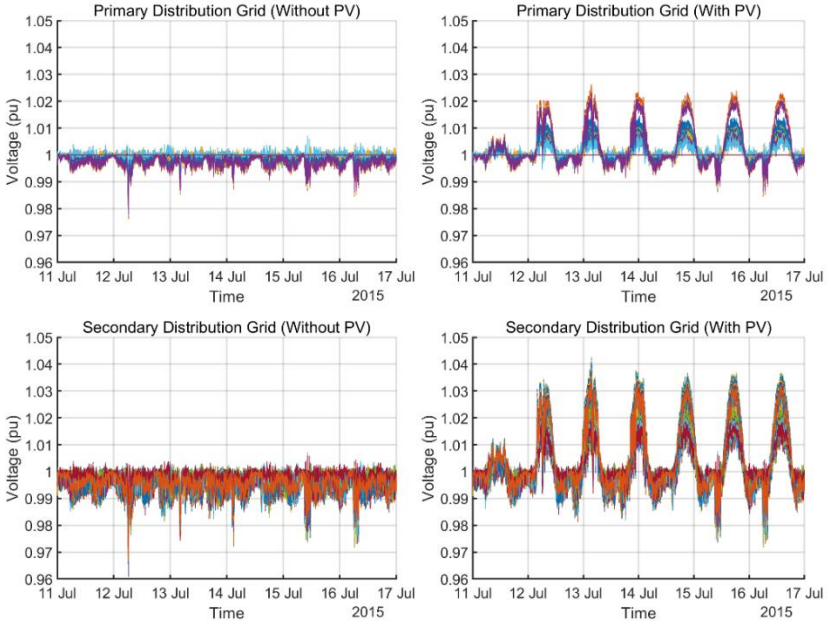

Figure 4.10 Voltage profiles of primary and secondary distribution grids with and without PV penetration (summer case)

4.4.2. VOLTAGE UNBALANCE

In a three-phase system, voltage unbalance problem occurs due to the differences in phase voltage magnitudes. It can be measured as the maximum deviation from the average phase voltage divided by the average of the phase voltages. Even though ANSI C84.1-2006 standard allows up to 3% voltage unbalance level, in most distribution grids, 2% limit is applied [115].

Voltage unbalance profiles including all three-phase primary nodes are shown in Figure 4.11 with and without PV systems for both winter and summer cases.

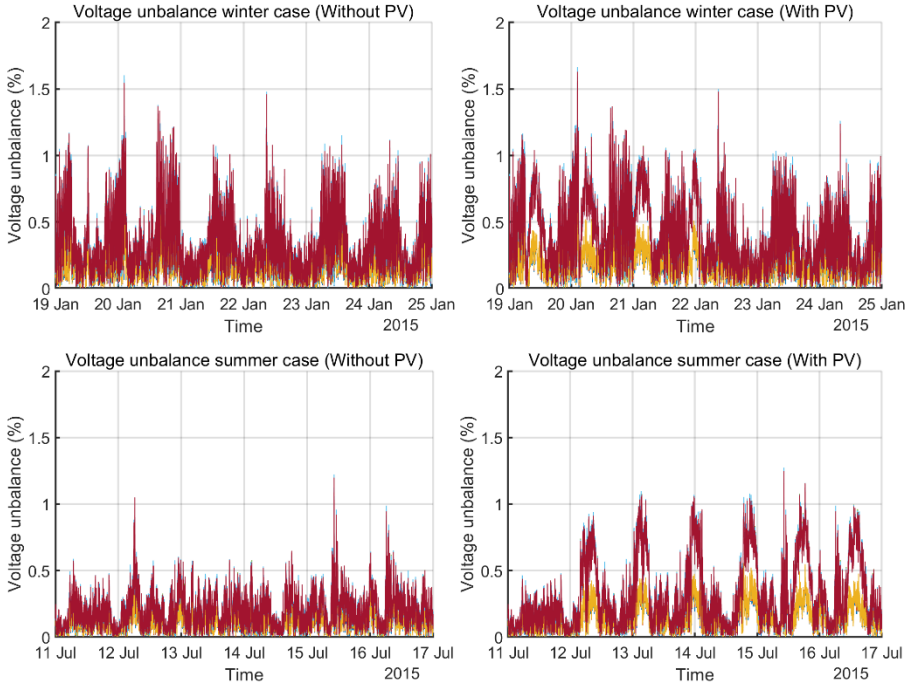

Figure 4.11 Voltage unbalance profiles including all primary nodes with and without PV penetration

As explained previously, distribution systems are inherently unbalanced due to unequal conductor spacings and unevenly distributed single-phase loads. This phenomenon can be seen in the winter case as voltage unbalance already reaches 1.5% at some intervals even without high PV penetration.

On the other hand, even though the results are not so clear to distinguish the PV impact from the default situation in winter case, it is more clear in summer that PV systems increase the degree of voltage unbalance to some extent. Actually, the impact could

be more severe if PV systems and loads were more unevenly distributed to the grid. Voltage unbalance problem is addressed more detailly in Chapter 6.

4.4.3. LINE LOADING

Each conductor is designed to operate continuously under a maximum current rating without causing any damage on the conductor itself or its surrounding insulation. Therefore, overhead lines and underground cables should not be overloaded more than their current-carrying capacities. To analyze the impact of PV systems on all lines and cables, Figure 4.12 is provided.

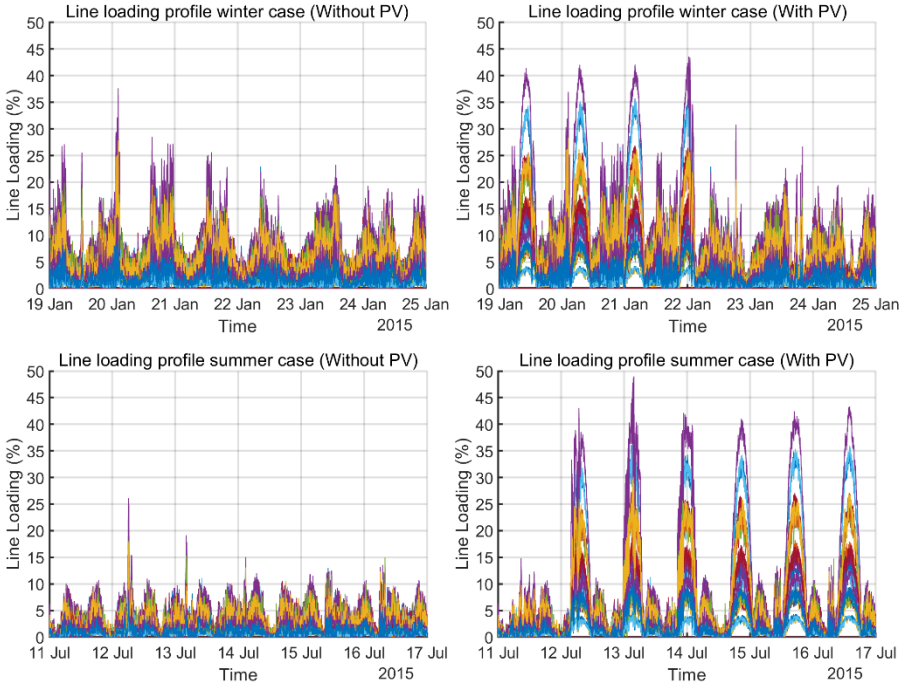

Figure 4.12 Line loading profiles including all lines and cables with and without PV penetration

As can be seen in the figure, PV systems increase the line loading up to 45% in winter and 50% in summer. According to the base loading, this corresponds to 20% and 30% increase in average for winter and summer cases respectively. It's important to note that these loading percentages are absolute values.

Due to PV systems change the direction of the current flow on the lines, the net contribution is actually more than these absolute values. For example, on the 20th of January, while the peak loading percentage due to consumption is around 37% in one direction, with PV systems the loading reaches 42% in the other direction which

corresponds to 79% net contribution from PV systems. Although these values are still within the safe limits, weaker lines may have some overloading problems especially in low consumption and high generation periods.

4.4.4. TRANSFORMER LOADING

End-users are interconnected to primary laterals via distribution transformers (service transformers) in secondary distribution grids. In the test system, 29 single-phase central-tapped distribution transformers (100 kVA each) are used to serve the 464 houses in total. Transformer loading profiles with and without PV systems are shown in Figure 4.13 for winter and summer cases, respectively.

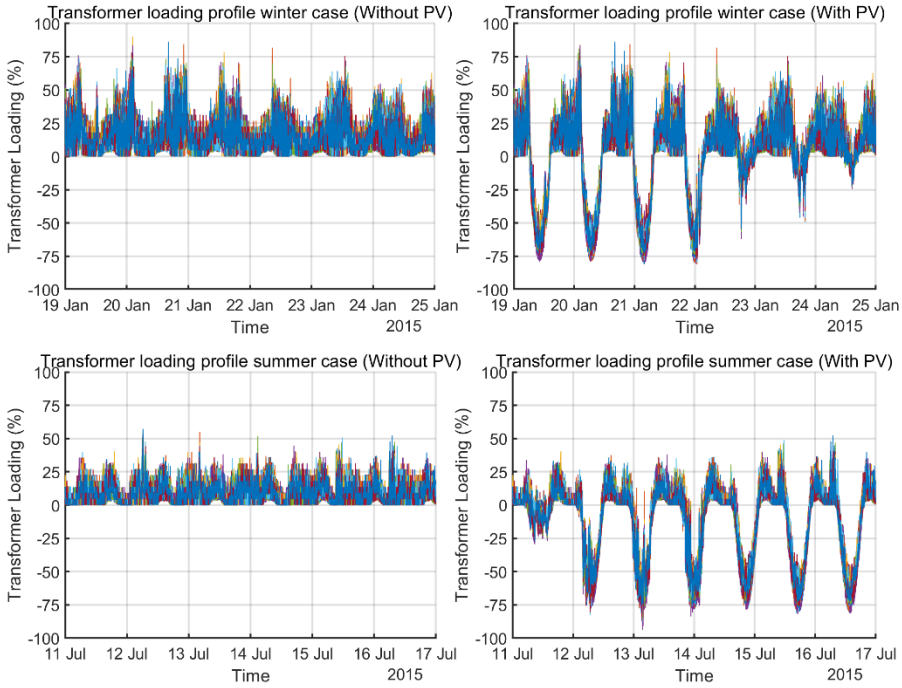

Figure 4.13 Transformer loading profiles including all secondary distribution transformers with and without PV penetration

Starting from the winter case, it can be observed that even without PV systems the transformer loadings may rise above 90% during the high consumption periods. With the integration of PV systems, generation offsets the consumption during the daylight and consequently, transformers are loaded in the opposite direction. To give an example, on the 20th of January, while the maximum loading is around 90% without PV systems, it becomes -80% due to high PV penetration. There is a huge net contribution as 170% from PV systems even in winter.

In summer periods due to an overall decrease in consumption, PV systems may push the loading levels up to 94%. Considering the peak loading is 54% without PV systems, the net contribution from PV systems have become 148% during the summer period. These high loading levels could be more severe in lower consumption and higher generation periods and damage the windings of transformers due to excessive heating.

4.4.5. SURPLUS POWER

Distribution systems are traditionally designed to draw power from subtransmission lines via substations. With the increase in PV penetration levels, powerflow has become bidirectional and now distribution systems may also inject power towards transmission lines. To investigate this phenomenon Figure 4.14 can be examined.

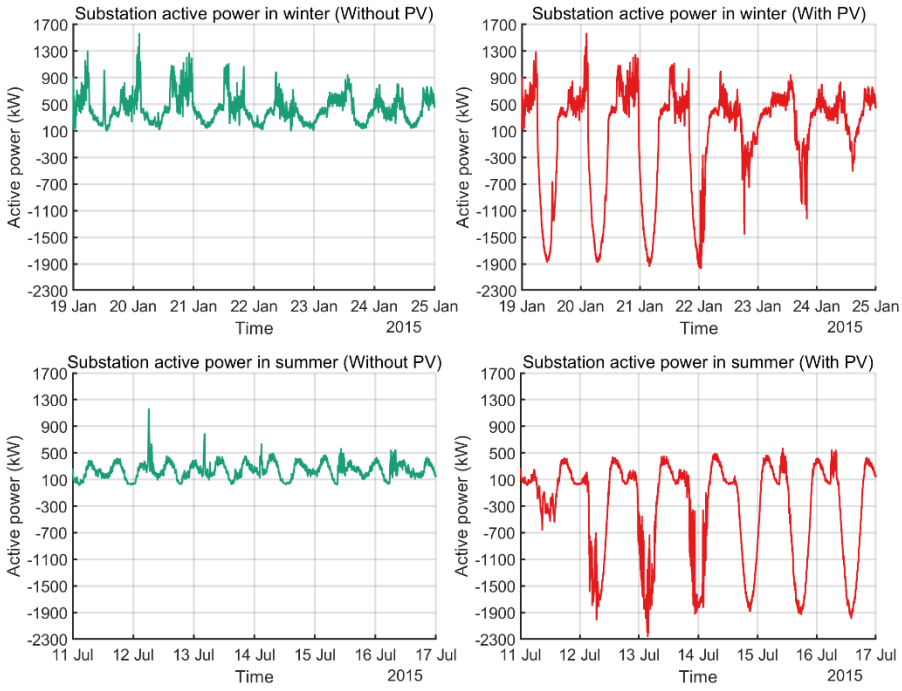

Figure 4.14 Voltage unbalance profiles of primary nodes with and without PV penetration

It can be seen that substantial amount of surplus power can be injected to the substation both in winter and summer periods. During the daylight, generation may overpass the consumption and consequently power can flow towards the subtransmission lines.

According to the quantitative results given in Table 4.2, PV systems cause a maximum surplus power injection of 1973 kW and 2270 kW in winter and summer, respectively. The net contribution from PV systems is approximately 3500 kW for both winter and summer periods.

Table 4.2 Substation active power with and without PV systems

	Winter		Summer	
	No PV	**PV**	**No PV**	**PV**
Max P_{drawn} (kW)	1570	1573	1169	577
Max $P_{injected}$ (kW)	0	-1973	0	-2270
PV contribution (kW)	-	-3543	-	-3439

Due to the peak load time do not coincide with the peak generation time in winter, PV systems do not contribute to reduce the peak load in winter. On the other hand, in summer, there happened some coincident and PV systems help to reduce the peak load by 592 kW.

4.4.6. POWER LOSS

Time-varying power loss profile with and without PV systems is illustrated in Figure 4.16 for the winter and summer case, respectively.

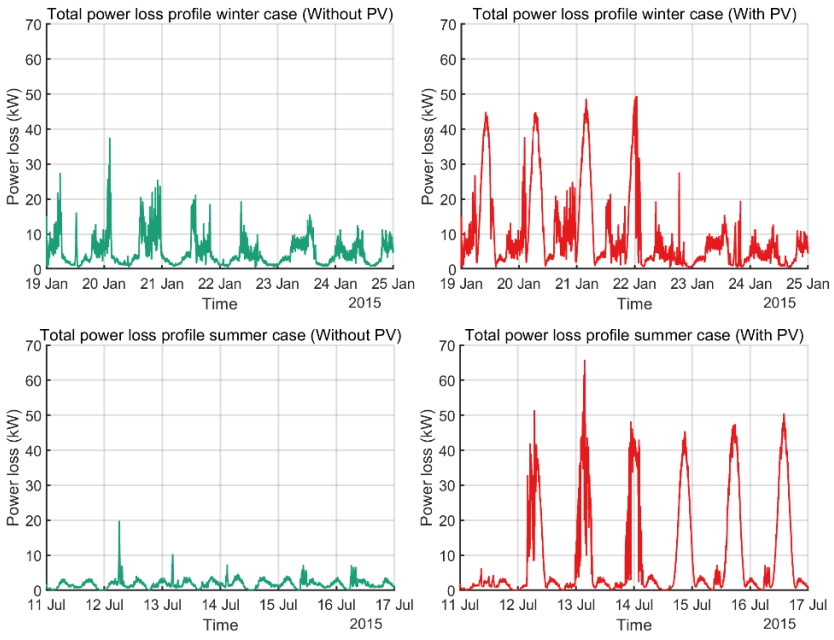

Figure 4.15 Total power loss profile with and without PV penetration

Total power loss in distribution systems is calculated by summing up the individual losses of overhead lines and underground cables, distribution transformers, and the voltage regulator. As can be seen from the figure, due to high PV penetration, power loss is significantly increased both in winter and summer periods. After the high PV penetration, maximum total loss is increased from 37 kW to 49 kW (1.32 times) in winter and from 19 kW to 65 kW (3.42 times) in summer.

4.4.7. STRESS ON VOLTAGE REGULATORS

To mitigate the voltage drops and rises in distribution grids, usually load tap changers and/or voltage regulators are used. Due to these devices have limited lifetime, number of tap changes should be kept as low as possible. The numbers of tap-changing count is given in Table 4.3 for the simulation cases.

Table 4.3 Number of tap-changing counts with and without PV systems

	Winter		**Summer**	
	No PV	**PV**	**No PV**	**PV**
Tap Change Phase A	1	16	0	5
Tap Change Phase B	1	14	1	5
Tap Change Phase C	3	18	1	7
Total	5	48	2	17

As can be seen from the table, the number of tap-changing operations are significantly increased after PVs are integrated to the system. While there were only 5 changes in winter case, it went up to 48 changes with PV systems. Similarly, number of changes in summer period is also increased from 2 to 17. It can be deduced that high PV penetration has an adverse impact on load tap changers and step voltage regulators.

4.5. SUMMARY AND DISCUSSION

In this chapter, technical impacts of high PV penetration is scrutinized in detail considering voltage variations, voltage unbalance, line and transformer loading, surplus power, power loss, and stress on voltage regulators. In the first part, a comprehensive overview is given about the PV integration challenges. It's stated that due to most PVs are interconnected to low-voltage distribution grids, there is a need for representing these grids as realistic as possible to evaluate the impacts more accurately. Therefore, in the second part, the distribution system is modeled as a whole including both primary and secondary sides. Then, the three-phase unbalanced powerflow technique is presented to make the sequential powerflow analysis using the generated time-series load and PV generation profiles as inputs. In the final stage, one by one technical impacts are analyzed and it's noticed that high PV penetration

may have some adverse impacts in distribution systems. Therefore, necessary measures should be taken in advance to achieve high PV penetration goals.

CHAPTER 5. REACTIVE POWER MANAGEMENT STRATEGIES TO MITIGATE THE VOLTAGE VARIATIONS

In this chapter, two different reactive power management strategies for PV inverters will be proposed to mitigate the voltage variations due to high PV penetration.

In the first strategy, it's aimed to reduce voltage rises by keeping the system complexity as minimum as possible. For the proposed method, only solar irradiance measurements are required from the weather stations. As in the traditional fixed power factor control strategies, individual local voltage or power measurements are not used. Therefore, it can replace the traditional fixed power factor control strategies by being as simple as them but still providing a more efficient and effective solution in terms of reducing the total number of tap changing operations, causing less line and transformer loadings, and also fewer power losses in average

In the second strategy, it's aimed to reduce both voltage rises and drops by providing inductive and capacitive power factors, depending on the net active power at the point of common coupling. To do so, system complexity is increased a bit and it's benefitted from individual local measurements as usually done in the traditional dynamic power factor control strategies. Considering weekly consumption and generation patterns, control parameters of PV inverters are adjusted and updated dynamically. While this strategy can mitigate the voltage variations successfully as the traditional dynamic power factor control methods, it outperforms them by further reducing the number of tap changing operations.

In the following sections, common technical solutions to mitigate the high PV penetration impacts are handled in detail with their advantages and disadvantages. Then, a very comprehensive literature review is provided. After that, traditional power factor control methods and proposed strategies are introduced respectively. Finally, the effectiveness of the proposed strategies is discussed and compared with the traditional counterpart methods.

5.1. TECHNICAL SOLUTIONS TO MITIGATE HIGH PV PENETRATION IMPACTS

Different solutions have been discussed and presented in the literature to mitigate the technical impacts of high PV penetration in distribution systems. These solutions may include

- Traditional voltage regulation devices such as on-load tap changers (OLTC), step voltage regulators (SVR), and switched capacitors (SC)
- Grid reinforcement
- Energy storage systems
- Demand-side management
- Active power curtailment
- Reactive power support

The main objective of the traditional voltage regulation devices, before the distributed generation sources are integrated into distribution grids, has been to compensate the voltage drops at the endpoints of the radial feeders. They are used to tolerate slow-changing voltage due to load variations over a longer timescale [116]. However, with the increase in PV penetration levels voltage variations have become more frequent and the inadequacy of these traditional devices to cope with the rapid voltage changes have appeared [117].

Utilities can also choose grid reinforcement option by increasing the conductor sizes of lines which in return will decrease the line resistance and consequently reduce the voltage variation impact of PV systems. Besides, service transformers may also be overloaded due to high reverse powerflow during low consumption and high generation periods. Therefore, transformers can also be replaced with bigger capacity variants. However, grid reinforcement solution is usually very costly and utilities usually see this as a measure of the last resort [118].

Although the capital cost of energy storage devices is still high nowadays, it may be a promising solution in the foreseeable future if the prices fall down to reasonable levels. Utilization of energy storage systems by grid operators is still very limited today due to regulatory frameworks which do not allow distribution system operators to directly own these devices [119]. On the other hand, residential and commercial customers may install batteries in conjunction with their PV systems and contribute to lessening high PV penetration impacts by limiting the active power injection to the electricity grid. However, as previously said the cost of the energy storage systems are still very high and should come down to affordable levels to become widespread.

Moreover, demand-side management techniques are also being proposed to better match the end-user consumption and generation profiles in an economical manner [120]. However, these techniques to a large extent depend on customers usage habits

which in nature are highly variable and include a great deal of uncertainty. Besides, without satisfactory incentives or benefits, there is no reason for end-users to change their usage habits and accordingly their comfort levels. Therefore, demand-side management option currently cannot be seen as a reliable solution for grid voltage control [121].

As it is well-known, R/X ratio is quite high in distribution grids, in other words, voltage is more sensitive to the active power variations than reactive power changes. Therefore, as a very effective solution, active power curtailment strategy can also be applied to mitigate high PV penetration impacts [122]. In this technique, some portion of the generated active power from PV systems is curtailed and not injected to the grid. However, this technique is economically not attractive to PV system owners which causes the spilling of generated solar energy. It can also lead to unfair curtailments and sometimes outages for producers who are located at the end of the feeders [123].

As another promising solution, reactive power support capabilities of PV inverters can be used to mitigate the rapid voltage variations. With the advances in power electronics and communication technologies, PV inverters have become so sophisticated that today they can provide ancillary services to the grid [124]. By choosing the inverter capacity a bit more, substantial amount of reactive power can be provided to the grid and voltage variations can be reduced [117]. National and international PV interconnection standards are currently being updated or have already been updated by technical committees to promote the reactive power support by utilizing PV inverters such as the new IEEE 1547-2018 standard [79].

Apart from these, distributed flexible AC transmission system devices (d-FACTs) such as Static VAr. compensator (SVC), dynamic voltage restorer (DVR), distributed static synchronous compensator (dSTATCOM), and unified power flow controller (UPFC) can also be installed. However, these devices are usually designed to be used in transmission systems and very expensive to be used in distribution systems [119].

It’s important to note that the aforementioned solutions can be applied individually or a few of them can be combined for a more effective solution. For example, OLTCs/SVRs and PV inverters can be used together to mitigate the slow and fast voltage variations, respectively. Or, PV inverters can be used for both active power curtailment and reactive power support at the same time. In the following section, a detailed literature review is provided for the studies which use individual or combined solutions, and they are also classified according to the adopted control infrastructure.

5.2. A COMPREHENSIVE LITERATURE REVIEW

Studies to mitigate high PV penetration impacts can be categorized into three main groups according to the applied control strategy as local control, centralized control, and decentralized control.

Briefly, local control is based on local power and/or local voltage measurements, and voltage regulation devices (PV inverters, OLTC, SVR, SC) do not need to communicate with each other or any central control unit. The second one, centralized control typically requires a central control unit which periodically gathers information from all available measurement points in the network and then optimizes the operating set-points of each controllable device and finally, sends these optimum set points back to the devices using a communication infrastructure. The last one, decentralized control divides the network into subnetworks and makes the optimization separately inside each subnetwork to determine the set-points of each controllable device with the minimum amount of information exchange between the subnetworks.

Starting from the local control studies, a location-dependent power factor control method is presented for the PV inverters combining two droop functions which are inherited from traditional cosφ(P) and Q(V) control to prevent the overvoltage problem [125]. A piecewise linear droop characteristic is used to determine the amount of reactive power injection as a function of measured voltage at the PV inverter connection point [118]. Technical and economic benefits of autonomous inverter control strategies are investigated and it is reported that with local PV inverter control strategies hosting capacity of the grid can be increased and also PV integration cost can be decreased [126]. A master/slave reactive power management scheme is proposed for voltage control utilizing OLTC for slow speed response, diesel generator for medium speed response, and PV/wind inverters for fast response [127]. Using historical voltage measurement of nodes and power production measurements of PV systems, piecewise constant and linear functions are optimized for Q(P) control with quadratic programming technique [128]. Two new VAr compensation methods are proposed to mitigate the fast voltage variations due to cloud transients by using the leftover capacity of PV inverter for reactive power control. While in the first method R/X ratio is used, in the second one Q/P sensitivity is used to change the power factor dynamically [96]. Active power curtailment is employed in conjunction with the droop based reactive power control to mitigate the overvoltage problem. Short term PV power forecast is used based on Kalman filter theory and on-site weather data [25]. During a critical system disturbance in the daytime, PV inverter is used as STATCOM by stopping active power injection and only providing reactive power until the disturbance is cleared [129]. Single point reactive power control method is presented by choosing only one node in the network and increasing the PV inverter capacity of that node substantially to cover the whole grid. Short circuit analysis is conducted to select the node [130]. Fuzzy logic control is used to dynamically change the reactive power of a three-phase PV inverter to compensate the fast voltage changes

[131]. A fair active power curtailment strategy is presented by optimizing the volt-watt control parameters for each PV inverter and then tested in a hardware-in-the-loop platform [26].

To continue with the centralized control studies, an adaptive VAr control algorithm is proposed to adjust the optimal reactive power values for each PV inverter. Adaptation comes from the choice of either power loss minimization or voltage regulation depending on the problem source at that moment [117]. An optimal powerflow study is conducted in a medium-voltage grid to determine the optimal reactive power references for all PV inverters. The method relies on active and reactive power measurements of all customers and producers in the grid [132]. An optimal active and reactive power dispatch strategy is proposed for PV inverters by minimizing power losses with ensuring the proper voltage regulation. A computationally affordable convex reformulation is derived by leveraging sparsity-promoting regularization approach for selection of PV inverters and also semidefinite relaxation technique is proposed to deal with the non-convexity of powerflow constraints [133]. A hierarchical control method is proposed which incorporates devices in succession until bringing voltage within allowable levels. STATCOM, battery energy storage system, reactive power support of PV inverters are activated one after another [134]. Another hierarchical control strategy is presented which tries to solve overvoltage problems by reactive power support of PV inverters first, then OLTC gets involved and finally active power is curtailed [135]. Two new reactive power compensation techniques are proposed to alleviate the overvoltage problem in LV distribution grids. While the first one is based on linear control scheme to equalize reactive power contribution of each PV inverter, the second one is based on a non-linear control scheme to also minimize the power loss in the network. It's reported that equal reactive power contribution does not solve the overvoltage problems at the end nodes of the feeders and for loss minimization usually, end nodes have to provide more reactive power support [136]. Operation of OLTC, SVR, and SCs are optimized with a centralized controller for long-timescale considering one-hour intervals and if PVs detect a significant reduction from the forecasted generation during that period, system switches to fast control mode until the output matches the forecast value. Nonconvex mixed integer nonlinear programming (MINLP) problem has been turned into the strictly convex quadratic programming problem by converting discrete variables into continuous variables [137]. A two-stage robust optimization model has been proposed to optimally dispatch active and reactive power setpoints of the selected PV inverters. While in the first stage subset of PV inverters which want to participate in ancillary service support is optimally selected, in the second stage, optimal setpoints are sent to the participating inverters considering the PV system active power output uncertainty [138]. Obtaining short term load and PV generation forecast at each 15-minute from the distribution system operator which includes the mean and variance values of active power injection, reactive power setpoints are dispatched to PV inverters by formulating the voltage regulation constraints as chance-constraints in the optimization problem [139]. A day-ahead optimal

scheduling method is presented to determine the set points of OLTC, SCs, and reactive power of PV inverters with 30-minute intervals over a 24 hour window. Multi-objective weights are determined with Edgeworth-Pareto optimization process and for the solution of the MINLP problem pattern search and genetic algorithms are proposed [140]. To mitigate the severe voltage variations due to PV ramp events, which may occur when solar irradiance suddenly changes because of cloud movements, a two-stage robust optimization based on intra-hour dispatch model is proposed for the coordination of OLTC and PV inverters with 1h horizon and 5min resolution. In the first stage, maximum admissible PV outputs and OLTC are co-optimized whereas, in the second stage, the feasibility of the first-stage decision variables is evaluated for any realization of PV ramp events [141]. Optimal power dispatch framework is proposed considering SVRs, SCs, PV inverters' active and reactive power setpoints in multi-phase unbalanced distribution systems. Power loss, active power curtailment, operation of SVRs and SCs are minimized to mitigate the voltage violations. Nonlinear and nonconvex optimal powerflow problem is solved based on the predictor-corrector primal-dual interior-point method which is affirmed to be more suitable for large systems in terms of convergence and scalability [142].

On the other hand, there are also a few decentralized control studies although not many as local and centralized studies but well worth to mention here. The distribution network is partitioned into clusters where each of them has some customer-owned PV systems and a single cluster energy manager (CEM). Using a decentralized optimization algorithm, i.e., the alternating direction method of multipliers (ADMM), operation of each cluster is optimized with a limited amount of information exchange (voltage related messages) between the clusters. By doing so, while the utility optimizes the network performance such as power loss minimization and voltage regulation, individual customers may also maximize their economic objectives such as minimizing their curtailed active power [122]. As in the previous study, the network is divided into subnetworks and ADMM is applied to realize the intra-regional optimization and inter-regional coordination. The nonconvexity introduced by SVRs is handled through the branch and bound method (BBM) by formulating the real value tap positions as linear inequality constraints [143]. A distributed control scheme is proposed by coordinating all PV inverters together to achieve the desired voltage profile in the grid. Nonconvex voltage regulation optimization problem is cast and solved based on a linearized model using a gradient descent based distributed scheme. In addition, a game-theoretic compensation scheme is proposed to incentivize the PV owners to provide voltage regulation [144]. A novel voltage support algorithm is developed based on distributed optimization and peer-to-peer communication of PV inverters. Jacobi-Proximal ADMM method is applied to optimize the required active power curtailment and reactive power support from each PV inverter. A push-sum gossip protocol is proposed to enable peer-to-peer data interchange between inverters [145].

Apart from these, there are also some hybrid control studies which are usually based on combination of the centralized and local control strategies. A hybrid control method is proposed where a centralized control unit optimizes the local PV control parameters considering different PV generation levels to deal with the uncertainty based on a 15-minute forecasted generation data. These local control functions are defined as piecewise linear functions which determine required active power curtailment and reactive power depending on the produced PV power locally. Central optimizer sends these optimal control parameters to each PV inverter and PV inverter choose the optimal set according to the instant production level at that moment [146]. A multi-objective genetic algorithm is used in a central unit to determine the optimal OLTC tap settings and reactive power curve parameters for PV inverters considering the traditional cosφ(P) and Q(V) local power factor controls [120]. Similar to the previous studies, curve parameters of two local control schemes, one for active power curtailment and the other one for reactive power support, are optimized using multi-objective particle swarm optimization in a central unit. Infrequent communication between the central controller and PV inverters such as one month is claimed to be sufficient [147]. A robust optimization framework is proposed taking into account the PV power uncertainty to update the local decision rules at each 15 to 30-minute time intervals. According to the linear decision rule, PV inverters adjust the reactive power contribution as a function of produced active power [148]. A two-stage voltage control strategy is proposed combining a central optimization and real-time local reactive power control. While in the first stage, OLTC, SC, and PV inverter setpoints are optimized based on 15-minute forecasted generation and load data, in the second stage, slope of the linear reactive power curve for each PV inverter is determined using a robust optimization framework to minimize the voltage deviations depending on the active power generation uncertainty in real-time [149].

Performance of the proposed control strategies is compared with each other considering different criteria as shown in Table 5.1.

Table 5.1 Performance comparison of the control strategies

Criteria	**Local control**	**Centralized control**	**Decentralized control**
Scalability	High	Low	Moderate
Communication requirement	Not necessary	High	High
Solution complexity	Low	Moderate	High
Global system optimality	Low	High	Moderate

To briefly summarize, local control is highly scalable by reason of its performance does not depend on the size of the network. Devices do not need to communicate with each other, and the solution complexity is very low. Devices operate independently and solution methodology only relies on the local measurements. The only drawback

of the local control is the global state of the network is usually not known, therefore solution can not guarantee the global optimality.

On the other hand, the centralized control has very low scalability. When the network grows, the amount of input data that should be handled by the central controller also grows and the computational efficiency decreases. It requires communication infrastructure which may increase the total system costs significantly. Due to devices only need to communicate with a central unit and do not need to communicate with each other, and also the optimization algorithms are well-developed, the system complexity is moderate. In terms of the global optimality, this type of control is best by virtue of handling all measurements at one place.

Decentralized control methods are actually being proposed to cope with the low scalability problem of centralized control. Although the scalability is not as high as local control, compared to centralized control it significantly increases the scalability of the solution. However, communication infrastructure requirement is still high and could be even more compared to the centralized one if peer-to-peer communication is required between the devices. Besides, the solution complexity is very high due to state-of-the-art optimization methods are needed. Lastly, studies have reported that global optimality performance is as not high as the centralized solution, getting closer for some cases.

Proposed reactive power management strategies in this chapter are based on local control which only relies on reactive power support by utilizing PV inverters. Therefore, traditional counterpart local reactive power control methods are also introduced in the following section.

5.3. TRADITIONAL LOCAL REACTIVE POWER CONTROL METHODS

To overcome voltage rise and frequent tap changing problems reactive power control capabilities of PV inverters can be utilized. The most used and preferred local reactive power control methods are shown in Figure 5.1. These methods can be classified as fixed (a) and dynamic power factor (b, c) control strategies.

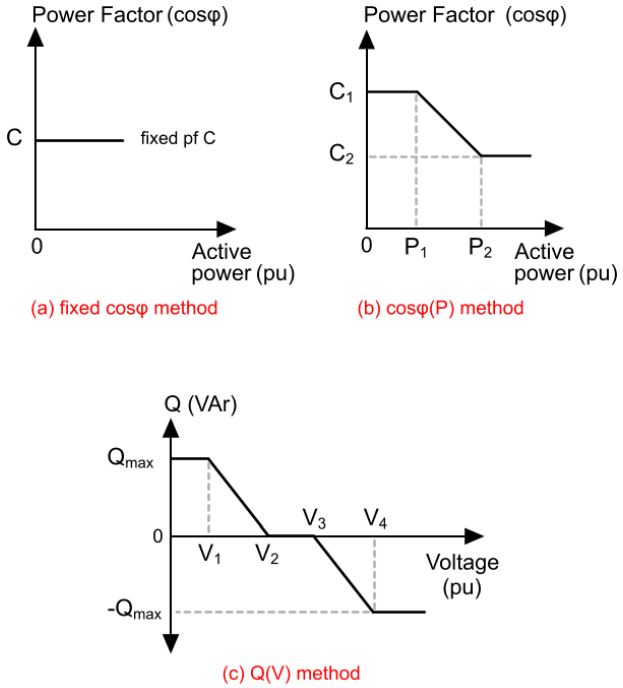

Figure 5.1 Traditional local reactive power control methods

In fixed cosφ method (a), power factor of the inverter is usually fixed to a predetermined value (C) aiming to reduce the voltage rise. The provided reactive power is proportional to the generated active power which can be obtained by

$$Q = C \times P \tag{5.1}$$

In cosφ(P) method (b), until a certain generated active power level (P_1), typically reactive power is not provided (C_1=1.0), after generated active power surpasses that predetermined P_1 level, power factor is linearly reduced up to the allowed minimum inductive power factor level (C_2). Even active generation continues to rise after this point, power factor stays constant at C_2 level. For any generated active power value (P), the corresponding power factor can be obtained by

$$\cos\varphi = \begin{cases} C_1, & P < P_1 \\ \dfrac{C_1 - C_2}{P_1 - P_2}\left(P - P_1\right) + C_1, & P_1 \le P \le P_2 \\ C_2, & P > P_2 \end{cases} \tag{5.2}$$

On the other hand, Q(*V*) method (c) does not depend on the generated active power parameter. Reactive power of the inverter is adjusted according to terminal voltage (*V*) of the connection point. In this method, not only inductive power factors but also the capacitive ones can be provided in case of any voltage drop events occur. For any measured terminal voltage, the corresponding reactive power amount can be obtained by

$$Q = \begin{cases} Q_{\max}, & V \le V_1 \\ \dfrac{Q_{\max}}{V_1 - V_2}\left(V - V_1\right) + Q_{\max}, & V_1 \le V < V_2 \\ 0, & V_2 \le V < V_3 \\ \dfrac{Q_{\max}}{V_3 - V_4}\left(V + V_3\right), & V_3 \le V < V_4 \\ -Q_{\max}, & V \ge V_4 \end{cases} \tag{5.3}$$

Fixed cosφ and cosφ(*P*) methods support grid voltage by only looking at the generated active power level. In these methods, it's assumed that grid voltage will always increase with the generated active power. Load variations are not considered in these methods. However, at some time periods where low generation meets high consumption, voltage drops can also be experienced. And, these methods may still think erroneously that voltage would be higher due to the generated PV active power. Related to this misbehavior, unnecessary reactive power absorption may occur which in return increase the power losses and component loading. These are the main drawbacks of the fixed cosφ and cosφ(*P*) methods [128].

On the other hand, Q(*V*) method does not rely on any active power measurements and always knows if the voltage is higher or lower at the connection point, so it behaves correctly to tolerate the voltage deviations. Yet, the biggest problem with this method is it may cause unequal reactive power provision among PV inverters depending on the difference of their locations in the grid. The inverters which are closer to the substation may experience fewer voltage variations than the ones which are closer to the end of the feeders. And consequently, inverters at the end of the feeder should provide more reactive power support to mitigate the voltage variations. This is the main drawback of the Q(*V*) method [125].

5.4. REACTIVE POWER MANAGEMENT STRATEGY I (RPMS-I)

The first technique is proposed to replace the traditional fixed power control strategies. As explained in the previous section, in these strategies, PV inverter is always operated at constant inductive power factor by aiming to reduce the voltage all the time at the maximum allowable power factor rate. However, that much power factor may not be necessary especially during the low generation times which may cause voltage drops. Considering this, a simple power factor regulation scheme is proposed in this section which regulates the inverter power factor in proportion to the solar irradiance measurements [150].

5.4.1. THE PROPOSED TECHNIQUE

The first technique only requires two solar irradiance components (global and diffuse horizontal irradiance) which can easily be obtained from weather stations. Instead of the fixed power factor, these solar irradiance measurements can be used to dynamically change power factor of the PV inverters. Despite the fact that the technique is proposed to replace fixed power factor strategies, it has the ability to regulate the power factor dynamically as in the cosφ(*P*) and Q(*V*) methods, yet individual local measurements, neither power nor voltage, are not needed in the proposed method. The power factor of all PV inverters can be regulated with the same solar irradiance measurements.

The power factor regulation scheme can be seen in Figure 5.2 (a). A simple linear curve is proposed to change the power factor of PV inverters depending on the estimated total solar irradiance (G_β).

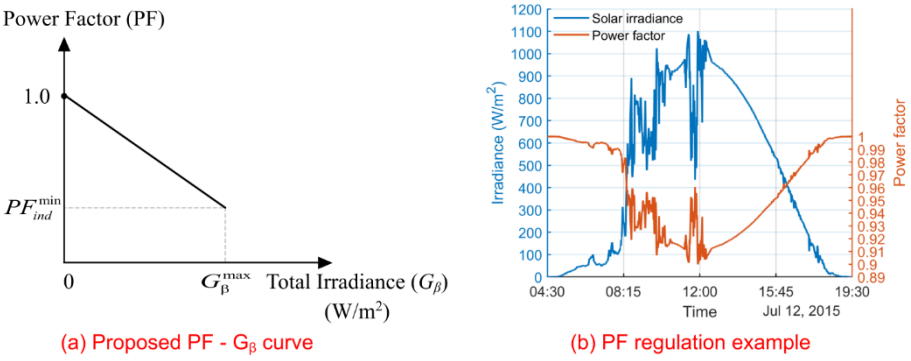

Figure 5.2 (a) Proposed power factor regulation scheme (RPMS-I), (b) power factor regulation example on a summer day

To estimate the total solar irradiance on tilted PV module surface, the process has been presented in Chapter 3. Two solar irradiance components which are measured

periodically for the horizontal surfaces can be obtained from meteorological stations and can be used to estimate the total solar irradiance. After estimation of G_β, the power factor can be obtained by

$$PF = 1.0 - \frac{1.0 - PF_{ind}^{\min}}{G_\beta^{\max}} G_\beta \tag{5.4}$$

where $PF_{ind}^{\min}$ variable indicates the allowed minimum inductive power factor limit which may vary depending on the grid codes. G_β represents the estimated total solar irradiance in W/m^2 where β subscript is used to specify the tilt angle of PV modules respected to the horizontal surface. $G_\beta^{\max}$ parameter shows the maximum total solar irradiance value that can fall onto PV module surfaces which is typically assumed to be 1000 W/m^2, but can be set to a different value depending on the historically recorded maximum values on the site location.

In Figure 5.2 (b), an example of the power factor regulation on a cloudy summer day is shown. As can be seen, during the low irradiance periods, which is usually the morning and evening hours, but also could be due to cloud coverage at any time instant during the day, power factor is approaching to unity power factor (1.0) due to low active power generation. On the other hand, when the irradiance approaches the maximum, the algorithm adjusts power factor to be close to the allowed minimum inductive power factor value which is predetermined to be 0.9 in the example.

5.4.2. SIMULATION SETUP AND CASES

As introduced in Chapter 4, a modified IEEE 13 bus distribution grid has been used as the simulation testbed with the integrated secondaries. A total number of 464 residential prosumers are modeled and each house is equipped with HVAC, EWH, and lighting loads, and a PV system of which generation capacity is randomly chosen between 4 and 8 kW. In addition, for each existing phase of a primary node, a single-phase central-tapped transformer (service transformer) has been installed to form a single-phase triplex node system. The capacity of each service transformer (100 kVA) is chosen to be able to serve 16 houses. Time-series load and PV profiles are used in the simulations which are generated in one-minute resolution with the modeling approach explained in Chapter 2 and Chapter 3, respectively.

Four different cases are considered as given in Table 5.3. The first one is base case where there is not any PV penetration in the grid, the second one represents the common fit-and-forget approach where PVs are operated at unity power factor without any reactive power support. The third case is commonly used fixed cosφ control where a constant inductive power factor is used and fixed at 0.9. Finally, the last case is the proposed method which is called as the reactive power management strategy I (RPMS-I).

Table 5.2 Simulation cases

Cases	Definition	Parameters
Base	No PVs in the grid	-
Fixed pf 1.0	PVs are connected without reactive power support	$C = 1.0$
Fixed pf 0.9	Fixed cosφ control (constant power factor)	$C = 0.9$
The proposed method (RPMS-I)	cosφ(G_β) control (dynamic power factor)	$PF_{ind}^{\min} = 0.9$ $G_\beta^{\max} = 1000$

One random week is chosen for both winter and summer and three-phase powerflow analysis is performed for these periods. Results are given and interpreted in the next section.

5.4.3. RESULTS

Results will be analyzed considering primary and secondary voltages profiles, line and service transformer loadings, stress on the voltage regulator (number of tap changes), and also total power loss in the following subsections.

5.4.3.1 Primary and secondary node voltages

Individual phase voltage profiles of one of the primary grid nodes choosing a random day from the whole simulation period are shown in Figure 5.3.

As can be seen, the voltage rises more in the fixed pf 1.0 case than the others which sometimes overpasses 1.02 p.u. limit when only ±2% regulation is allowed in the primary nodes. On the other hand, fixed pf 0.9 method and RPMS-I are becoming very successful to prevent overvoltage issues. Due to RPMS-I does not cause unnecessary voltage drops in low generation periods, it performs better compared to the fixed pf 0.9 method. When the generation increases especially at noon times, RPMS-I method starts to behave like fixed pf 0.9 method and allows inverters to work close to the allowable inductive power factor limit to reduce the voltage.

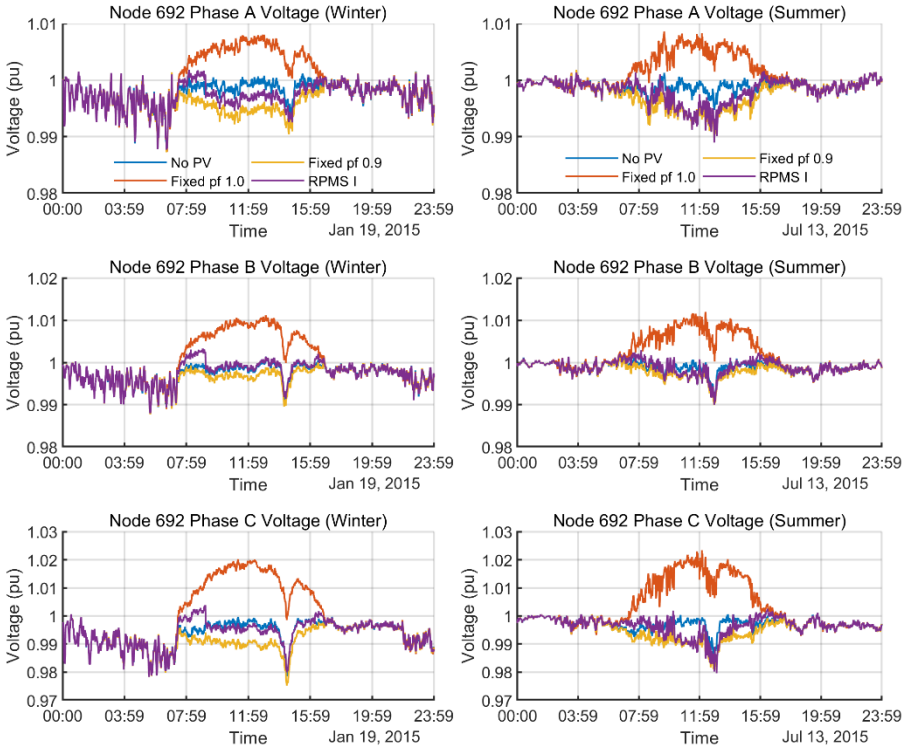

Figure 5.3 Voltage profile of a primary grid node (Node 692) in winter (left) and summer (right)

Voltage metrics which measures the performance of the methods are given in Table 5.3 which includes all primary grid nodes and one week simulation period for both winter and summer cases.

Table 5.3 Performance comparison with voltage metrics in the primary distribution grid

Voltage Impact Metrics	**Primary Distribution Grid (Winter)**				**Primary Distribution Grid (Summer)**			
	No PV	**PF 1.0**	**PF 0.9**	**RPMS-I**	**No PV**	**PF 1.0**	**PF 0.9**	**RPMS-I**
$V_{rise\_violation}$ (total)	0	856	0	0	0	1390	0	0
$V_{drop\_violation}$ (total)	57	20	93	26	34	0	187	169
$V_{deviation}$	0.98	5.16	4.70	1.83	0.98	7.64	6.87	4.37

As can be seen in the table, both fixed pf 0.9 and RPMS-I methods successfully mitigate all voltage rise violations compared to the no reactive power control case (fixed pf 1.0). On the other hand, due to consumption profiles are not taken into

account, both reactive power control methods may sometimes cause voltage drops. Proposed RPMS-I method improves this drawback compared to the fixed pf 0.9 method and by causing fewer voltage drops and also more successful reducing the voltage deviations.

In Figure 5.4, the voltage profiles of two randomly chosen houses which are located in secondaries are shown for both winter and summer cases.

As can be seen, the secondary nodes are more vulnerable to voltage variations than primary grids. If no reactive power control is applied, voltages at some houses can rise up to 1.04 p.u. which is well above the ±3% regulation limit. On the other hand, with both fixed pf 0.9 and RPMS-I methods, voltage rises can be mitigated also in the secondary distribution grids. Compared to the fixed pf 0.9 method, proposed RPMS-I method is becoming more successful to reduce the undesired voltage drops in secondaries.

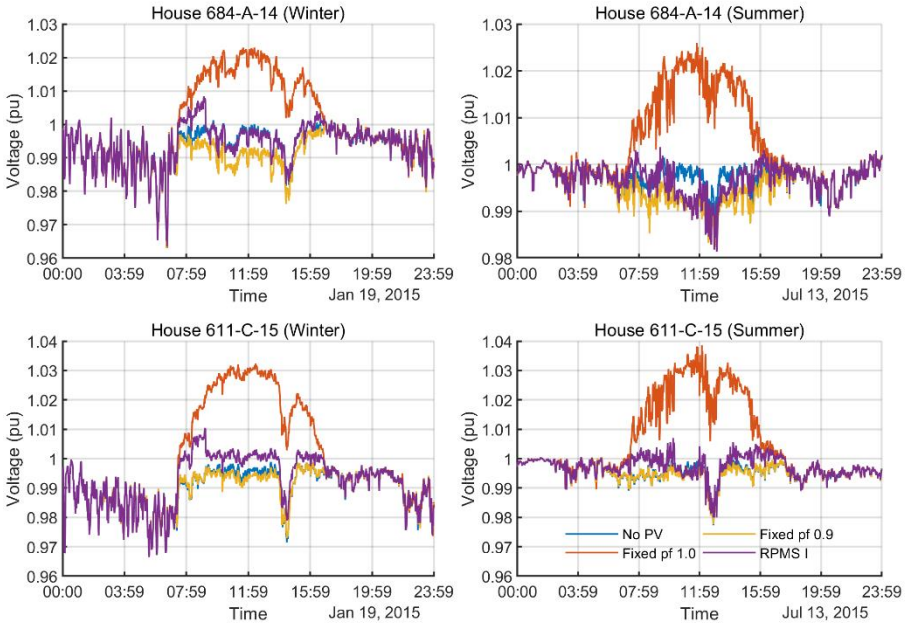

Figure 5.4 Voltage profile of two random houses in secondaries in winter (left) and summer (right)

Voltage metrics which measures the performance of the methods including the whole secondary distribution grid nodes are given in Table 5.4 for both winter and summer cases.

Similar to the primary grid results, both fixed pf 0.9 and RPMS-I methods successfully mitigate all voltage rise violations compared to the no reactive power control case

(fixed pf 1.0). Due to the nature of inductive power factor control methods, sometimes voltage drops are also experienced in secondary distribution grids. RPMS-I reduces this drawback compared to the fixed pf 0.9 method and cuts almost half of these drops. Lastly, according to the voltage deviation index, RPMS-I method performs better than the fixed pf 0.9 method in voltage deviation reduction.

Table 5.4 Performance comparison with voltage metrics in the secondary distribution grid

Voltage Impact Metrics	**Secondary Distribution Grid (Winter)**				**Secondary Distribution Grid (Summer)**			
	No PV	**PF 1.0**	**PF 0.9**	**RPMS-I**	**No PV**	**PF 1.0**	**PF 0.9**	**RPMS-I**
$V_{rise\_violation}$ **(total)**	0	32951	0	0	0	50929	0	0
$V_{drop\_violation}$ **(total)**	631	215	504	261	452	0	423	239
$V_{deviation}$	50.0	303.1	77.8	72.4	49.7	455.6	100.8	86.0

5.4.3.2 Line loadings

Average and maximum line loading ratios including all lines and cables in the grid are given in Table 5.5 and Table 5.6 for winter and summer cases, respectively.

First of all, it can be deduced that reactive power control mechanisms always cause an increase in line loading ratios compared to the pure active power injection method. It can be seen that both fixed pf 0.9 and RPMS-I methods increase the maximum loading ratios by 5-8% compared to fixed pf 1.0 method.

Table 5.5 Average and maximum line loading ratios in winter

Cases	**Winter (average)**			**Winter (maximum)**		
	I_{a_avg} **(%)**	I_{b_avg} **(%)**	I_{c_avg} **(%)**	I_{a_max} **(%)**	I_{b_max} **(%)**	I_{c_max} **(%)**
NO PV	1.71	1.66	2.35	23.3	20.0	25.6
PF 1.0	4.85	4.55	6.30	35.7	35.9	43.6
PF 0.9	5.79	5.42	7.57	41.0	41.9	51.0
RPMS-I	5.20	4.87	6.78	40.7	41.5	50.6

On the other hand, no matter what type of control is chosen, maximum line loading ratios have never reached critical levels. Although the difference between the fixed pf 0.9 and RPMS-I method is not that significant, the proposed method causes less line loading compared to the fixed pf 0.9 method.

Table 5.6 Average and maximum line loading ratios in summer

Cases	Summer (average)			Summer (maximum)		
	I_{a_avg} (%)	I_{b_avg} (%)	I_{c_avg} (%)	I_{a_max} (%)	I_{b_max} (%)	I_{c_max} (%)
NO PV	1.57	1.40	2.00	20.8	23.1	26.1
PF 1.0	5.12	4.85	6.74	40.8	40.1	49.0
PF 0.9	6.14	5.78	8.09	46.6	45.9	57.0
RPMS-I	5.71	5.38	7.52	46.2	45.7	57.0

To visually compare the line loading performances, Figure 5.5 is also provided which shows the main feeder loading profiles.

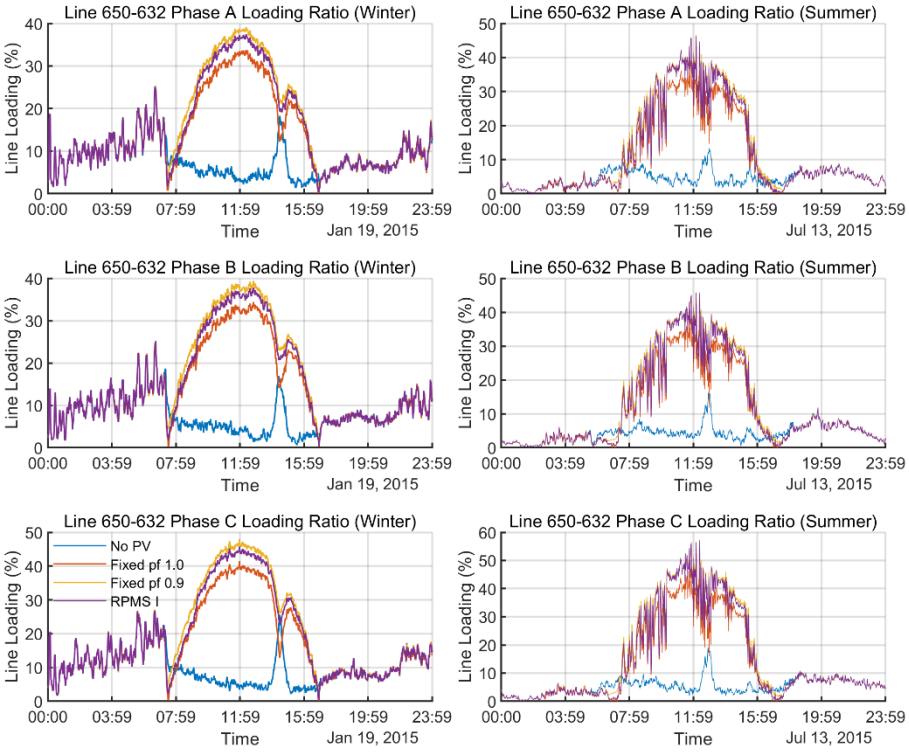

Figure 5.5 Line loading profile of the main feeder line in winter (left) and summer (right)

As can be seen in the figure, loading ratios usually reach the peak values around the noon hours. While fixed pf 1.0 method is the best in terms of line loading criteria, among reactive power control methods, the proposed one gives slightly better performance than the fixed pf 0.9 method.

5.4.3.3 Service transformer loadings

Recorded average and maximum loading ratios including all service transformers are given in Table 5.7. In addition, for two randomly selected service transformers, loading profiles are illustrated in Figure 5.6.

Table 5.7 Average and maximum transformer loading ratios in winter and summer

Cases	Winter		Summer	
	S_{avg}(%)	S_{max}(%)	S_{avg}(%)	S_{max}(%)
NO PV	10.1	69.3	8.8	57.2
PF 1.0	-23.3	-81.1	-27.5	-93.6
PF 0.9	-27.8	-91.6	-32.4	-99.5
RPMS-I	-25.6	-91.0	-30.4	-99.1

* - sign indicates the reverse powerflow

Similar to the line loading results, reactive power control methods also cause an increase in transformer loading ratios compared to the pure active power injection method which can reach up to 10% as experienced in the winter case. As can be seen in the figure, the loading ratio gets higher around noon hours due to high reverse powerflow. On the other hand, proposed RPMS-I method gives slightly better performance compared to the fixed pf 0.9 method in terms of fewer loading ratios.

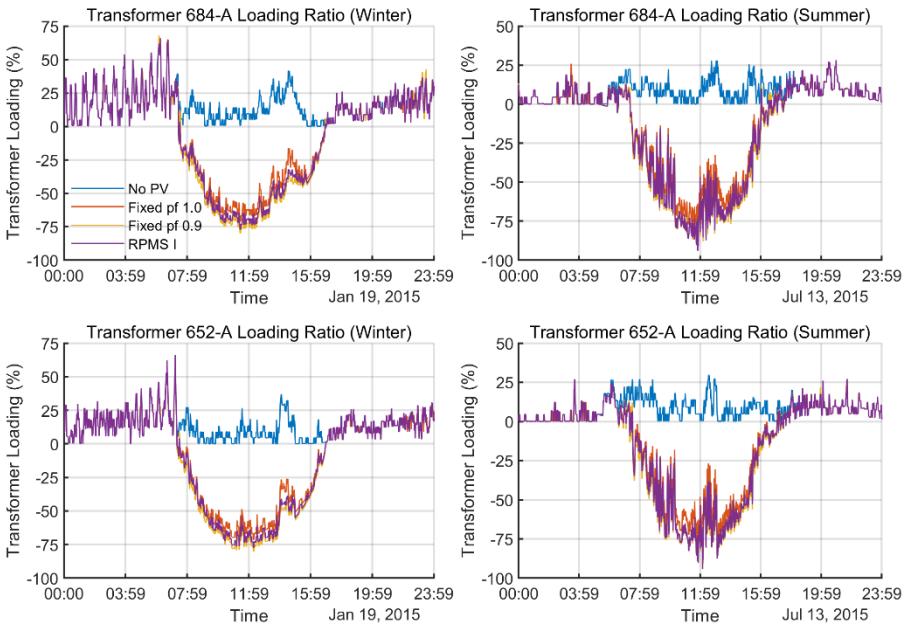

Figure 5.6 Loading profile of two random transformers in winter (left) and summer (right)

5.4.3.4 Stress on the voltage regulator

The performances of the methods are also compared in terms of their impacts on step voltage regulator (SVR) tap changing operation. Total number of tap changes considering each phase individually are given for one-week winter and summer simulation periods in Table 5.8.

Table 5.8 Total number of SVR tap changing operations in winter and summer

Cases	Winter				Summer			
	Phase A	Phase B	Phase C	Total	Phase A	Phase B	Phase C	Total
NO PV	1	1	3	5	0	1	1	2
PF 1.0	16	14	18	48	5	5	7	17
PF 0.9	1	1	3	5	2	2	3	7
RPMS-I	1	1	3	5	2	2	3	7

First of all, it can be deduced that in the case of high PV penetration without reactive power support, number of tap changes of the SVR significantly increases. On the other hand, both reactive power control methods contribute to relieving the stress on the SVR. None of the methods are superior to each other, they equally reduce the tap changing counts.

5.4.3.5 Power loss

Recorded average and maximum power loss values considering one-week winter and summer periods are given in Table 5.9.

Table 5.9 Recorded average and maximum power loss in winter and summer

Cases	Winter		Summer	
	$PL_{\_avg}$ (kW)	$PL_{\_max}$ (kW)	$PL_{\_avg}$ (kW)	$PL_{\_max}$ (kW)
NO PV	2.46	21.96	1.92	19.86
PF 1.0	14.36	49.44	15.73	65.86
PF 0.9	19.53	68.51	21.61	86.94
RPMS-I	16.44	68.18	19.51	86.71

It can be seen that reactive power control methods also cause an increase in power loss compared to the pure active power injection method. On the other hand, the proposed RMPS-I method achieves to reduce average and maximum power loss a few

kW more compared to the fixed pf 0.9 method. Maximum power loss values are very close to each other due to at peak generation periods RPMS-I method tries to absorb maximum allowable reactive power as the fixed pf 0.9 method. In order to compare the methods visually, Figure 5.7 is also provided. Although it is not easy to distinguish results in summer case, it can be clearly seen from the winter case that RPMS-I method achieves to reduce power loss compared to the fixed pf 0.9 method.

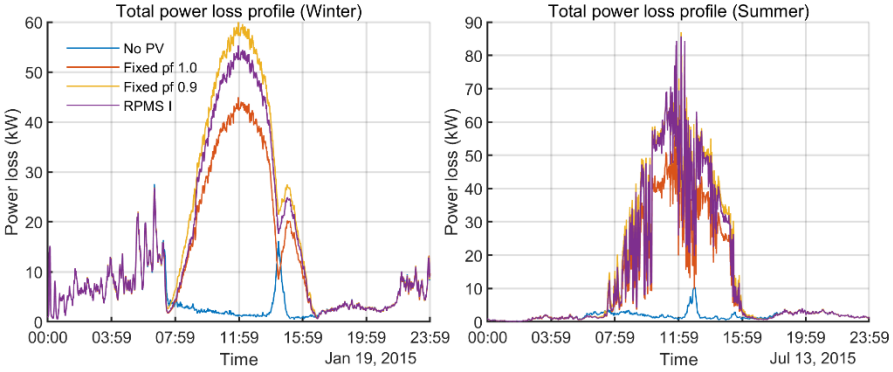

Figure 5.7 Total power loss profile in winter (left) and summer (right)

5.4.4. DISCUSSION AND CONCLUSION

In this section, a simple power factor control strategy is proposed for PV inverters as a competitor to traditional fixed power factor control strategy. The new method does not require any individual local power or voltage measurements, therefore the system complexity is kept as simple as possible. It only relies on solar irradiance measurements which can easily be obtained from the weather stations. Compared to the fit-and-forget approach both traditional and proposed methods are successful to mitigate the voltage rises. In addition, both methods have the ability to reduce the number of tap changing operations on step voltage regulators. However, due to local consumption patterns are not taken into account in both methods, at some instants small voltage drops may also be seen due to only providing inductive power factors. Considering this, the proposed method performs better than the traditional fixed power factor method by reducing the voltage drops to some extent. On the other hand, as the main drawbacks of the reactive power control strategies, loading ratios of lines and transformers, and also power losses are generally increased a bit compared to the pure active power injection. In this context, proposed method has performed better than the constant power factor control method by reducing the average line and transformer loadings, and also the average power losses in the grid.

5.5. REACTIVE POWER MANAGEMENT STRATEGY II (RPMS-II)

The second technique is proposed in an attempt to reduce both voltage rises and voltage drops. To do so, PV inverters are operated to be able to provide both inductive and capacitive power factors depending on the net active power. In this case, as in the other traditional dynamic power factor control methods, individual local measurements are used. Benefitting from the instantaneous imbalance of load and generation, a novel dynamic power factor control strategy is proposed [151].

5.5.1. THE PROPOSED TECHNIQUE

Voltage drops usually happen at low-generation and high-consumption periods. Sometimes, cloud coverage can also reduce the generation significantly which may cause sudden voltage drops even though the consumption levels do not change considerably. Power factor control strategies which only provide inductive power factors cannot mitigate this problem, on the contrary, they may even increase the severity of this issue. To solve this, reactive power control strategies either should watch the local voltages directly as in the traditional Q(*V*) method or check the generation/consumption balance to have an indirect idea about the voltage. The latter approach has been considered in this part by measuring the net active power at the connection point.

The proposed power factor regulation scheme can be seen in Figure 5.8.

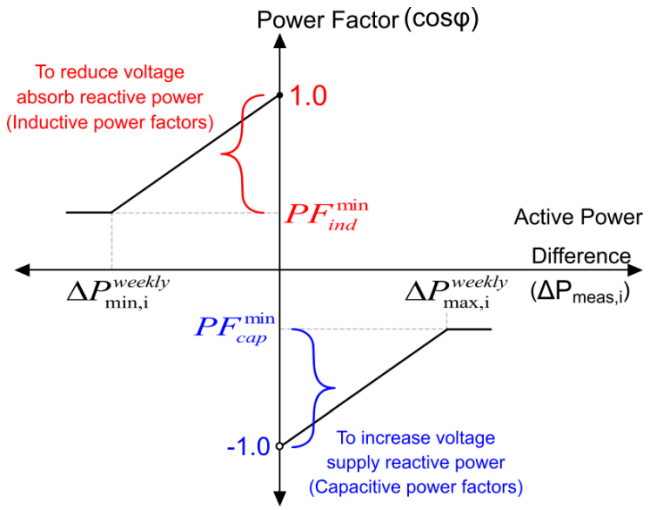

Figure 5.8 Proposed power factor control scheme (RPMS-II)

In Figure 5.8, $\Delta P_{meas,i}$ represents measured net active power of the i^{th} house in the grid. The negative sign for $\Delta P_{meas,i}$ indicates that generation ($P_{G,i}$) is bigger than the consumption ($P_{L,i}$), whereas the positive sign indicates quite the opposite which shows the situation that consumption is bigger than the generation.

$\Delta P_{\min,i}^{weekly}$ and $\Delta P_{\max,i}^{weekly}$ parameters represent the weekly recorded minimum and maximum active power differences of the i^{th} house, respectively. These parameters are dynamically being updated for each house to take weekly load and generation pattern into account.

According to the reactive power control scheme, the instantaneous power factor of PV inverters can be determined by

$$\Delta P_{meas,i} = P_{L,i} - P_{G,i} \tag{5.5}$$

$$PF_{new,i} = \begin{cases} PF_{ind}^{\min}, & \Delta P_{meas,i} < \Delta P_{\min,i}^{weekly} \\ 1.0 + \Delta P_{meas,i} \dfrac{PF_{ind}^{\min} - 1.0}{\Delta P_{\min,i}^{weekly}}, & \Delta P_{\min,i}^{weekly} \le \Delta P_{meas,i} < 0 \\ 1.0, & \Delta P_{meas,i} = 0 \\ -1.0 + \Delta P_{meas,i} \dfrac{PF_{cap}^{\min} - (-1.0)}{\Delta P_{\max,i}^{weekly}}, & 0 < \Delta P_{meas,i} \le \Delta P_{\max,i}^{weekly} \\ PF_{cap}^{\min}, & \Delta P_{\max,i}^{weekly} < P_{meas,i} \end{cases} \tag{5.6}$$

Where

$$\Delta P_{\min,i}^{weekly} = \min\left\{\Delta P_{meas,i}^{k} \quad k = 1,2,\ldots,7\right\} \tag{5.7}$$

$$\Delta P_{\max,i}^{weekly} = \max\left\{\Delta P_{meas,i}^{k} \quad k = 1,2,\ldots,7\right\} \tag{5.8}$$

Here, it is important to note that the relation between power factor and measured net active power assumed to be linear. In addition, to comply with the requirements of each country's specific grid codes, power factor is not allowed to go beyond predefined minimum inductive ($PF_{ind}^{\min}$) and capacitive power factor ($PF_{cap}^{\min}$) values.

5.5.2. SIMULATION SETUP AND CASES

The same simulation setup is used as explained detailly in section 5.4.2, so it is not repeated here.

On the other hand, five different simulation cases are considered as given in Table 5.10. The first one is the base case where there is not any PV penetration in the grid, the second one represents the common fit-and-forget approach where PVs are operated at unity power factor without providing any reactive power support. The third case is the traditional Volt/Var control scheme where reactive power is regulated depending on local voltage. The fourth case is the traditional cosφ(P) control where power factor is regulated depending on the active power generation. And finally, the last case is the proposed method (RPMS-II) which regulates the power factor depending on the net active power.

Table 5.10 Simulation cases

Cases	**Definition**	**Parameters**
Base (No PV)	No PVs in the grid	-
Fixed pf 1.0	PVs are connected without reactive power support	$C = 1.0$
Q(V)	Voltage dependent control (dynamic power factor)	$V_1 = 0.98$, $V_2 = 0.99$ $V_3 = 1.01$, $V_4 = 1.02$ $PF = \{(-1.0, -0.9], [0.9, 1.0]\}$
Cosφ(P)	Active power generation dependent control (dynamic power factor)	$P_1 = 0.5$ p.u. $P_2 = 1.0$ p.u. $C_1 = 1.0$ $C_2 = 0.9$
The proposed method (RPMS-II)	PF(ΔP) net active power dependent control (dynamic power factor)	$PF_{ind}^{\min} = 0.9$ $PF_{cap}^{\min} = -0.9$ $\Delta P_{\min,i}^{weekly}$ and $\Delta P_{\max,i}^{weekly}$ are changed weekly for each house individually

One random week is chosen considering both winter and summer cases and three-phase powerflow analysis is performed for these periods. Results are given and interpreted in the next section.

5.5.3. RESULTS

Results are analyzed considering primary and secondary node voltages profiles, line and service transformer loadings, stress on the voltage regulator (number of tap changes), and also the total power loss in the following subsections.

5.5.3.1 Primary and secondary node voltages

Individual phase voltage profiles of one of the primary grid nodes choosing a random day from the whole simulation period are shown in Figure 5.9.

Compared to the fixed pf 1.0 case, all dynamic power factor control methods successfully mitigate the voltage rises and maintain it below the 1.02 p.u. limit. In addition, during the daylight hours when PVs generate active power, none of the dynamic methods seems to cause voltage drops as seen in the figure for these particular winter and summer days.

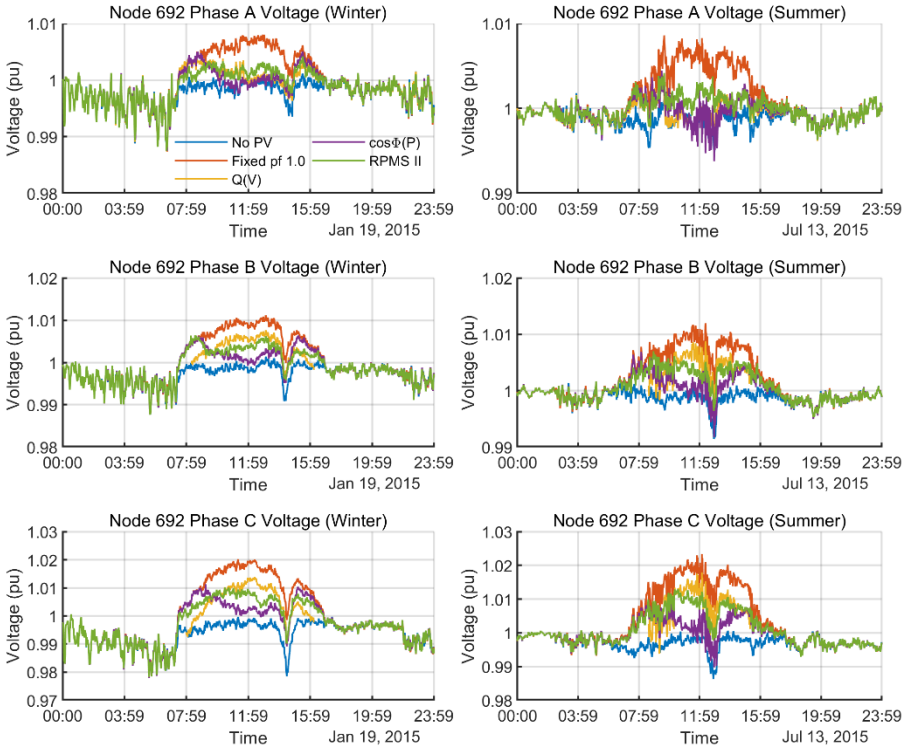

Figure 5.9 Voltage profile of a primary grid node (Node 692) in winter (left) and summer (right)

To be able to compare the methods quantitatively, Table 5.11 and 5.12 are given for the winter and summer cases, respectively. Still, during one-week simulation periods, neither in winter nor in summer, voltage rises are not experienced. However, some small number of voltage drops are recorded in the winter case. It's because of morning and evening hours where sometimes generation almost falls to zero and consumption reaches very high values. On the other hand, the performances of the Q(V), cosφ(P), and proposed methods are very close to each other. The difference is not much to

make a fair grading, but they all perform well to mitigate the variations in the primary nodes.

Table 5.11 Comparison with voltage metrics including all nodes in the primary grid (winter)

Voltage Impact Metrics	**Primary Distribution Grid (Winter)**				
	No PV	**PF 1.0**	**Q(V)**	**Cosφ(P)**	**RPMS-II**
$\mathbf{V_{rise\_violation}}$ **(total)**	0	856	0	0	0
$\mathbf{V_{drop\_violation}}$ **(total)**	57	20	14	15	18
$\mathbf{V_{deviation}}$	0.9881	5.1682	1.20	1.24	1.17

Table 5.12 Comparison with voltage metrics including all nodes in the primary grid (summer)

Voltage Impact Metrics	**Primary Distribution Grid (Summer)**				
	No PV	**PF 1.0**	**Q(V)**	**Cosφ(P)**	**RPMS-II**
$\mathbf{V_{rise\_violation}}$ **(total)**	0	1390	0	0	0
$\mathbf{V_{drop\_violation}}$ **(total)**	34	0	0	0	0
$\mathbf{V_{deviation}}$	0.98	7.64	1.70	1.53	1.63

To continue with the secondaries, Figure 5.10 is provided which shows the voltage profiles of two randomly chosen houses. Moreover, Table 5.13 and Table 5.14 are given to be able to compare the methods with voltage quality metrics.

Except the fixed pf 1.0 strategy, all dynamic power factor control methods can successfully mitigate the voltage variations in secondaries as in the primary grid. The voltage drops seen in winter case are due to morning and evening hours as explained in the primary grid evaluation part. On the other hand, according to the voltage deviation index, it seems that Q(V), cosφ(P), and RPMS-II methods are performing very close to each other. The small difference between them may be insignificant in real-life application.

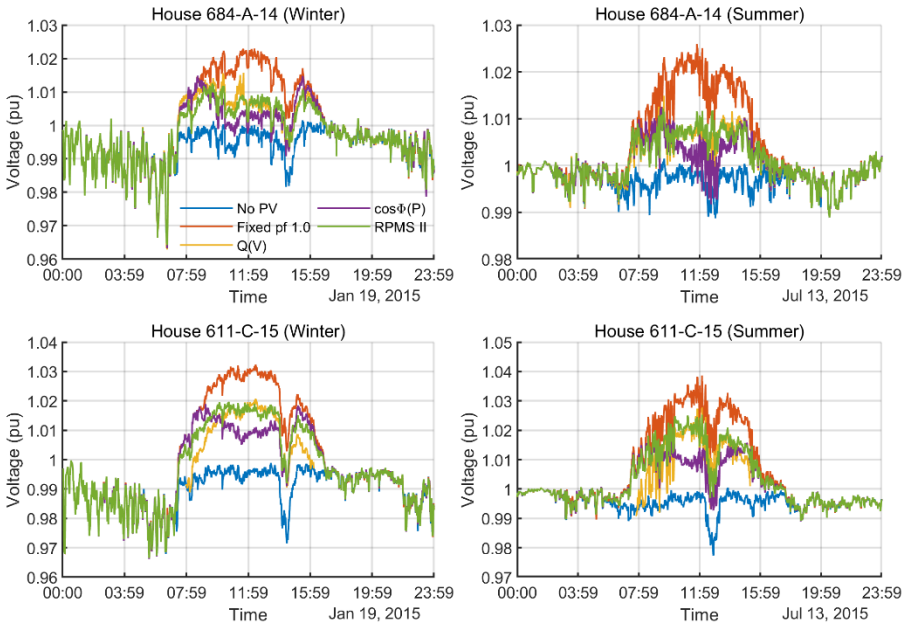

Figure 5.10 Voltage profile of two random houses in secondaries in winter (left) and summer (right)

Table 5.13 Comparison with voltage metrics including all nodes in secondaries (winter)

Voltage Impact Metrics	**Primary Distribution Grid (Winter)**				
	No PV	**PF 1.0**	**Q(V)**	**Cosφ(P)**	**RPMS-II**
$V_{rise\_violation}$ (total)	0	32951	0	0	0
$V_{drop\_violation}$ (total)	631	215	183	202	202
$V_{deviation}$	50.07	303.10	82.68	80.93	87.81

Table 5.14 Comparison with voltage metrics including all nodes in secondaries (summer)

Voltage Impact Metrics	**Primary Distribution Grid (Summer)**				
	No PV	**PF 1.0**	**Q(V)**	**Cosφ(P)**	**RPMS-II**
$V_{rise\_violation}$ (total)	0	50929	0	0	0
$V_{drop\_violation}$ (total)	452	0	0	0	0
$V_{deviation}$	49.70	455.69	110.27	104.82	114.37

5.5.3.2 Line loadings

Average and maximum line loading ratios including all lines and cables in the grid are given in Table 5.15 and Table 5.16 for winter and summer cases, respectively.

Table 5.15 Average and maximum line loading ratios in winter

Cases	Winter (average)			Winter (maximum)		
	I_{a_avg} (%)	I_{b_avg} (%)	I_{c_avg} (%)	I_{a_max} (%)	I_{b_max} (%)	I_{c_max} (%)
NO PV	1.71	1.66	2.35	23.33	20.09	25.66
PF 1.0	4.85	4.50	6.10	34.71	34.90	42.62
Q(V)	4.92	4.55	6.29	36.48	35.81	43.53
Cosφ(P)	5.07	4.77	6.57	38.44	39.10	46.80
RPMS-II	5.02	4.70	6.51	37.23	36.98	44.84

Table 5.16 Average and maximum line loading ratios in summer

Cases	Summer (average)			Summer (maximum)		
	I_{a_avg} (%)	I_{b_avg} (%)	I_{c_avg} (%)	I_{a_max} (%)	I_{b_max} (%)	I_{c_max} (%)
NO PV	1.57	1.40	2.00	20.84	23.18	26.12
PF 1.0	5.12	4.80	6.67	40.89	38.12	47.00
Q(V)	5.21	4.84	6.73	41.92	39.96	48.81
Cosφ(P)	5.40	5.11	7.08	45.26	44.73	54.63
RPMS-II	5.28	4.99	6.94	41.82	41.26	50.06

As can be seen from the tables, although average line loading ratios are more or less same for all PV penetration cases, when reactive power is provided maximum loading levels usually increase compared to the pure active power injection strategy. It can be deduced that neither of the reactive power support strategies reaches the critical line loading levels, so it would be safe to use any of them. On the other hand, Q(V) and proposed RPMS-II strategies seem superior to cosφ(P) method by reducing the maximum loading ratios a few percents more.

These results can also be verified visually from the main feeder line loading profiles as shown in Figure 5.11. Although the differences are in the order of a few percentages, during the peak active power injection hours Q(V) gives slightly better performance than the RPMS-II, but they both outperform the traditional cosφ(P) method.

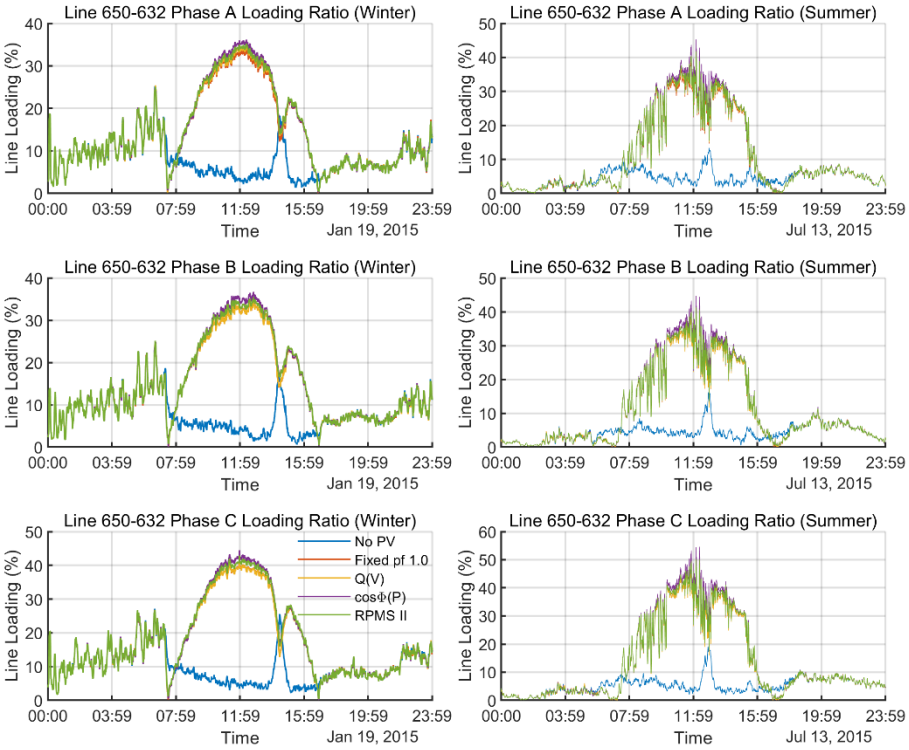

Figure 5.11 Line loading profile of the main feeder line in winter (left) and summer (right)

5.5.3.3 Service transformer loadings

Recorded average and maximum loading ratios considering all service transformers in the secondaries are given in Table 5.17. In addition, for two randomly selected service transformers, loading profiles are also illustrated in Figure 5.12.

Table 5.17 Average and maximum transformer loading ratios in winter and summer

Cases	Winter		Summer	
	S_{avg}(%)	S_{max}(%)	S_{avg}(%)	S_{max}(%)
NO PV	10.10	69.34	8.88	57.21
PF 1.0	-23.35	-81.14	-27.50	-93.66
Q(V)	-23.42	-81.57	-27.60	-93.65
Cosφ(P)	-24.38	-86.15	-28.80	-101.90
RPMS-II	-24.12	-83.70	-28.24	-95.99

* - sign indicates the reverse powerflow

Due to high reverse powerflow, especially during the high generation periods, transformers are being loaded significantly when PVs are integrated into the grid. Compared to the winter, transformers may reach higher loading ratios in summer periods. Therefore, distribution system operators should monitor transformers more carefully in case of high PV penetration.

On the other hand, among reactive power control methods, cosφ(P) seems to be the only one method which overpasses 100% loading ratio in summer. Both Q(V) and proposed RPMS-II methods achieve to stay below the critical loading level. Compared to RPMS-I, Q(V) method has the ability to reduce the loading ratios a few percents during the maximum generation periods.

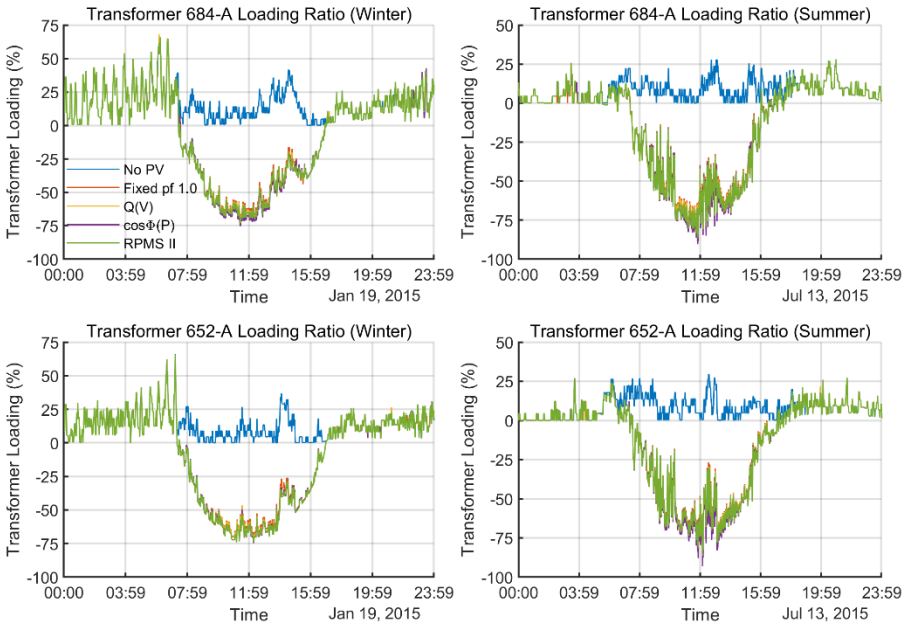

Figure 5.12 Loading profile of two random transformers in winter (left) and summer (right)

5.5.3.4 Stress on the voltage regulator

The performances of the methods are also compared in terms of their impacts on step voltage regulator (SVR) tap changing operations. Total number of tap changes considering each phase individually are given in Table 5.18 for one-week winter and summer simulation periods.

It can be seen that, when PVs are integrated into the grid, the tap-changing operations of conventional voltage regulators significantly increase. In terms of SVR operation, winter seems to be more problematic than the summer periods. This could be due to more cloudy days in winter which may affect the PV generation and cause more

frequent voltage drops. On the other hand, to reduce the number of SVR operations, reactive power support capabilities of PV inverters can be used. As can be seen in the table, SVR operations can be cut to half in winter with cosφ(P) and proposed RPMS-II methods. Moreover, with the RPMS-II strategy, tap-changing operations are completely eliminated in the summer. However, performance of the Q(V) method is not as good as the other reactive power control methods even though it can also reduce the tap-changing counts a bit.

Table 5.18 Total number of SVR tap changing operations in winter and summer

Number of Tap changes	Winter				Summer			
	Phase A	Phase B	Phase C	Total	Phase A	Phase B	Phase C	Total
NO PV	1	1	3	5	0	1	1	2
PF 1.0	16	14	18	48	5	5	7	17
Q(V)	8	14	18	40	0	5	7	12
Cosφ(P)	8	6	10	24	0	0	2	2
RPMS-II	8	6	10	24	0	0	0	0

5.5.3.5 Power loss

Recorded average and maximum power loss values considering one-week winter and summer periods are given in Table 5.19.

Table 5.19 Recorded average and maximum power loss in winter and summer

Cases	Winter		Summer	
	PL_{avg} (kW)	PL_{max} (kW)	PL_{avg} (kW)	PL_{max} (kW)
NO PV	2.46	21.96	1.92	19.86
PF 1.0	14.36	49.44	15.73	65.86
Q(V)	14.52	50.22	15.95	66.97
Cosφ(P)	15.86	58.53	17.61	81.71
RPMS-II	15.61	54.13	17.02	70.47

As in line and transformer loading, power loss is also increased with high PV penetration. Reactive power control methods cause a further increase in power loss values in exchange for better voltage regulation. Among them, Q(V) method seems to perform much better by keeping the losses as minimum as possible. The proposed

RPMS-II method is the second-best performer which outperforms the cosφ(P) strategy.

For visual comparison , Figure 5.13 is provided choosing a random day in one-week winter and summer simulation periods. Although it is not easy to distinguish results in summer case, winter profiles are more clear to give an idea about the performance of the methods. First of all, no matter what type of control is applied, it can be seen that power loss is increased with high PV penetration. Starting from the sunrise, it gradually increases as the generation gets higher and reaches a peak around noon, and then it gradually decreaces until the sunset.

In terms of the power loss performances of reactive power control strategies, Q(V) method becomes the best by approaching the performance of pure active power injection strategy (fixed pf 1.0). On the other hand, the proposed RPMS-II method comes second by achieving to reduce the power loss more than the traditional cosφ(P) strategy.

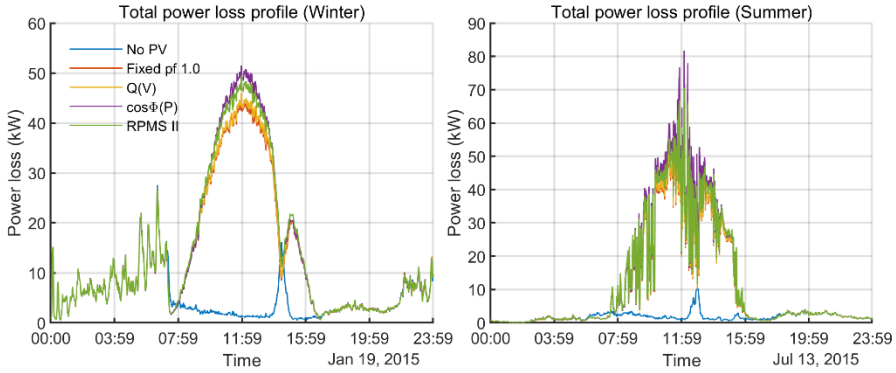

Figure 5.13 Total power loss profile in winter (left) and summer (right)

5.5.4. DISCUSSION AND CONCLUSION

In this section, a novel reactive power management strategy (RPMS-II) is proposed as a competitor to the traditional dynamic power factor control strategies, Q(V) and cosφ(P). In the previous section, while proposing the first strategy (RPMS-I), it has been aimed to keep the system complexity as minimum as possible by not measuring any individual local measurements. On the other hand, in RPMS-II, individual local power measurements are used to provide better voltage regulation support aiming to also mitigate the undesired voltage drops. As the counterpart Q(V) and cosφ(P) methods, RPMS-II has also been very successful to mitigate the voltage variations. In addition, it has performed better than the Q(V) and cosφ(P) methods in terms of reducing the total number of tap-changing operations on the step voltage regulator. Although, as the main drawbacks of all reactive power support strategies, line and transformer loadings, and power loss are increased a bit, they have never reached the

critical levels with the Q(V) and RPMS-II methods. In exchange for better voltage regulation support, these drawbacks are acceptable. To also mitigate these problems, other solutions such as active power curtailment strategies or energy storage systems can also be integrated into the system. However, these strategies also come with their own drawbacks as they increase the installation and operational costs.

CHAPTER 6. VOLTAGE UNBALANCE MITIGATION USING THREE-PHASE SENSITIVITY ANALYSIS AND REACTIVE POWER SUPPORT

Practically, electrical power is generated and consumed instantaneously. This instantaneous interaction poses a great challenge for system operators to maintain the power quality at a certain level all the time. In this chapter, as one of the power quality issues, voltage unbalance problem is addressed in distribution grids. Due to uneven conductor spacings, unequal load distribution, and multi-phase characteristics, distribution grids are more inclined to this problem.

Voltage unbalance problem may arise due to the differences of phase voltage magnitudes. It can be measured as the maximum deviation divided by the average of the three phase magnitudes. ANSI C84.1-2006 standard recommends that voltage unbalance should be limited to 3%. Similarly, other standards such as IEC 61000-2-2:2002 and EN 50160-1999 also allow voltage unbalance limit as high as 3% for systems with large single phase-loads.

Furthermore, in recent years, there is an increasing pattern of single-phase PV system installations in secondary distribution grids. These renewable energy resources may also introduce additional uncertainty in voltage levels and forthrightly affect the degree of phase imbalances. Therefore, the impact of different PV penetration levels should also be considered and investigated thoroughly.

In this chapter, benefitting from three-phase voltage sensitivity analysis and reactive power support capabilities of PV inverters, two different methods are proposed to mitigate the voltage unbalance. While in the first method, only individual phases of local nodes contribute to the mitigation strategy (self-node balancing), in the second method, interactions between all problematic nodes is also considered (cooperative balancing).

Following this section, a literature review is provided for voltage unbalance studies. Then, an enhanced version of voltage sensitivity analysis is introduced to be used for both of the voltage unbalance mitigation strategies. After explaining the proposed strategies, their performance is tested with some study cases that consist of different PV penetration levels. Finally, results are discussed.

6.1. LITERATURE REVIEW

A very detailed voltage regulation review has already been provided in Chapter 5. Therefore, in this section, only the studies which will particularly tackle voltage unbalance problem are reviewed.

Studies in literature typically adopt a centralized control approach to mitigate voltage unbalance. Due to the nature of the problem, it concerns all the three phases. Therefore, individual and independent local single-phase control approach is not suitable for mitigation of the voltage unbalance [119].

A multi-objective optimal power flow study is conducted in a three-phase four-wire LV distribution network to minimize voltage deviation, voltage unbalance, network loss, active power curtailment cost and also the inverter loss which is associated with the reactive power support. Sequential quadratic programming algorithm with multiple starting points is used to ensure global optima. Optimal setpoints which determine the active power curtailment and reactive power support amount are sent to PV inverters by a central controller [180]. A communication-based two-stage voltage control technique is proposed by coordinating OLTC and rooftop single-phase PV systems. While in the first stage, OLTC is used to keep the voltage in the secondary grid within allowable limits, in the second stage, reactive power support by PV inverters is utilized to mitigate the voltage unbalance. Q-V droop controller is proposed to make each phase voltage equal to the measured average node voltage [181]. A probabilistic voltage management system in distribution network is proposed to regulate the voltage and mitigate voltage unbalance by keeping them within limits with some confidence level. The location and size of d-STATCOM, size of the embedded energy storage system, location of OLTC are optimized by a modified particle swarm optimization algorithm considering also the reactive power support capabilities of PV inverters. To reduce the computational burden in the optimization process, key states of the load and generation are identified by k-means clustering algorithm [182]. A combined voltage scheme is presented to improve the voltage profile, fluctuations, and unbalance by coordinating OLTC, battery energy storage systems, electric vehicles, and PV/Wind hybrid generation systems. In this scheme, batteries are located at the end of the feeders and controlled by a central controller. To mitigate voltage unbalance, the central controller determines the required active power injections of the battery inverters [183]. Apart from these, a manual [162] and a dynamic [163] network reconfiguration strategies are proposed to minimize the voltage unbalance, but significant network modifications may not be a preferred solution by system operators at all.

6.2. ENHANCED VOLTAGE SENSITIVITY ANALYSIS

For some applications of power systems, sensitivity analysis provides a practical way to reduce complex nonlinear equations to simple linear equations. These simplified network relationships may help system operators to develop more efficient network management strategies. Generally, three different methods are being used in the literature for sensitivity analysis. First one is called Jacobian matrix method which is specifically used in Newton-Raphson power flow method or its derivatives [152]. The second method, Perturb and observe is not related to any specific power flow algorithm, thus has the flexibility to work with any software package [153]. There is also Adjoint networks method which uses a modified Tellegen theorem but not widely used as the aforementioned methods [154].

Sensitivity analysis is mostly used in applications which require fast response such as voltage regulation [155], [156], [157], [158], [159]; voltage stability [160], [161]; voltage unbalance [162], [163]; detection of fault location [164]; harmonic analysis [165]; power system stability [166], [167]; and reactive power management [168], [169].

Additionally, it has also been used in other applications that spanning a larger time frame such as power system planning [170], [171]; optimal DG location [172], [173]; optimal capacitor location [153], [174]; network reconfiguration [162], [175]; power loss minimization [152], [176]; reliability [177], ranking of generators and loads [178]; and PV hosting capacity investigation [179].

Multiphase unbalanced distribution grids have some unique features such as an increase in phase-A voltage at one node may cause a decrease in phase-B voltage at another node or vice versa. Even though this sounds a bit chaotic, it can be transformed into useful information to reduce the degree of unbalance. As proposed in the following sections, relationships of all node phases with each other can be revealed with an enhanced three-phase voltage sensitivity analysis and this information can be provided to PV inverters to optimally adjust the reactive power deviations for each phase separately. In this way, degree of voltage unbalance at each node can be reduced to permissible level.

In this chapter, an enhanced Perturb and Observe method is also introduced to obtain the three-phase voltage sensitivity matrices of the grid. In proposed strategies, only V/Q sensitivity is required, but V/P, V/(P-Q), and other sensitivities can also be obtained by following the same steps.

The methodology will be explained on the well-known IEEE 13 node test feeder, which is a multiphase distribution grid with both overhead lines and underground cable systems. Although the grid is inherently unbalanced due to large number of unequal single-phase loads, an additional unbalance is introduced by uneven

conductor spacings. The grid is visualized with modified node IDs as shown in Figure 6.1.

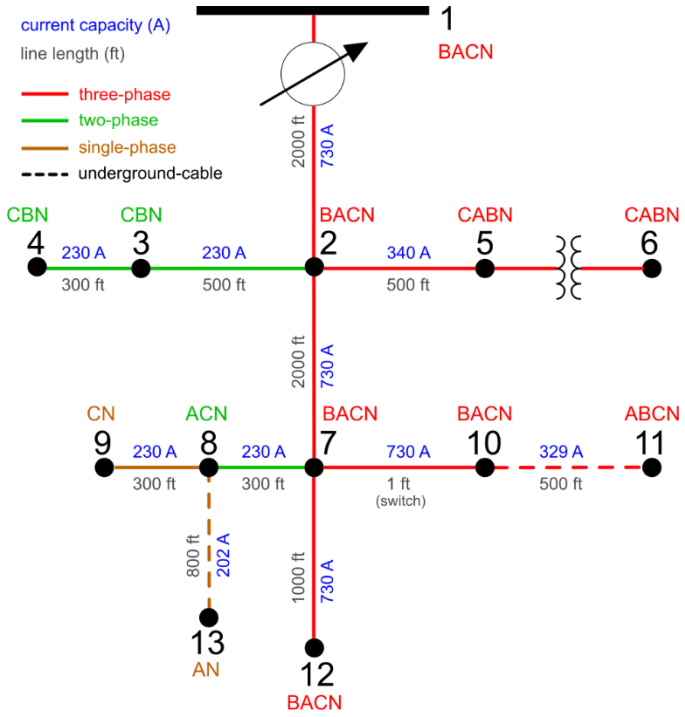

Figure 6.1 IEEE13 test grid with modified node IDs and phase sequences

In literature, generally, sensitivity matrices are calculated for only one state of the network. If operation point changes from one state to another, then a new sensitivity matrix should be calculated. Therefore, a practical solution is needed to update the matrices to adapt dynamically changing grid conditions.

To do so, a selected grid variable, reactive power in this case, is varied with small enough intervals, both positive and negative deviations from the current state. Then, voltage variations are observed. **Algorithm 1** is provided to obtain *N*-dimensional (*N* different operation points) three-phase $\boldsymbol{\Delta|V|/\Delta Q}$ matrix. The flowchart of the algorithm can be seen in Figure 6.2.

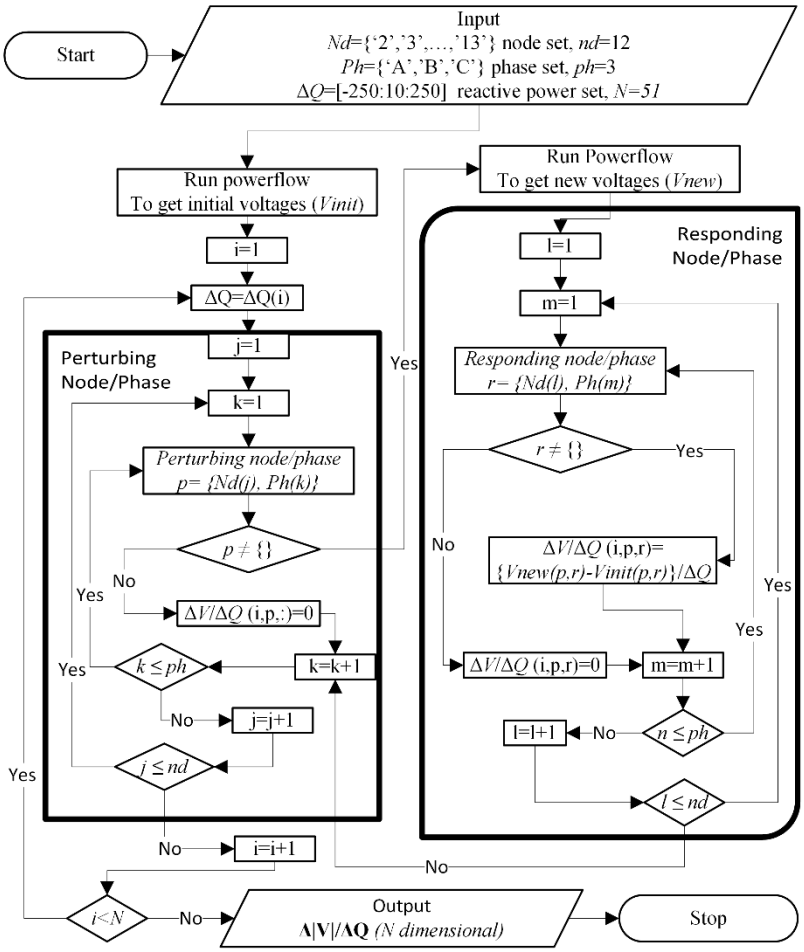

Figure 6.2 Flowchart of Algorithm 1, to obtain N-dimensional three-phase voltage sensitivity matrix

After voltage variations are analyzed throughout the grid, linearity in voltage deviations (at responding node) according to the reactive power changes (at perturbing node) is observed within that specific ΔQ range. This observation is also illustrated in Figure 6.3 for some of the node/phase couples.

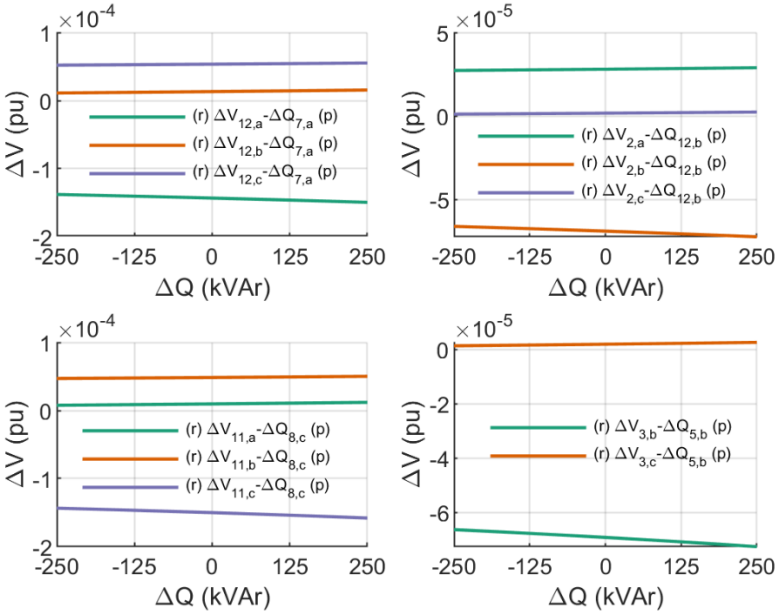

Figure 6.3 Voltage deviations at responding node/phase (r) according to reactive power changes at perturbing node/phase (p)

Based on this observation, it is thought that linear regression can be used to model the variations of voltage sensitivity coefficients. Applying the least-squares method, using the *N*-dimensional $\boldsymbol{\Delta|V|/\Delta Q}$ matrix as the input, linear equation coefficients are obtained with **Algorithm 2** as shown in Figure 6.4.

Then, for any specific responding node/phase and perturbing node/phase interaction, voltage - reactive power sensitivity is approximated as

$$\frac{\partial |V_r|}{\partial Q_p} \approx a_{p,r} + b_{p,r} \cdot \Delta Q_p \tag{6.1}$$

Here, $a_{p,r}$ and $b_{p,r}$ are the fitted coefficients of the linear regression model in which p and r subscripts represent perturbing and responding node/phase couples, respectively.

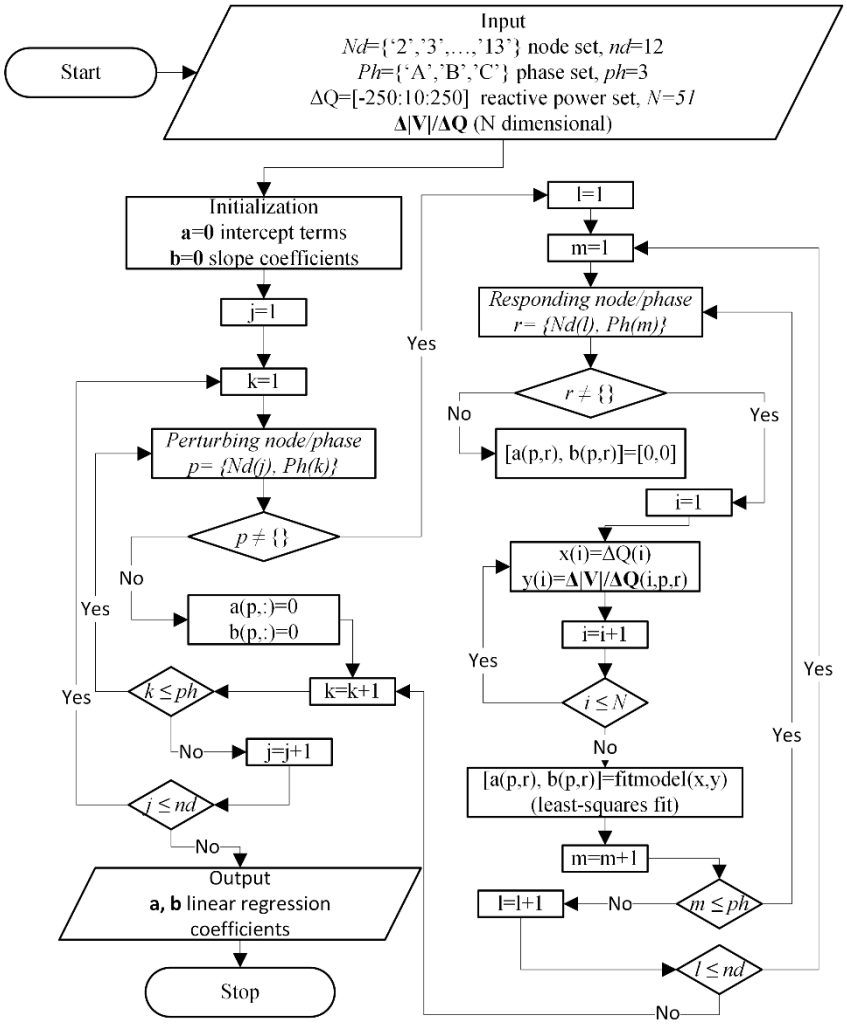

Figure 6.4 Flowchart of Algorithm 2, to calculate linear regression coefficients to model the variations of voltage sensitivity coefficients

6.3. VOLTAGE UNBALANCE MITIGATION STRATEGY I (VUMS-I, SELF-NODE BALANCING)

In the first strategy, it is assumed that VUMS-I algorithm will only consider unbalanced node(s)'s own phases while adjusting reactive power deviations for each phase. Even though all the nodes in the grid may affect each other to a certain degree, this interaction will be disregarded by the algorithm. This strategy is introduced as a

practical life challenge for the possibility of not having a proper communication infrastructure between the nodes. However, while evaluating the performance of the algorithm, the effect of all other nodes will also be considered as in reality.

As illustrated in Figure 6.5, the purpose of the proposed strategy will be to pull node phase voltages back to the allowed voltage unbalance zone. To do so, reactive power absorbing/supplying capabilities of PV inverters will be used.

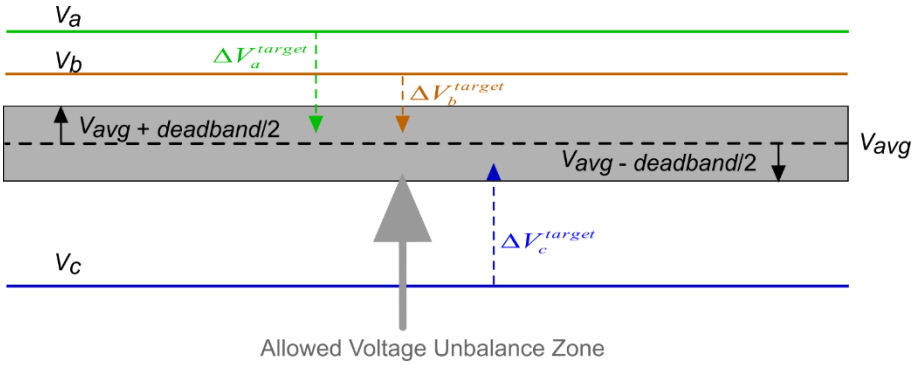

Figure 6.5 Demonstration of phase voltage adjustments to bring them in allowed zone

To provide more technical details, firstly VUMS-I algorithm detects all the nodes which have the voltage unbalance problem and then forms a set of *J* which contains these nodes

$$J = \left\{ j \quad | \quad j \in Nd, \quad V_{j,unb} \geq 3\% \right\} \tag{6.2}$$

Then, finds the average phase voltage value for the *i* th node in this *J* set

$$V_{i,avg} = \frac{V_{i,a} + V_{i,b} + V_{i,c}}{3}, \quad i \in J \tag{6.3}$$

After that, the algorithm checks each phase if its voltage is above or below the average. If it is above the average, then it sets the target phase voltage between the average and a bit above (determined by deadband). Otherwise, if it is below the average, then it does this in the opposite direction as illustrated in Figure 6.5.

$$V_{i,ph}^{target} = \begin{cases} V_{i,avg} \leq V_{i,ph}^{target} \leq V_{i,avg} + (db/2), & V_{i,ph} > V_{i,avg} \\ V_{i,avg} - (db/2) \leq V_{i,ph}^{target} \leq V_{i,avg}, & V_{i,ph} \leq V_{i,avg} \end{cases} \tag{6.4}$$

For a good starting point, target voltage can be set to the arithmetic average of these low and high boundaries

$$V_{i,ph}^{target} = \begin{cases} V_{i,avg} + (db/4), & V_{i,ph} > V_{i,avg} \\ V_{i,avg} - (db/4), & V_{i,ph} \le V_{i,avg} \end{cases} \tag{6.5}$$

Then, the required voltage deviation for each phase can be calculated by

$$\Delta V_{i,ph}^{target} = V_{i,ph}^{target} - V_{i,ph} \tag{6.6}$$

Now, all needs to be done is adjusting phase reactive power (ΔQ) deviations such that the new phase voltages move to the boundaries defined in (6.4) and helps to bring voltage unbalance below the limit. New phase voltage deviations can be calculated by superposition principle as

$$\Delta V_{i,a}^{new} = \frac{\partial |V_{i,a}|}{\partial Q_{i,a}} \times \Delta Q_{i,a} + \frac{\partial |V_{i,a}|}{\partial Q_{i,b}} \times \Delta Q_{i,b} + \frac{\partial |V_{i,a}|}{\partial Q_{i,c}} \times \Delta Q_{i,c} \tag{6.7}$$

$$\Delta V_{i,b}^{new} = \frac{\partial |V_{i,b}|}{\partial Q_{i,a}} \times \Delta Q_{i,a} + \frac{\partial |V_{i,b}|}{\partial Q_{i,b}} \times \Delta Q_{i,b} + \frac{\partial |V_{i,b}|}{\partial Q_{i,c}} \times \Delta Q_{i,c} \tag{6.8}$$

$$\Delta V_{i,c}^{new} = \frac{\partial |V_{i,c}|}{\partial Q_{i,a}} \times \Delta Q_{i,a} + \frac{\partial |V_{i,c}|}{\partial Q_{i,b}} \times \Delta Q_{i,b} + \frac{\partial |V_{i,c}|}{\partial Q_{i,c}} \times \Delta Q_{i,c} \tag{6.9}$$

Even though the voltages found in (6.5) would be the optimum solution, it's known that it is not so easy to get exact voltage values for all phases, because phases will affect each other and there will be deviations from these target points.

Therefore, an optimization algorithm is written to minimize the difference between new and target phase voltage deviations as

$$\min f = \sum_{j=1}^{Nj} \sum_{ph=1}^{Nph} \left| \Delta V_{j,ph}^{new} - \Delta V_{j,ph}^{target} \right| \tag{6.10}$$

which is subject to equalities in (6.5), (6.7), (6.8), and (6.9) and inequality in (6.4). Here, N_j is the number of nodes having voltage unbalance problem and N_{ph} is the number of available phases for each of those nodes. To find optimal reactive power deviations for each phase, a simple linear programming algorithm is used in Matlab.

6.4. VOLTAGE UNBALANCE MITIGATION STRATEGY II (VUMS-II, COOPERATIVE BALANCING)

In the second strategy, not only unbalanced node(s)'s own phases (self-effect) but also the impact of other node phases on unbalanced node (mutual-effect) will be considered by the algorithm. Therefore, some modifications are made in (6.7), (6.8), and (6.9) of the VUMS-I algorithm for VUMS-II as

$$\Delta V_{i,a}^{new} = \underbrace{\frac{\partial |V_{i,a}|}{\partial Q_{i,a}} \times \Delta Q_{i,a} + \frac{\partial |V_{i,a}|}{\partial Q_{i,b}} \times \Delta Q_{i,b} + \frac{\partial |V_{i,a}|}{\partial Q_{i,c}} \times \Delta Q_{i,c}}_{\text{self effect (node i)}} + \underbrace{\sum_{\substack{k \\ k \neq i}}^{n} \left(\frac{\partial |V_{i,a}|}{\partial Q_{k,a}} \times \Delta Q_{k,a} + \frac{\partial |V_{i,a}|}{\partial Q_{k,b}} \times \Delta Q_{k,b} + \frac{\partial |V_{i,a}|}{\partial Q_{k,c}} \times \Delta Q_{k,c} \right)}_{\text{mutual effect (node i and k) } \{k \in J \text{ and } k \neq i\}} \tag{6.11}$$

$$\Delta V_{i,b}^{new} = \underbrace{\frac{\partial |V_{i,b}|}{\partial Q_{i,a}} \times \Delta Q_{i,a} + \frac{\partial |V_{i,b}|}{\partial Q_{i,b}} \times \Delta Q_{i,b} + \frac{\partial |V_{i,b}|}{\partial Q_{i,c}} \times \Delta Q_{i,c}}_{\text{self effect (node i)}} + \underbrace{\sum_{\substack{k \\ k \neq i}}^{n} \left(\frac{\partial |V_{i,b}|}{\partial Q_{k,a}} \times \Delta Q_{k,a} + \frac{\partial |V_{i,b}|}{\partial Q_{k,b}} \times \Delta Q_{k,b} + \frac{\partial |V_{i,b}|}{\partial Q_{k,c}} \times \Delta Q_{k,c} \right)}_{\text{mutual effect (node i and k) } \{k \in J \text{ and } k \neq i\}} \tag{6.12}$$

$$\Delta V_{i,c}^{new} = \underbrace{\frac{\partial |V_{i,c}|}{\partial Q_{i,a}} \times \Delta Q_{i,a} + \frac{\partial |V_{i,c}|}{\partial Q_{i,b}} \times \Delta Q_{i,b} + \frac{\partial |V_{i,c}|}{\partial Q_{i,c}} \times \Delta Q_{i,c}}_{\text{self effect (node i)}} + \underbrace{\sum_{\substack{k \\ k \neq i}}^{n} \left(\frac{\partial |V_{i,c}|}{\partial Q_{k,a}} \times \Delta Q_{k,a} + \frac{\partial |V_{i,c}|}{\partial Q_{k,b}} \times \Delta Q_{k,b} + \frac{\partial |V_{i,c}|}{\partial Q_{k,c}} \times \Delta Q_{k,c} \right)}_{\text{mutual effect (node i and k) } \{k \in J \text{ and } k \neq i\}} \tag{6.13}$$

In cooperative balancing, there should be at least two unbalanced nodes in the grid. Otherwise, included mutual effect terms will disappear and VUMS-II algorithm will simply behave like VUMS-I algorithm. On the other hand, balanced nodes which do not have voltage unbalance problem are not considered in this mitigation strategy. However, some or all other balanced nodes in the grid can also be included in the cooperative balancing strategy to improve the voltage unbalance. On a side note, some nodes may not contain all the three phases, meaning that they may either be single

and/or two-phase. Those nodes are exempted and not considered in neither of the mitigation strategies.

Optimization procedure will remain same for VUMS-II except the replacement of equations (6.7), (6.8), and (6.9) by (6.11), (6.12), and (6.13), respectively. A detailed flowchart of both strategies is provided in Figure 6.6.

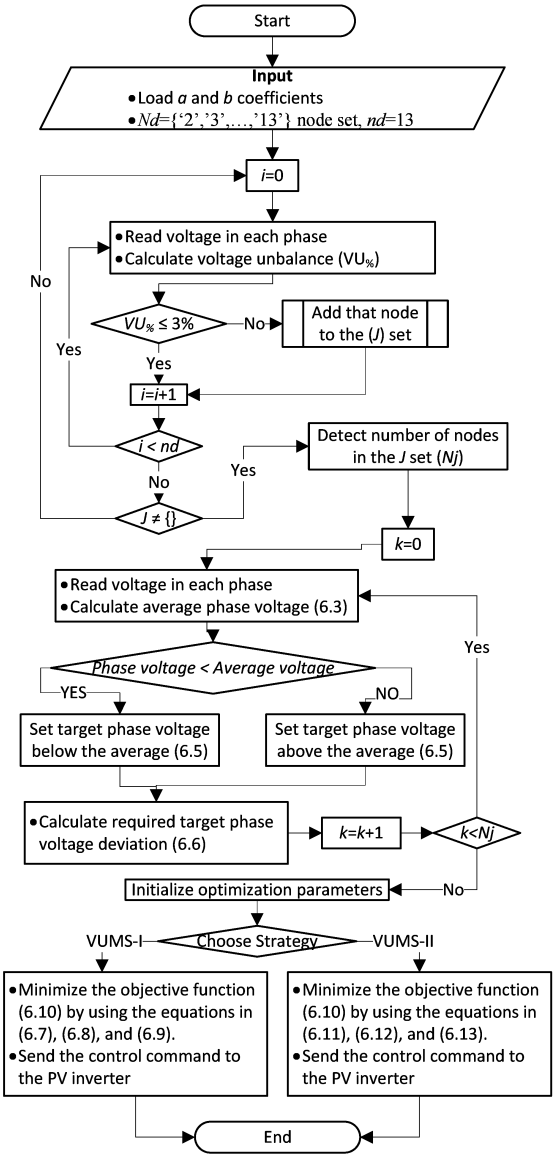

Figure 6.6 Flowchart of the voltage unbalance mitigation strategies, VUMS-I and VUMS-II

6.5. STUDY CASES

Considering different PV penetration levels, five different cases are formed as given in Table 6.1. Here, the initial network state is represented by Case1 where no modification is done, hence there will not be any PV systems in this case. PV penetration percentages are defined by scaling the PV systems according to the total active power load of the whole grid and equally distributed to each existing phase.

Active power curtailment is not considered in any of the cases to keep the profits of prosumers at default level, but to make provision against possible overloading issues on individual phase lines, maximum support of reactive power is limited to 50% of PV inverter capacity. At peak generation times to provide this amount of reactive power, inverter capacity should be chosen 11.8% bigger. However, this can also be achieved with 10.56% active power curtailment even though this option is not considered in this study.

Table 6.1 Study cases

Case ID	PV Pen. Level (%)	PV Pen. whole grid (kW)	Corresponding PV Pen. for phase A (kW)	Corresponding PV Pen. for phase B (kW)	Corresponding PV Pen. for phase C (kW)
Case1	0	0	0	0	0
Case2	25	870	270	270	330
Case3	50	1740	540	540	660
Case4	75	2610	810	810	990
Case5	100	3480	1080	1080	1320

6.6. RESULTS

Results will be analyzed and interpreted case by case considering voltage unbalance ($VU_{\%}$), minimum and maximum voltage values (V_{min} and V_{max}), maximum loading ratios of lines and substation (L_{max} and S_{max}), and finally total active and reactive power losses (P_{loss} and Q_{loss}), respectively.

Even though the main purpose has been to mitigate the voltage unbalance problem, the indirect impacts of proposed methods to other important grid parameters are also investigated. As a side note, only a switch exists between node ‘7’ and ‘10’, thus results are almost identical for these nodes in all cases, but both nodes are included in the analysis as they are regarded different nodes initially.

6.6.1. VOLTAGE UNBALANCE

As can be seen from Table 6.2, in the initial case (Case1), voltage unbalance problem exists ranging from 4.56% to 5.01% at four of the nodes ('7', '10', '11', and '12').

Table 6.2 Voltage unbalance for the default conditions

Case ID	Default	
	Node IDs having VU problem	**Corresponding VU% local each node | total whole grid**
Case1	7,10,11,12	[**4.56**, **4.56**, **5.01**, **4.56**] | 29.79
Case2	7,10,11,12	[**4.03**, **4.03**, **4.46**, **4.02**] | 25.86
Case3	7,10,11,12	[**3.55**, **3.55**, **3.97**, **3.53**] | 22.45
Case4	7,10,11,12	[**3.13**, **3.13**, **3.54**, **3.09**] | 19.95
Case5	11	[2.74, 2.74, **3.14**, 2.70] | 17.84

The first remarkable deduction is that increasing PV penetration levels in the grid to some extent contributes to lessening the voltage unbalances. Even though, it will not be enough to completely mitigate voltage unbalances without large amount of PV penetration levels, it might naturally help relatively more balanced grids without taking extra measures.

However, increasing PV penetration beyond some levels may also cause other technical problems such as violation of maximum voltage limit which will be investigated in the next subsection.

On the other hand, as shown in Table 6.3, the proposed methods almost in every case mitigate the voltage unbalances successfully. Only at node '11' in Case2, i.e., 25% PV penetration case, even though $VU_{\%}$ is significantly reduced from 4.46% to 3.20% and 3.09%, respectively, due to ±15 kVAr reactive power support limit for each node phase they couldn't pull $VU_{\%}$ back to below 3%. Yet, when the reactive power support is increased to ±30 kVAr as in Case3, they also managed to mitigate the VU problem at Node '11'.

Moreover, the proposed methods do not only contribute to balancing voltage at individual nodes, but they also help to reduce the total voltage unbalance percentage

in the whole grid. Even though only problematic nodes join the voltage mitigation strategy, other healthy nodes may also benefit from this indirectly.

Table 6.3 Voltage unbalance for the proposed strategies

	VUMS-I		VUMS-II	
Case ID	**Node IDs having VU problem**	**Corresponding VU% local each node | total whole grid**	**Node IDs having VU problem**	**Corresponding VU% local each node | total whole grid**
Case1	7,10,11,12	No Q support (No PV)	7,10,11,12	No Q support (No PV)
Case2	11	[2.79, 2.79, **3.20**, 2.70] | 17.07	11	[2.68, 2.68, **3.09**, 2.59] | 16.72
Case3	-	[1.77, 1.77, 2.15, 1.64] | 11.15	-	[1.49, 1.49, 1.87, 1.31] | 9.26
Case4	-	[0.95, 0.95, 0.62, 1.13] | 10.90	-	[0.89, 0.89, 1.28, 0.71] | 6.60
Case5	-	[1.62, 1.62, 1.97, 1.57] | 9.86	-	[1.62, 1.62, 1.97, 1.57] | 9.86

6.6.2. MINIMUM AND MAXIMUM VOLTAGE LEVELS

As another important criterion, minimum and maximum voltage levels should also be analyzed in PV penetration cases. Even though minimum voltage levels may not be problematic as the other, it is included in this analysis as given in Table 6.4.

Table 6.4 Minimum and maximum voltage levels

	V_{min} (pu)			V_{max} (pu)		
Case ID	**Default**	**VUMS-I**	**VUMS-II**	**Default**	**VUMS-I**	**VUMS-II**
Case1	0.9739	-	-	1.0553	-	-
Case2	0.9876	0.9951	0.9935	1.0571	1.0453	1.0450
Case3	0.9963	1.0074	1.0070	1.0590	1.0441	1.0376
Case4	1.0022	1.0178	1.0145	1.0610	1.0492	1.0402
Case5	1.0079	1.0199	1.0199	1.0630	1.0520	1.0520

As can be seen from the table, PV system installations generally increase voltage levels in the grid. Having said that, the test grid in this study is already suffering from the maximum voltage violation. Thus, adding more generation resources will not help the grid. According to the results, for each additional 25% increase in PV penetration,

the maximum voltage level is also increased by 0.002 p.u. approximately. Therefore, this extra burden should also be mitigated.

The logic behind both proposed methods has been to pull phase voltages back to their average value. This idea also helped us to decrease maximum voltage levels in the grid. Considering all the cases and both methods, maximum voltage levels are decreased successfully between 0.01 and 0.02 p.u. Even at 100% PV penetration level, the proposed methods performed better than the default no PV case.

6.6.3. LINE AND SUBSTATION LOADING RATIOS

In Table 6.5, maximum loading ratios of all lines (L_{max}) and substation (S_{max}) are given. It can be deduced that increasing PV penetration level helps to decrease line and substation loading ratios. This impact can be reasoned to decreasing net load amount in the grid.

Table 6.5 Maximum loading ratios of all lines and substation

	L_{max} (%)			S_{max} (%)		
Case ID	**Default**	**VUMS-I**	**VUMS-II**	**Default**	**VUMS-I**	**VUMS-II**
Case1	80.35	-	-	79.42	-	-
Case2	62.79	61.30	61.08	62.48	62.09	61.78
Case3	53.99	53.65	53.41	46.98	45.28	46.98
Case4	49.89	48.99	49.74	34.49	31.31	36.13
Case5	45.86	46.31	46.31	28.73	27.88	27.88

On the other hand, it is seen that the proposed methods do not increase loading ratios which could be another advantage. This is also illustrated in Figure 6.7 with the time-varying loading profiles of the main feeder and substation for the 50% PV penetration case (Case3).

Generally, due to reactive power support, current magnitudes are increased on the lines and transformers that in return may cause an increase in loading ratios. However, the algorithm used in the proposed methods is arranging reactive power deviations so that not only inductive or capacitive power factors are being used, but combination of them at the same time. Otherwise, it would not be possible to raise the lowest phase voltage and lower the highest phase voltage.

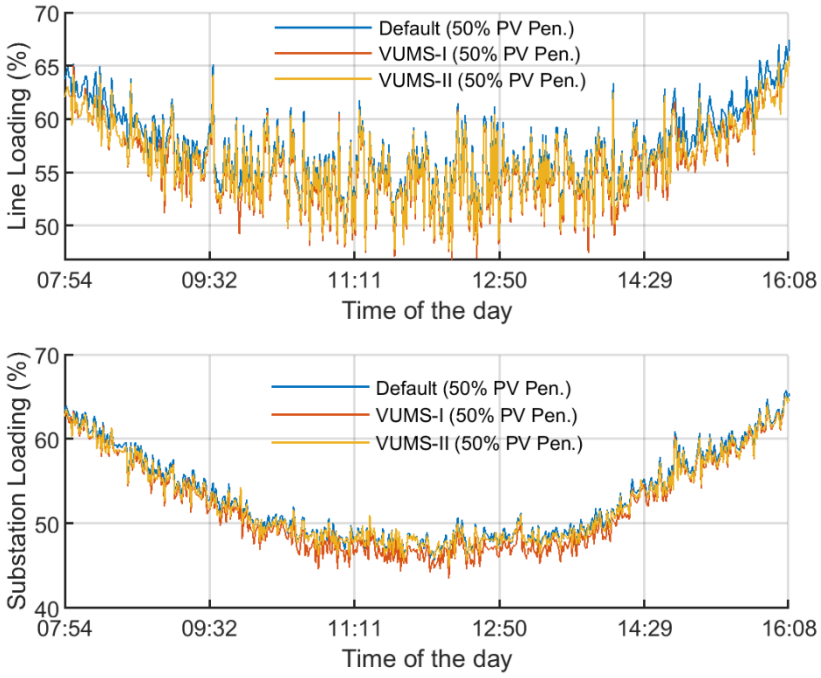

Figure 6.7 Loading profiles of the main feeder and substation

6.6.4. ACTIVE AND REACTIVE POWER LOSS

As another important grid parameter, power loss is also considered for the performance comparison. According to the results in Table 6.6, PV penetration naturally helps to decrease both active and reactive power losses. The reason as explained in loading ratio subsection is due to decreasing net load amount in total.

Table 6.6 Active and reactive power loss

	P_{loss} (kW)			Q_{loss} (kVAr)		
Case ID	**Default**	**VUMS-I**	**VUMS-II**	**Default**	**VUMS-I**	**VUMS-II**
Case1	111.04	-	-	324.76	-	-
Case2	74.33	71.47	71.05	213.65	203.73	201.97
Case3	47.85	42.90	44.90	133.10	117.10	122.93
Case4	31.10	25.66	30.04	81.54	63.63	77.32
Case5	23.67	21.02	21.02	57.70	50.39	50.39

On the other hand, both active and reactive power losses may also be reduced further with the proposed methods. Due to naturally balancing reactive power deviations in the nodes, we see an indirect benefit of reduced power losses in the grid. This observable decrease in total active and reactive power loss is also illustrated in Figure 6.8 with time-varying loss profiles for the 50% PV penetration case (Case3).

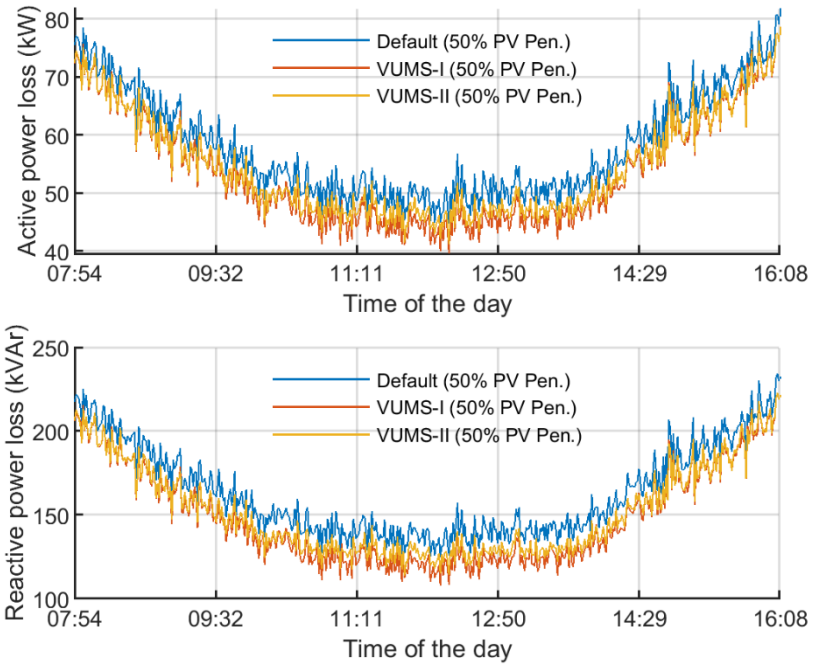

Figure 6.8 Total active and reactive power loss profile

6.6.5. OVERALL PERFORMANCE COMPARISON (CASE AVERAGES)

Considering the case averages, Table 6.7 is provided to be able to easily compare the proposed strategies with each other and the default conditions. As done in the upper section, overall results are given for the voltage unbalance, minimum and maximum voltage levels, line and substation loading ratios, and power losses.

- Voltage unbalance

It is demonstrated that VU can be reduced from 3.45% to 1.82% and 1.73% at individual nodes; and from 21.52% to 12.24% and 10.61% in the whole grid by VUMS-I and VUMS-II methods, respectively. $VU_{\%}$ at individual nodes successfully pulled back well below 3% limit. Besides, total $VU_{\%}$ in whole grid has also been reduced more than 40% in average. Even though, both methods give satisfactory

performances, VUMS-II method in average has been slightly better than VUMS-I method in voltage unbalance mitigation.

Table 6.7 Performance comparison (case averages)

	Case averages			Difference compared with the default	
Parameter	**Default**	**VUMS-I**	**VUMS-II**	**VUMS-I**	**VUMS-II**
$VU_{\%}$	3.45	1.82	1.73	−47.24 (%)	−49.85 (%)
$VU_{\%}$ [a]	21.52	12.24	10.61	−43.12 (%)	−50.69 (%)
V_{min} **(p.u.)**	0.9985	1.0101	1.0097	+0.0116 (pu)	+0.0112 (pu)
V_{max} **(p.u..)**	1.0600	1.0477	1.0437	−0.0123 (pu)	−0.0163 (pu)
L_{max} **(%)**	53.13	52.56	52.63	−1.07 (%)	−0.94 (%)
S_{max} **(%)**	43.17	41.64	43.19	−3.54 (%)	+0.04 (%)
P_{loss} **(kW)**	44.23	40.26	41.75	−8.97 (%)	−5.60 (%)
Q_{loss} **(kVAr)**	121.49	108.71	113.15	−10.51 (%)	−6.86 (%)

- Minimum and maximum voltage levels

In comparison to default, the maximum voltage levels are decreased by 0.0123 and 0.0163 p.u., and the minimum voltage levels are increased by 0.0116 and 0.0112 p.u. with VUMS-I and VUMS-II methods, respectively. It can be said that VUMS-II strategy performs slightly better than VUMS-I in maximum voltage reduction.

- Line and substation loading ratios

Even though the difference is not much compared to the default situation, maximum line loading can be reduced by 1.07% and 0.94% with VUMS-I and VUMS-II methods, respectively. In addition, substation loading ratio can also be lowered by 3.54% with VUMS-I method, but VUMS-II method does not make a significant change on it.

- Power loss

While total active power loss is reduced by 8.97% and 5.60% in average; reactive power loss is reduced by 10.51% and 6.86% with VUMS-I and VUMS-II methods, respectively. For the power loss performance evaluation, it can be said that VUMS-I method gives slightly better performance.

6.7. SUMMARY AND DISCUSSION

Balancing generation and consumption while maintaining a certain power quality is becoming more and more challenging for system operators. In this chapter, as one of the power quality issues, voltage unbalance problem is addressed in distribution grids. Because of unequal single-phase load distribution, uneven conductor spacings and increase in single-phase PV system penetrations, multiphase distribution grids are more vulnerable to the voltage unbalance.

Two novel voltage unbalance mitigation strategies are proposed benefitting from three-phase voltage sensitivity analysis and reactive power support capabilities of PV inverters. In the first method, while only individual phases of local nodes contribute to the mitigation strategy (self-node balancing), in the second method, interactions between all problematic nodes are also considered (cooperative balancing). In addition, a linear regression model is also introduced to consider fluctuations in voltage sensitivities for multiphase distribution grids.

Study cases are formed considering different PV penetration levels on a well-known multiphase IEEE13 test feeder. According to the results, in average, voltage unbalance is successfully reduced from 3.45% to 1.82% and 1.73% by the first and second proposed method, respectively. Not only decreasing voltage unbalance by at least 40% but as an indirect contribution, maximum voltage levels and total power loss are also decreased with the proposed strategies. In this way, PV penetration levels can also be increased thanks to the proposed methods.

Due to providing an effective solution to voltage unbalance problem without any negative impacts on the other grid elements, distribution system operators may integrate the proposed strategies into their network management systems to build a more complete smart grid network management solution.

CHAPTER 7. CONCLUSIONS

In this thesis, reactive power management strategies based on PV inverters are developed to mitigate the voltage variations and voltage unbalance by including the behavior of secondary distribution systems under high PV penetration levels. Since the development of the strategies is based on a detailed model of the system, a comprehensive load model is constructed as the first step of the thesis to include the individual characteristics of end-users with high-resolution time-varying probabilistic load profiles. And then, apart from the irradiance and temperature effects on PV generation, wind speed effect is also included in the model of the PV generation system to more accurately estimate the variations of PV system output. After that, high PV penetration impacts on distribution systems are scrutinized considering voltage variations, voltage unbalance, line and transformer loadings, surplus power, power loss, and stress on voltage regulators. It's worthy of note that secondary distribution grids are more vulnerable to voltage variations than primary distribution grids. Regarding this issue, voltage level control problems impose a limit for PV penetration in secondaries. In that manner, it's observed that the number of tap changing operations on voltage regulators are also significantly increased as a consequence of high PV penetration. Because frequent switching may reduce their lifetime considerably, it may not be so feasible to use them to mitigate the fast voltage variations. On the other hand, power loss, loading of line and transformers are also affected by the high PV penetration. While line loadings still remain far from the critical levels, distribution transformers are almost fully loaded especially during the noon hours. As a result, voltage variation and voltage unbalance in terms of power quality problems are the main critical issues in distribution systems under high PV penetration level.

Within this scope, two different techniques, called RPMS-I and RPMS-II, are proposed to mitigate the voltage variations. Both techniques utilize reactive power support capabilities of PV inverters and do not require any communication among PV inverters. While in RPMS-I, only one global measurement is needed for all the inverters with an attempt to reduce the system complexity, in RPMS-II, individual local measurements are used to increase the system accuracy. According to the results, both techniques have been successful to reduce the voltage rises due to high PV penetration. Providing both inductive and capacitive power factors with RPMS-II, voltage drops are also effectively mitigated during the time intervals where consumption is greater than the generation. It's shown that reactive power management via PV inverters is a very promising solution to deal with the voltage variations.

On the other hand, regarding voltage unbalance problem, two different techniques, called as VUMS-I and VUMS-II, are proposed based on three-phase voltage sensitivity analysis and reactive power support capabilities of PV inverters to mitigate

the voltage unbalance due to single-phase load and PV installations on single-phase laterals in distribution systems. While in VUMS-I, coordination of PV inverters is limited among the individual node phases to reduce the system complexity, in VUMS-II, coordination of PV inverters is extended among all unbalanced node phases to include the mutual effect between the nodes. According to the results, both techniques have been successful to pull back the voltage unbalance levels to the allowable zone. Besides, maximum voltage levels and total power loss are also decreased with the proposed techniques. The effectiveness of the proposed techniques is investigated and confirmed to effectively mitigate the voltage unbalanced problem in distribution systems.

The main contributions of this thesis can be summarized as follows:

- End-user loads in secondary distribution grids are individually modeled adopting a probabilistic approach. High-resolution time-varying load profiles are generated individually for each load.
- Apart from the irradiance and temperature effects on PV generation, wind effect is also investigated to more accurately estimate the variations of PV system output. High-resolution time-varying PV generation profiles are generated for each PV system separately.
- The distribution system is modeled in detail including both primary and secondary sides. Using the generated high-resolution time-varying load and PV generation profiles, a very detailed technical impact analysis is conducted on a large scale from customer connection points to the substation.
- Using global solar irradiance measurements from weather stations and utilizing reactive power support capabilities of PV inverters, a simple analytical approach is proposed to mitigate the voltage rises (less costly, in terms of reduced system complexity and the number of sensors).
- Using local active power measurements of load and PV generation and utilizing reactive power support capabilities of PV inverters, another simple analytical approach is proposed to mitigate both voltage rises and drops (more costly, in terms of the increased number of sensors).
- A self-node balancing strategy is proposed to mitigate the voltage unbalance by coordinating the PV inverters only within the same unbalanced node. It's benefitted from the three-phase voltage sensitivity analysis and reactive power support capabilities of PV inverters.
- A cooperative-node balancing strategy is proposed to mitigate the voltage unbalance problem by coordinating the PV inverters in all unbalanced nodes. It's benefitted from the three-phase voltage sensitivity analysis and reactive power support capabilities of PV inverters.

On the other hand, based on the foundations of this thesis, there will be some future work to contribute to increasing renewable energy penetration levels further in distribution grids. These works can be defined as short-term and medium-term goals as follows

- In short-term, a decentralized control strategy will be designed by combining the best parts of local (scalability) and centralized (global optimality) control strategies aiming to simultaneously minimize voltage variations, voltage unbalance, and total power loss almost in real-time.

- In medium-term, a peer-to-peer energy exchange framework will be designed by utilizing the state-of-the-art blockchain technology where consumers and prosumers can securely exchange energy with each other without the requirement of any middleman. By doing so, reverse power flows can be reduced and locally generated renewable energy can also be consumed locally.

LITERATURE LIST

[1] D. A. Senshaw and J. W. Kim, “Meeting conditional targets in nationally determined contributions of developing countries: Renewable energy targets and required investment of GGGI member and partner countries,” *Energy Policy*, vol. 116, pp. 433–443, May 2018.

[2] International Energy Agency, “Trends 2018 in Photovoltaic Applications.” [Online]. Available: http://www.iea-pvps.org/index.php?id=trends. [Accessed: 28-Apr-2019].

[3] SolarPower Europe, “Global Market Outlook 2018-2022,” 2018. [Online]. Available: http://www.solarpowereurope.org. [Accessed: 07-Apr-2019].

[4] E. Kabir, P. Kumar, S. Kumar, A. A. Adelodun, and K.-H. Kim, “Solar energy: Potential and future prospects,” *Renew. Sustain. Energy Rev.*, vol. 82, pp. 894–900, Feb. 2018.

[5] R. E. Brown, “Impact of Smart Grid on distribution system design,” in *2008 IEEE Power and Energy Society General Meeting - Conversion and Delivery of Electrical Energy in the 21st Century*, 2008, pp. 1–4.

[6] H. E. Z. Farag and El-Saadany, “A Novel Cooperative Protocol for Distributed Voltage Control in Active Distribution Systems,” *IEEE Trans. Power Syst.*, vol. 28, no. 2, pp. 1645–1656, May 2013.

[7] E. O’Shaughnessy, D. Cutler, K. Ardani, and R. Margolis, “Solar plus: A review of the end-user economics of solar PV integration with storage and load control in residential buildings,” *Appl. Energy*, vol. 228, pp. 2165–2175, Oct. 2018.

[8] R. Zafar, A. Mahmood, S. Razzaq, W. Ali, U. Naeem, and K. Shehzad, “Prosumer based energy management and sharing in smart grid,” *Renew. Sustain. Energy Rev.*, vol. 82, pp. 1675–1684, Feb. 2018.

[9] D. Srinivasan, L. T. Trung, and C. Singh, “Bidding and Cooperation Strategies for Electricity Buyers in Power Markets,” *IEEE Syst. J.*, vol. 10, no. 2, pp. 422–433, Jun. 2016.

[10] A. Kaygusuz, C. Keles, B. B. Alagoz, and A. Karabiber, “Renewable energy integration for smart sites,” *Energy Build.*, vol. 64, pp. 456–462, Sep. 2013.

[11] V. C. Gungor *et al.*, "Smart Grid Technologies: Communication Technologies and Standards," *IEEE Trans. Ind. Informatics*, vol. 7, no. 4, pp. 529–539, Nov. 2011.

[12] G. P. J. Verbong, S. Beemsterboer, and F. Sengers, "Smart grids or smart users? Involving users in developing a low carbon electricity economy," *Energy Policy*, vol. 52, pp. 117–125, Jan. 2013.

[13] L. Wang, R. Yan, and T. K. Saha, "Voltage Management for Large Scale PV Integration into Weak Distribution Systems," *IEEE Trans. Smart Grid*, vol. 9, no. 5, pp. 4128–4139, Sep. 2018.

[14] F. J. Ruiz-Rodriguez, J. C. Hernández, and F. Jurado, "Voltage unbalance assessment in secondary radial distribution networks with single-phase photovoltaic systems," *Int. J. Electr. Power Energy Syst.*, vol. 64, pp. 646–654, Jan. 2015.

[15] S. Hashemi and J. Østergaard, "Methods and strategies for overvoltage prevention in low voltage distribution systems with PV," *IET Renew. Power Gener.*, vol. 11, no. 2, pp. 205–214, Feb. 2017.

[16] A. Nguyen *et al.*, "High PV penetration impacts on five local distribution networks using high resolution solar resource assessment with sky imager and quasi-steady state distribution system simulations," *Sol. Energy*, vol. 132, pp. 221–235, Jul. 2016.

[17] D. Cheng, B. A. Mather, R. Seguin, J. Hambrick, and R. P. Broadwater, "Photovoltaic (PV) Impact Assessment for Very High Penetration Levels," *IEEE J. Photovoltaics*, vol. 6, no. 1, pp. 295–300, Jan. 2016.

[18] D. Owaki, S. Horie, K. Yukita, T. Matsumura, Y. Goto, and K. Hirose, "Study on power interchange for surplus electric power by distributed power supply in micro grid," in *2017 IEEE 12th International Conference on Power Electronics and Drive Systems (PEDS)*, 2017, pp. 142–146.

[19] E. Reihani, M. Motalleb, R. Ghorbani, and L. Saad Saoud, "Load peak shaving and power smoothing of a distribution grid with high renewable energy penetration," *Renew. Energy*, vol. 86, pp. 1372–1379, Feb. 2016.

[20] P. Chaudhary and M. Rizwan, "Voltage regulation mitigation techniques in distribution system with high PV penetration: A review," *Renew. Sustain. Energy Rev.*, vol. 82, pp. 3279–3287, Feb. 2018.

[21] J. Deboever, S. Grijalva, M. J. Reno, and R. J. Broderick, “Fast Quasi-Static Time-Series (QSTS) for yearlong PV impact studies using vector quantization,” *Sol. Energy*, vol. 159, pp. 538–547, Jan. 2018.

[22] S. J. Steffel, P. R. Caroselli, A. M. Dinkel, J. Q. Liu, R. N. Sackey, and N. R. Vadhar, “Integrating Solar Generation on the Electric Distribution Grid,” *IEEE Trans. Smart Grid*, vol. 3, no. 2, pp. 878–886, Jun. 2012.

[23] A. J. Collin, G. Tsagarakis, A. E. Kiprakis, and S. McLaughlin, “Development of low-voltage load models for the residential load sector,” *IEEE Trans. Power Syst.*, vol. 29, no. 5, pp. 2180–2188, 2014.

[24] A. Singhal, V. Ajjarapu, J. C. Fuller, and J. Hansen, “Real-Time Local Volt/VAR Control Under External Disturbances with High PV Penetration,” *IEEE Trans. Smart Grid*, pp. 1–1, 2018.

[25] S. Ghosh, S. Rahman, and M. Pipattanasomporn, “Distribution Voltage Regulation Through Active Power Curtailment With PV Inverters and Solar Generation Forecasts,” *IEEE Trans. Sustain. Energy*, vol. 8, no. 1, pp. 13–22, Jan. 2017.

[26] M. G. Kashani, M. Mobarrez, and S. Bhattacharya, “Smart Inverter Volt-Watt Control Design in High PV-Penetrated Distribution Systems,” *IEEE Trans. Ind. Appl.*, vol. 55, no. 2, pp. 1147–1156, Mar. 2019.

[27] I. I. Avramidis, V. A. Evangelopoulos, P. S. Georgilakis, and N. D. Hatziargyriou, “Demand side flexibility schemes for facilitating the high penetration of residential distributed energy resources,” *IET Gener. Transm. Distrib.*, vol. 12, no. 18, pp. 4079–4088, Oct. 2018.

[28] M. Zeraati, M. E. Hamedani Golshan, and J. M. Guerrero, “Distributed Control of Battery Energy Storage Systems for Voltage Regulation in Distribution Networks With High PV Penetration,” *IEEE Trans. Smart Grid*, vol. 9, no. 4, pp. 3582–3593, Jul. 2018.

[29] M. Kraiczy, T. Stetz, and M. Braun, “Parallel operation of transformers with on load tap changer and photovoltaic systems with reactive power control,” *IEEE Trans. Smart Grid*, vol. 9, no. 6, pp. 6419–6428, 2018.

[30] G. M. Tina, D. Garozzo, and P. Siano, “Scheduling of PV inverter reactive power set-point and battery charge/discharge profile for voltage regulation in low voltage networks,” *Int. J. Electr. Power Energy Syst.*, vol. 107, pp. 131–139, May 2019.

[31] W. Kong, Z. Y. Dong, D. J. Hill, J. Ma, J. H. Zhao, and F. J. Luo, "A Hierarchical Hidden Markov Model Framework for Home Appliance Modeling," *IEEE Trans. Smart Grid*, vol. 9, no. 4, pp. 3079–3090, 2018.

[32] L. Chuan, A. Ukil, and S. Member, "Modeling and Validation of Electrical Load Profilling in Residential Buildings in Singapore," *2015 IEEE Power Energy Soc. Gen. Meet.*, vol. 30, no. 5, pp. 1–10, 2014.

[33] L. M. Korunovic, J. V. Milanovic, S. Z. Djokic, K. Yamashita, S. M. Villanueva, and S. Sterpu, "Recommended parameter values and ranges of most frequently used static load models," *IEEE Trans. Power Syst.*, vol. 33, no. 6, pp. 5923–5934, 2018.

[34] W. Kong, Z. Y. Dong, J. Ma, D. J. Hill, J. Zhao, and F. Luo, "An Extensible Approach for Non-Intrusive Load Disaggregation with Smart Meter Data," *IEEE Trans. Smart Grid*, vol. 9, no. 4, pp. 3362–3372, 2018.

[35] R. Drenyovszki, L. Kovacs, K. Tornai, A. Olah, and I. Pinter, "Bottom-up modeling of domestic appliances with markov chains and semi-markov processes," *Kybernetika*, vol. 53, no. 6, pp. 1100–1117, 2017.

[36] R. Zhang, Y. Xu, Z. Y. Dong, and K. P. Wong, "Measurement-based dynamic load modelling using time-domain simulation and parallel-evolutionary search," *IET Gener. Transm. Distrib.*, vol. 10, no. 15, pp. 3893–3900, 2016.

[37] V. V. G. Krishnan, S. C. Srivastava, and S. Chakrabarti, "A robust decentralized wide area damping controller for wind generators and facts controllers considering load model uncertainties," *IEEE Trans. Smart Grid*, vol. 9, no. 1, pp. 360–372, 2018.

[38] A. Gerossier, T. Barbier, and R. Girard, "A novel method for decomposing electricity feeder load into elementary profiles from customer information," *Appl. Energy*, vol. 203, pp. 752–760, 2017.

[39] S. A. Saleh, P. Pijnenburg, and E. Castillo-Guerra, "Load Aggregation from Generation-Follows-Load to Load-Follows-Generation: Residential Loads," *IEEE Trans. Ind. Appl.*, vol. 53, no. 2, pp. 833–842, 2017.

[40] K. McKenna and A. Keane, "Residential Load Modeling of Price-Based Demand Response for Network Impact Studies," *IEEE Trans. Smart Grid*, vol. 7, no. 5, pp. 2285–2294, 2016.

[41] M. Sepehr, R. Eghtedaei, A. Toolabimoghadam, Y. Noorollahi, and M. Mohammadi, "Modeling the electrical energy consumption profile for

residential buildings in Iran," *Sustain. Cities Soc.*, vol. 41, no. May, pp. 481–489, 2018.

[42] Tushar, S. Pandey, A. K. Srivastava, P. Markham, and M. Patel, "Online Estimation of Steady-State Load Models Considering Data Anomalies," *IEEE Trans. Ind. Appl.*, vol. 54, no. 1, pp. 712–721, 2018.

[43] K. N. Hasan, K. Bailey, S. J. Stott, J. V. Milanovic, and X. Tang, "Estimation and Validation of Characteristic Load Profile Through Smart Grid Trials in a Medium Voltage Distribution Network," *IEEE Trans. Power Syst.*, vol. 33, no. 2, pp. 1848–1859, 2017.

[44] L. M. Korunovic, S. Martinez Villanueva, S. Z. Djokic, K. Yamashita, and J. V. Milanovic, "International Industry Practice on Power System Load Modeling," *IEEE Trans. Power Syst.*, vol. 28, no. 3, pp. 3038–3046, 2012.

[45] I. R. S. Casella, B. C. S. Sanches, A. J. S. Filho, and C. E. Capovilla, "A Dynamic Residential Load Model Based on a Non-homogeneous Poisson Process," *J. Control. Autom. Electr. Syst.*, vol. 27, no. 6, pp. 670–679, 2016.

[46] Z. Guo, Z. J. Wang, S. Member, and A. Kashani, "Home Appliance Load Modeling From Aggregated Smart Meter Data," *IEEE Trans. Power Syst.*, vol. 30, no. 1, pp. 1–8, 2014.

[47] G. Le Ray, E. M. Larsen, P. Pinson, and S. Member, "Evaluating price-based demand response in practice — with application to the EcoGrid EU Experiment," *IEEE Trans. Smart Grid*, vol. 3053, no. c, pp. 1–10, 2016.

[48] Z. A. Khan and D. Jayaweera, "Approach for smart meter load profiling in Monte Carlo simulation applications," *IET Gener. Transm. Distrib.*, vol. 11, no. 7, pp. 1856–1864, 2017.

[49] R. Li, C. Gu, F. Li, G. Shaddick, and M. Dale, "Development of Low Voltage Network Templates - Part II: Peak Load Estimation by Clusterwise Regression," *IEEE Trans. Power Syst.*, vol. 30, no. 6, pp. 3045–3052, 2015.

[50] M. Manbachi, H. Farhangi, A. Palizban, and S. Arzanpour, "Quasi real-time ZIP load modeling for Conservation Voltage Reduction of smart distribution networks using disaggregated AMI data," *Sustain. Cities Soc.*, vol. 19, pp. 1–10, 2015.

[51] B. Dawoud, E. Amer, and D. Gross, "Performance analysis of CCHP and CHP systems operating following the thermal and electric load," *Int. J. energy Res.*, vol. 31, no. August 2007, pp. 135–147, 2007.

[52] M. F. Romero, L. Gallego, J. Meyer, and S. Müller, "Characterization of non-linear household loads for frequency domain modeling," *Ing. e Investig.*, vol. 35, no. 2Sup, pp. 65–72, Nov. 2015.

[53] A. Marini, M. A. Latify, M. S. Ghazizadeh, and A. Salemnia, "Long-term chronological load modeling in power system studies with energy storage systems," *Appl. Energy*, vol. 156, pp. 436–448, 2015.

[54] I. A. Sajjad, G. Chicco, and R. Napoli, "Effect of aggregation level and sampling time on load variation profile - A statistical analysis," *Proc. Mediterr. Electrotech. Conf. - MELECON*, no. April, pp. 208–212, 2014.

[55] M. Bastani, A. E. Thanos, H. Damgacioglu, N. Celik, and C. H. Chen, "An evolutionary simulation optimization framework for interruptible load management in the smart grid," *Sustain. Cities Soc.*, vol. 41, no. May, pp. 802–809, 2018.

[56] A. Ballanti and L. F. Ochoa, "Voltage-Led Load Management in Whole Distribution Networks," *IEEE Trans. Power Syst.*, vol. 33, no. 2, pp. 1544–1554, 2018.

[57] P. J. Douglass and I. Trintis, "Balancing distribution systems with three-phase active front end rectifiers: field experiment results," *IET Gener. Transm. Distrib.*, vol. 11, no. 15, pp. 3749–3755, 2017.

[58] M. C. Baechler, T. L. Gilbride, P. C. Cole, M. G. Hefty, and K. Ruiz, "Guide to Determining Climate Regions by County PREPARED BY Pacific Northwest National Laboratory," *Pacific Northwest Natl. Lab. Oak Ridge Natl. Lab.*, 2015.

[59] A. Andreas and S. Wilcox, "Solar Resource & Meteorological Assessment Project (SOLRMAP): Rotating Shadowband Radiometer (RSR)," Los Angeles, California (Data); NREL Report No. DA-5500-56502, 2012.

[60] U.S. Energy Information Administration, "2009 Residential Energy Consumption Survey," 2009. [Online]. Available: https://www.eia.gov/consumption/residential/data/2009/. [Accessed: 07-May-2017].

[61] International Code Council, "2009 International Energy Conservation Code," 2009. [Online]. Available: https://codes.iccsafe.org/content/document/747?site_type=public/. [Accessed: 15-Feb-2019].

[62] S. M. Kay, *Intuitive probability and random processes using MATLAB®*. 2006.

[63] E. Wilson, C. E. Metzger, S. Horowitz, and R. Hendron, "2014 Building America House Simulation Protocols," Golden, CO, NREL Report No. TP-5500-60988, 2014.

[64] Z. T. Taylor, K. Gowri, and S. Katipamula, "GridLAB-D technical support document: Residential end-use module version 1.0," Richland, WA, PNNL-17694, 2008.

[65] B. Hendron and J. Burch, "Tool for Generating Realistic Residential Hot Water Event Schedules," in *SimBuild 2010*, 2010.

[66] K. P. Schneider and J. C. Fuller, "Detailed end use load modeling for distribution system analysis," in *IEEE PES General Meeting*, 2010, pp. 1–7.

[67] I. Richardson, M. Thomson, D. Infield, and A. Delahunty, "Domestic lighting: A high-resolution energy demand model," *Energy Build.*, vol. 41, no. 7, pp. 781–789, Jul. 2009.

[68] R. Hasan, S. Mekhilef, M. Seyedmahmoudian, and B. Horan, "Grid-connected isolated PV microinverters: A review," *Renew. Sustain. Energy Rev.*, vol. 67, pp. 1065–1080, 2017.

[69] J. Sommerfeld, L. Buys, and D. Vine, "Residential consumers' experiences in the adoption and use of solar PV," *Energy Policy*, vol. 105, no. May 2016, pp. 10–16, 2017.

[70] L. Fara and D. Craciunescu, "Output Analysis of Stand-alone PV Systems: Modeling, Simulation and Control," *Energy Procedia*, vol. 112, no. October 2016, pp. 595–605, 2017.

[71] P. G. V. Sampaio and M. O. A. González, "Photovoltaic solar energy: Conceptual framework," *Renew. Sustain. Energy Rev.*, vol. 74, no. March, pp. 590–601, 2017.

[72] M. Kumar and A. Kumar, "Performance assessment and degradation analysis of solar photovoltaic technologies: A review," *Renew. Sustain. Energy Rev.*, vol. 78, no. March, pp. 554–587, 2017.

[73] M. A. Green *et al.*, "Solar cell efficiency tables (Version 53)," *Prog. Photovoltaics Res. Appl.*, vol. 27, no. 1, pp. 3–12, 2019.

[74] T. D. Lee and A. U. Ebong, "A review of thin film solar cell technologies and challenges," *Renew. Sustain. Energy Rev.*, vol. 70, no. November 2016, pp. 1286–1297, 2017.

[75] A. A. Babatunde, S. Abbasoglu, and M. Senol, "Analysis of the impact of dust, tilt angle and orientation on performance of PV Plants," *Renew. Sustain. Energy Rev.*, vol. 90, no. October 2017, pp. 1017–1026, 2018.

[76] A. R. Malekpour and A. Pahwa, "A Dynamic Operational Scheme for Residential PV Smart Inverters," *IEEE Trans. Smart Grid*, vol. 8, no. 5, pp. 2258–2267, 2017.

[77] S. S. Rangarajan, E. R. Collins, J. C. Fox, and D. P. Kothari, "A survey on global PV interconnection standards," *2017 IEEE Power Energy Conf. Illinois, PECI 2017*, pp. 1–8, 2017.

[78] I. de la Parra, M. Muñoz, E. Lorenzo, M. García, J. Marcos, and F. Martínez-Moreno, "PV performance modelling: A review in the light of quality assurance for large PV plants," *Renew. Sustain. Energy Rev.*, vol. 78, no. March, pp. 780–797, 2017.

[79] IEEE, "IEEE Standard for Interconnection and Interoperability of Distributed Energy Resources with Associated Electric Power Systems Interfaces," *IEEE Std 1547-2018 (Revision of IEEE Std 1547-2003)*. 2018.

[80] A. K. Yadav and S. S. Chandel, "Tilt angle optimization to maximize incident solar radiation: A review," *Renewable and Sustainable Energy Reviews*. 2013.

[81] R. Perez, P. Ineichen, R. Seals, J. Michalsky, and R. Stewart, "Modeling daylight availability and irradiance components from direct and global irradiance," *Sol. Energy*, 1990.

[82] M. Alsayed, M. Cacciato, G. Scarcella, and G. Scelba, "Multicriteria Optimal Sizing of Photovoltaic-Wind Turbine Grid Connected Systems," *IEEE Trans. Energy Convers.*, vol. 28, no. 2, pp. 370–379, Jun. 2013.

[83] N. Gökmen, W. Hu, P. Hou, Z. Chen, D. Sera, and S. Spataru, "Investigation of wind speed cooling effect on PV panels in windy locations," *Renew. Energy*, 2016.

[84] E. Skoplaki, A. G. Boudouvis, and J. A. Palyvos, "A simple correlation for the operating temperature of photovoltaic modules of arbitrary mounting," *Sol. Energy Mater. Sol. Cells*, 2008.

[85] D. L. King, S. Gonzalez, G. M. Galbraith, and W. E. Boyson, “Performance Model for Grid-Connected Photovoltaic Inverters, SAND2007-5036,” 2007.

[86] T. Stetz, J. von Appen, M. Braun, and G. Wirth, “Cost-Optimal Inverter Sizing for Ancillary Services - Field Experience in Germany and Future Considerations,” in *Proc. 26th EU PVSEC*, 2011.

[87] P. Gilman, “SAM Photovoltaic Model Technical Reference,” NREL/TP-6A20-64102, 2015.

[88] G. Pillai, G. Putrus, N. Pearsall, and T. Georgitsioti, “The effect of distribution network on the annual energy yield and economic performance of residential PV systems under high penetration,” *Renew. Energy*, vol. 108, pp. 144–155, 2017.

[89] F. Katiraei and J. Aguero, “Solar PV Integration Challenges,” *IEEE Power Energy Mag.*, vol. 9, no. 3, pp. 62–71, May 2011.

[90] J. von Appen, M. Braun, T. Stetz, K. Diwold, and D. Geibel, “Time in the Sun: The Challenge of High PV Penetration in the German Electric Grid,” *IEEE Power Energy Mag.*, vol. 11, no. 2, pp. 55–64, Mar. 2013.

[91] J. Widén, E. Wäckelgård, J. Paatero, and P. Lund, “Impacts of distributed photovoltaics on network voltages: Stochastic simulations of three Swedish low-voltage distribution grids,” *Electr. Power Syst. Res.*, vol. 80, no. 12, pp. 1562–1571, 2010.

[92] M. Thomson and D. G. Infield, “Impact of widespread photovoltaics generation on distribution systems,” *IET Renew. Power Gener.*, vol. 1, no. 1, p. 33, 2007.

[93] R. Tonkoski, D. Turcotte, and T. H. M. El-Fouly, “Impact of high PV penetration on voltage profiles in residential neighborhoods,” *IEEE Trans. Sustain. Energy*, vol. 3, no. 3, pp. 518–527, 2012.

[94] R. Torquato, D. Salles, C. O. Pereira, P. C. M. Meira, and W. Freitas, “A Comprehensive Assessment of PV Hosting Capacity on Low-Voltage Distribution Systems,” *IEEE Trans. Power Deliv.*, vol. 33, no. 2, pp. 1002–1012, 2018.

[95] R. Tonkoski, I. S. Member, L. A. C. Lopes, and I. S. Member, “Voltage Regulation in Radial Distribution Feeders with High Penetration of Photovoltaic,” *2008 IEEE Energy 2030 Conf.*, no. Lv, pp. 1–7, 2008.

[96] F. C. L. Trindade, T. S. D. Ferreira, M. G. Lopes, and W. Freitas, "Mitigation of Fast Voltage Variations during Cloud Transients in Distribution Systems with PV Solar Farms," *IEEE Trans. Power Deliv.*, vol. 32, no. 2, pp. 921–932, 2017.

[97] M. Karimi, H. Mokhlis, K. Naidu, S. Uddin, and A. H. A. Bakar, "Photovoltaic penetration issues and impacts in distribution network - A review," *Renew. Sustain. Energy Rev.*, vol. 53, pp. 594–605, 2016.

[98] D. Schwanz, F. Moller, S. K. Ronnberg, J. Meyer, and M. H. J. Bollen, "Stochastic Assessment of Voltage Unbalance Due to Single-Phase-Connected Solar Power," *IEEE Trans. Power Deliv.*, vol. 32, no. 2, pp. 852–861, 2017.

[99] T. Stetz, M. Kraiczy, M. Braun, and S. Schmidt, "Technical and economical assessment of voltage control strategies in distribution grids," *Prog. Photovoltaics Res. Appl.*, vol. 21, no. 6, pp. 1292–1307, Sep. 2013.

[100] H. Pezeshki and P. Wolfs, "Impact of high PV penetration on distribution transformer life time," in *2013 IEEE Power & Energy Society General Meeting*, 2013, pp. 1–5.

[101] X. Liu, A. Aichhorn, L. Liu, and H. Li, "Coordinated control of distributed energy storage system with tap changer transformers for voltage rise mitigation under high photovoltaic penetration," *IEEE Trans. Smart Grid*, 2012.

[102] M. A. Eltawil and Z. Zhao, "Grid-connected photovoltaic power systems: Technical and potential problems-A review," *Renew. Sustain. Energy Rev.*, vol. 14, no. 1, pp. 112–129, 2010.

[103] J. Susanto, F. Shahnia, and D. Ludwig, "A framework to technically evaluate integration of utility-scale photovoltaic plants to weak power distribution systems," *Appl. Energy*, vol. 231, no. September, pp. 207–221, 2018.

[104] S. Eftekharnejad, V. Vittal, G. T. Heydt, B. Keel, and J. Loehr, "Impact of Increased Penetration of Photovoltaic Generation on Power Systems," *Power Syst. IEEE Trans.*, vol. 28, no. 2, pp. 893–901, 2013.

[105] M. E. Baran, H. Hooshyar, Z. Shen, and A. Huang, "Accommodating High PV Penetration on," *IEEE Trans. Smart Grid*, vol. 3, no. 2, pp. 1039–1046, 2012.

[106] T. Adefarati and R. C. Bansal, “Reliability assessment of distribution system with the integration of renewable distributed generation,” *Appl. Energy*, vol. 185, pp. 158–171, 2017.

[107] J. C. Hernández, A. Medina, and F. Jurado, “Impact comparison of PV system integration into rural and urban feeders,” *Energy Convers. Manag.*, vol. 49, no. 6, pp. 1747–1765, 2008.

[108] H. Pezeshki, P. J. Wolfs, and G. Ledwich, “Impact of high PV penetration on distribution transformer insulation life,” *IEEE Trans. Power Deliv.*, vol. 29, no. 3, pp. 1212–1220, 2014.

[109] M. Braun *et al.*, “Is the distribution grid ready to accept large-scale photovoltaic deployment? State of the art, progress, and future prospects,” *Prog. Photovoltaics Res. Appl.*, vol. 20, no. 6, pp. 681–697, Sep. 2012.

[110] C. Lupangu and R. C. Bansal, “A review of technical issues on the development of solar photovoltaic systems,” *Renew. Sustain. Energy Rev.*, vol. 73, no. February 2016, pp. 950–965, 2017.

[111] M. Thomson and D. G. Infield, “Network power-flow analysis for a high penetration of distributed generation,” *IEEE Trans. Power Syst.*, vol. 22, no. 3, pp. 1157–1162, 2007.

[112] W. H. Kersting, *Distribution system modeling and analysis*, 4th Edition. 2017.

[113] N. Gökmen, W. Hu, and Z. Chen, “Technical Impacts of Overhead-Line to Underground-Cable Transition in Distribution Grids,” in *International Conference on Advances in Power System Control, Operation and Management, APSCOM 2018*, 2018.

[114] R. D. Zimmerman, “Comprehensive Distribution Power Flow: Modeling Formulation Solution Algorithm and Analysis,” Cornell University, 1995.

[115] F. Ghassemi and M. Perry, “Review of voltage unbalance limit in the GB grid code CC. 6.1. 5 (b),” 2014. [Online]. Available: https://www.nationalgrideso.com/document/14271/download.

[116] M. M. Aly, M. Abdel-Akher, Z. Ziadi, and T. Senjyu, “Assessment of reactive power contribution of photovoltaic energy systems on voltage profile and stability of distribution systems,” *Int. J. Electr. Power Energy Syst.*, vol. 61, pp. 665–672, Oct. 2014.

[117] H.-G. Yeh, D. F. Gayme, and S. H. Low, "Adaptive VAR Control for Distribution Circuits With Photovoltaic Generators," *IEEE Trans. Power Syst.*, vol. 27, no. 3, pp. 1656–1663, Aug. 2012.

[118] P. Jahangiri and D. C. Aliprantis, "Distributed Volt/VAr Control by PV Inverters," *IEEE Trans. Power Syst.*, vol. 28, no. 3, pp. 3429–3439, Aug. 2013.

[119] N. Efkarpidis, T. De Rybel, and J. Driesen, "Optimization control scheme utilizing small-scale distributed generators and OLTC distribution transformers," *Sustain. Energy, Grids Networks*, vol. 8, pp. 74–84, Dec. 2016.

[120] M. JUAMPEREZ, G. YANG, and S. B. KJÆR, "Voltage regulation in LV grids by coordinated volt-var control strategies," *J. Mod. Power Syst. Clean Energy*, vol. 2, no. 4, pp. 319–328, Dec. 2014.

[121] S. Hashemi, J. Ostergaard, T. Degner, R. Brandl, and W. Heckmann, "Efficient Control of Active Transformers for Increasing the PV Hosting Capacity of LV Grids," *IEEE Trans. Ind. Informatics*, vol. 13, no. 1, pp. 270–277, Feb. 2017.

[122] E. Dall'Anese, S. V. Dhople, B. B. Johnson, and G. B. Giannakis, "Decentralized Optimal Dispatch of Photovoltaic Inverters in Residential Distribution Systems," *IEEE Trans. Energy Convers.*, vol. 29, no. 4, pp. 957–967, Dec. 2014.

[123] I. T. Papaioannou, A. Purvins, and C. S. Demoulias, "Reactive power consumption in photovoltaic inverters: a novel configuration for voltage regulation in low-voltage radial feeders with no need for central control," *Prog. Photovoltaics Res. Appl.*, vol. 23, no. 5, pp. 611–619, May 2015.

[124] A. Safayet, P. Fajri, and I. Husain, "Reactive Power Management for Overvoltage Prevention at High PV Penetration in a Low-Voltage Distribution System," *IEEE Trans. Ind. Appl.*, vol. 53, no. 6, pp. 5786–5794, Nov. 2017.

[125] E. Demirok, P. C. González, K. H. B. Frederiksen, D. Sera, P. Rodriguez, and R. Teodorescu, "Local Reactive Power Control Methods for Overvoltage Prevention of Distributed Solar Inverters in Low-Voltage Grids," *IEEE J. Photovoltaics*, vol. 1, no. 2, pp. 174–182, Oct. 2011.

[126] T. Stetz, F. Marten, and M. Braun, "Improved Low Voltage Grid-Integration of Photovoltaic Systems in Germany," *IEEE Trans. Sustain. Energy*, vol. 4, no. 2, pp. 534–542, Apr. 2013.

[127] M. S. El Moursi, H. H. Zeineldin, J. L. Kirtley, and K. Alobeidli, “A Dynamic Master/Slave Reactive Power-Management Scheme for Smart Grids With Distributed Generation,” *IEEE Trans. Power Deliv.*, vol. 29, no. 3, pp. 1157–1167, Jun. 2014.

[128] S. Weckx and J. Driesen, “Optimal Local Reactive Power Control by PV Inverters,” *IEEE Trans. Sustain. Energy*, vol. 7, no. 4, pp. 1624–1633, Oct. 2016.

[129] R. K. Varma and E. M. Siavashi, “PV-STATCOM: A New Smart Inverter for Voltage Control in Distribution Systems,” *IEEE Trans. Sustain. Energy*, vol. 9, no. 4, pp. 1681–1691, Oct. 2018.

[130] M. Hasheminamin, V. G. Agelidis, A. Ahmadi, P. Siano, and R. Teodorescu, “Single-point reactive power control method on voltage rise mitigation in residential networks with high PV penetration,” *Renew. Energy*, vol. 119, pp. 504–512, Apr. 2018.

[131] A. Selim, M. Abdel-Akher, M. M. Aly, S. Kamel, and T. Senjyu, “Fast quasi-static time-series analysis and reactive power control of unbalanced distribution systems,” *Int. Trans. Electr. Energy Syst.*, vol. 29, no. 1, p. e2673, Jan. 2019.

[132] A. Bonfiglio, M. Brignone, F. Delfino, and R. Procopio, “Optimal Control and Operation of Grid-Connected Photovoltaic Production Units for Voltage Support in Medium-Voltage Networks,” *IEEE Trans. Sustain. Energy*, vol. 5, no. 1, pp. 254–263, Jan. 2014.

[133] E. Dall’Anese, S. V. Dhople, and G. B. Giannakis, “Optimal Dispatch of Photovoltaic Inverters in Residential Distribution Systems,” *IEEE Trans. Sustain. Energy*, vol. 5, no. 2, pp. 487–497, Apr. 2014.

[134] F. H. M. Rafi, M. J. Hossain, and J. Lu, “Hierarchical controls selection based on PV penetrations for voltage rise mitigation in a LV distribution network,” *Int. J. Electr. Power Energy Syst.*, vol. 81, pp. 123–139, Oct. 2016.

[135] H.-T. Yang and J.-T. Liao, “Hierarchical reactive power regulation strategies for high-penetration photovoltaic distribution systems,” *Int. J. Energy Res.*, vol. 40, no. 3, pp. 332–342, Oct. 2016.

[136] M. Castilla, M. Velasco, J. Miret, P. Martí, and A. Momeneh, “Comparative study of reactive power control methods for photovoltaic inverters in low-voltage grids,” *IET Renew. Power Gener.*, vol. 10, no. 3, pp. 310–318, Mar. 2016.

[137] T. Van Dao, S. Chaitusaney, Y. Hayashi, and H. Ishii, "Optimal coordination of voltage controllable devices in distribution systems using power-based models and quadratic programming," *IEEJ Trans. Electr. Electron. Eng.*, vol. 12, pp. S54–S64, Jun. 2017.

[138] T. Ding, C. Li, Y. Yang, J. Jiang, Z. Bie, and F. Blaabjerg, "A Two-Stage Robust Optimization for Centralized-Optimal Dispatch of Photovoltaic Inverters in Active Distribution Networks," *IEEE Trans. Sustain. Energy*, vol. 8, no. 2, pp. 744–754, Apr. 2017.

[139] S. Ibrahim, A. Cramer, X. Liu, and Y. Liao, "PV inverter reactive power control for chance-constrained distribution system performance optimisation," *IET Gener. Transm. Distrib.*, vol. 12, no. 5, pp. 1089–1098, Mar. 2018.

[140] Y. Chen, M. Strothers, and A. Benigni, "All-day coordinated optimal scheduling in distribution grids with PV penetration," *Electr. Power Syst. Res.*, vol. 164, pp. 112–122, Nov. 2018.

[141] J. Li, Z. Xu, J. Zhao, and C. Wan, "A Coordinated Dispatch Model for Distribution Network Considering PV Ramp," *IEEE Trans. Power Syst.*, vol. 33, no. 1, pp. 1107–1109, Jan. 2018.

[142] Q. Nguyen, H. V. Padullaparti, K.-W. Lao, S. Santoso, X. Ke, and N. Samaan, "Exact Optimal Power Dispatch in Unbalanced Distribution Systems With High PV Penetration," *IEEE Trans. Power Syst.*, vol. 34, no. 1, pp. 718–728, Jan. 2019.

[143] Y. Liu, L. Guo, C. Lu, Y. Chai, S. Gao, and B. Xu, "A Fully Distributed Voltage Optimization Method for Distribution Networks Considering Integer Constraints of Step Voltage Regulators," *IEEE Access*, vol. 7, pp. 60055–60066, 2019.

[144] C. Wu, G. Hug, and S. Kar, "Smart Inverter for Voltage Regulation: Physical and Market Implementation," *IEEE Trans. Power Syst.*, vol. 33, no. 6, pp. 6181–6192, Nov. 2018.

[145] H. Almasalma, S. Claeys, and G. Deconinck, "Peer-to-peer-based integrated grid voltage support function for smart photovoltaic inverters," *Appl. Energy*, vol. 239, pp. 1037–1048, Apr. 2019.

[146] S. Weckx, C. Gonzalez, and J. Driesen, "Combined Central and Local Active and Reactive Power Control of PV Inverters," *IEEE Trans. Sustain. Energy*, vol. 5, no. 3, pp. 776–784, Jul. 2014.

[147] A. Chanhome and S. Chaitusaney, “Applying control scheme function of PV inverter for minimizing voltage fluctuation and imbalance with consideration of maximum PV generation,” *IEEJ Trans. Electr. Electron. Eng.*, vol. 12, pp. S42–S53, Jun. 2017.

[148] R. A. Jabr, “Linear Decision Rules for Control of Reactive Power by Distributed Photovoltaic Generators,” *IEEE Trans. Power Syst.*, vol. 33, no. 2, pp. 2165–2174, Mar. 2018.

[149] R. A. Jabr, “Robust Volt/VAr Control With Photovoltaics,” *IEEE Trans. Power Syst.*, vol. 34, no. 3, pp. 2401–2408, May 2019.

[150] N. Gokmen, W. Hu, and Z. Chen, “A simple PV inverter power factor control method based on solar irradiance variation,” in *2017 IEEE Manchester PowerTech*, 2017, pp. 1–6.

[151] N. Gokmen, W. Hu, X. Xu, and Z. Chen, “A novel reactive power control strategy for distribution grids with large scale rooftop PV systems,” in *2018 IEEE PES Asia-Pacific Power and Energy Engineering Conference (APPEEC)*, 2018, pp. 382–387.

[152] H. M. Ayres, D. Salles, and W. Freitas, “A practical second-order based method for power losses estimation in distribution systems with distributed generation,” *IEEE Trans. Power Syst.*, vol. 29, no. 2, pp. 666–674, 2014.

[153] F. Tamp and P. Ciufo, “A Sensitivity Analysis Toolkit for the Simplification of MV Distribution Network Voltage Management,” *IEEE Trans. Smart Grid*, vol. 5, no. 2, pp. 559–568, Mar. 2014.

[154] R. Gurram and B. Subramanyam, “Sensitivity analysis of radial distribution network – adjoint network method,” *Int. J. Electr. Power Energy Syst.*, vol. 21, no. 5, pp. 323–326, 1999.

[155] R. Aghatehrani and R. Kavasseri, “Reactive Power Management of a DFIG Wind System in Microgrids Based on Voltage Sensitivity Analysis,” *IEEE Trans. Sustain. Energy*, vol. 2, no. 4, pp. 451–458, Oct. 2011.

[156] B. Bakhshideh Zad, H. Hasanvand, J. Lobry, and F. Vallée, “Optimal reactive power control of DGs for voltage regulation of MV distribution systems using sensitivity analysis method and PSO algorithm,” *Int. J. Electr. Power Energy Syst.*, vol. 68, pp. 52–60, Jun. 2015.

[157] R. Aghatehrani and R. Kavasseri, "Sensitivity-analysis-based sliding mode control for voltage regulation in microgrids," *IEEE Trans. Sustain. Energy*, vol. 4, no. 1, pp. 50–57, 2013.

[158] S. Weckx, R. DeHulst, and J. Driesen, "Voltage Sensitivity Analysis of a Laboratory Distribution Grid With Incomplete Data," *IEEE Trans. Smart Grid*, vol. 6, no. 3, pp. 1271–1280, 2015.

[159] Z. Zhang, L. F. Ochoa, and G. Valverde, "A Novel Voltage Sensitivity Approach for the Decentralized Control of DG Plants," *IEEE Trans. Power Syst.*, vol. 33, no. 2, pp. 1566–1576, 2018.

[160] Y. H. Choi, S. Seo, S. Kang, and B. Lee, "Justification of effective reactive power reserves with respect to a particular bus using linear sensitivity," *IEEE Trans. Power Syst.*, vol. 26, no. 4, pp. 2118–2124, 2011.

[161] J. Ma, X. Ma, Z. Y. Dong, D. J. Hill, and L. Z. Zhu, "Input sensitivity analysis via transfer function matrix," *IEEE Trans. Power Syst.*, vol. 29, no. 6, pp. 3120–3121, 2014.

[162] R. Yan and T. K. Saha, "Voltage Variation Sensitivity Analysis for Unbalanced Distribution Networks Due to Photovoltaic Power Fluctuations," *IEEE Trans. Power Syst.*, vol. 27, no. 2, pp. 1078–1089, May 2012.

[163] S. H. Soltani, M. Rashidinejad, and A. Abdollahi, "Dynamic phase balancing in the smart distribution networks," *Int. J. Electr. Power Energy Syst.*, vol. 93, pp. 374–383, 2017.

[164] P.-C. Chen, V. Malbasa, Y. Dong, and M. Kezunovic, "Sensitivity Analysis of Voltage Sag Based Fault Location With Distributed Generation," *IEEE Trans. Smart Grid*, vol. 6, no. 4, pp. 2098–2106, 2015.

[165] Z. Liu, J. Rong, G. Zhao, and Y. Luo, "Harmonic Assessment for Wind Parks Based on Sensitivity Analysis," *IEEE Trans. Sustain. Energy*, vol. 8, no. 4, pp. 1373–1382, 2017.

[166] K. N. Hasan, R. Preece, and J. Milanović, "Application of game theoretic approaches for identification of critical parameters affecting power system small-disturbance stability," *Int. J. Electr. Power Energy Syst.*, vol. 97, no. August 2017, pp. 344–352, 2018.

[167] K. N. Hasan, R. Preece, and J. V. Milanovic, "Priority Ranking of Critical Uncertainties Affecting Small-Disturbance Stability Using Sensitivity

Analysis Techniques," *IEEE Trans. Power Syst.*, vol. 32, no. 4, pp. 2629–2639, 2017.

[168] E. S. Hoji, a Padilha-Feltrin, and J. Contreras, "Reactive Control for Transmission Overload Relief Based on Sensitivity Analysis and Cooperative Game Theory," *Ieee Trans. Power Syst.*, vol. 27, no. 3, pp. 1192–1203, 2012.

[169] K. H. Youssef, "A New Method for Online Sensitivity-Based Distributed Voltage Control and Short Circuit Analysis of Unbalanced Distribution Feeders," *IEEE Trans. Smart Grid*, vol. 6, no. 3, pp. 1–1, 2014.

[170] S. F. Santos *et al.*, "Impacts of Operational Variability and Uncertainty on Distributed Generation Investment Planning: A Comprehensive Sensitivity Analysis," *IEEE Trans. Sustain. Energy*, vol. 8, no. 2, pp. 855–869, 2017.

[171] P. Wiest, D. Gross, K. Rudion, and A. Probst, "Rapid identification of worst-case conditions: improved planning of active distribution grids," *IET Gener. Transm. Distrib.*, vol. 11, no. 9, pp. 2412–2417, 2017.

[172] V. V. S. N. Murthy and A. Kumar, "Comparison of optimal DG allocation methods in radial distribution systems based on sensitivity approaches," *Int. J. Electr. Power Energy Syst.*, vol. 53, no. 1, pp. 450–467, 2013.

[173] A. R. R. De Souza *et al.*, "Sensitivity analysis to connect distributed generation," *Int. J. Electr. Power Energy Syst.*, vol. 46, no. 1, pp. 145–152, 2013.

[174] A. A. Abou El-Ela, M. T. Mouwafi, A.-M. Kinawy, and R. A. El-Sehiemy, "Optimal capacitor placement in distribution systems for power loss reduction and voltage profile improvement," *IET Gener. Transm. Distrib.*, vol. 10, no. 5, pp. 1209–1221, 2016.

[175] A. Gonzalez, F. M. Echavarren, L. Rouco, and T. Gomez, "A Sensitivities Computation Method for Reconfiguration of Radial Networks," *IEEE Trans. Power Syst.*, vol. 27, no. 3, pp. 1294–1301, Aug. 2012.

[176] Z. Lu, J. Liu, Y. Liu, R. Ding, and F. Yang, "The interval sensitivity analysis and optimization of the distribution network parameters considering the load uncertainty," *Int. J. Electr. Power Energy Syst.*, vol. 64, pp. 931–936, 2015.

[177] J. Mitra and M. Benidris, "Reliability and sensitivity analysis of composite power systems considering voltage and reactive power constraints," *IET Gener. Transm. Distrib.*, vol. 9, no. 12, pp. 1245–1253, 2015.

[178] F. Ni, M. Nijhuis, P. H. Nguyen, and J. F. G. Cobben, "Variance-Based Global Sensitivity Analysis for Power Systems," *IEEE Trans. Power Syst.*, vol. 33, no. 2, pp. 1–1, 2017.

[179] A. Dubey and S. Santoso, "On Estimation and Sensitivity Analysis of Distribution Circuit's Photovoltaic Hosting Capacity," *IEEE Trans. Power Syst.*, vol. 32, no. 4, pp. 2779–2789, 2017.

[180] X. Su, M. A. S. Masoum, and P. J. Wolfs, "Optimal PV Inverter Reactive Power Control and Real Power Curtailment to Improve Performance of Unbalanced Four-Wire LV Distribution Networks," *IEEE Trans. Sustain. Energy*, vol. 5, no. 3, pp. 967–977, Jul. 2014.

[181] N. Safitri, F. Shahnia, and M. A. S. Masoum, "Coordination of single-phase rooftop pvs in unbalanced three-phase residential feeders for voltage profiles improvement," *Aust. J. Electr. Electron. Eng.*, vol. 13, no. 2, pp. 77–90, Apr. 2016.

[182] H. Pezeshki, A. Arefi, G. Ledwich, and P. Wolfs, "Probabilistic Voltage Management Using OLTC and dSTATCOM in Distribution Networks," *IEEE Trans. Power Deliv.*, vol. 33, no. 2, pp. 570–580, Apr. 2018.

[183] V. Behravesh, R. Keypour, and A. Akbari Foroud, "Control strategy for improving voltage quality in residential power distribution network consisting of roof-top photovoltaic-wind hybrid systems, battery storage and electric vehicles," *Sol. Energy*, vol. 182, pp. 80–95, Apr. 2019.

ISSN (online): 2446-1636
ISBN (online): 978-87-7210-500-0

AALBORG UNIVERSITY PRESS